Cool Gas in High-Redshift Galaxies

C.L. Carilli[1] and F. Walter[2]

[1]National Radio Astronomy Observatory, Socorro, New Mexico 87801; email: ccarilli@nrao.edu

[2]Max-Planck-Institut für Astronomie, D-69117 Heidelberg, Germany; email: walter@mpia.de

Annu. Rev. Astron. Astrophys. 2013. 51:105–61

The *Annual Review of Astronomy and Astrophysics* is online at astro.annualreviews.org

This article's doi:
10.1146/annurev-astro-082812-140953

Keywords

galaxy formation, radio lines: molecular, radio lines: mm, radio lines: cm, molecular gas, atomic fine structure lines, galaxies

Abstract

Over the past decade, observations of the cool interstellar medium (ISM) in distant galaxies via molecular and atomic fine structure line (FSL) emission have gone from a curious look into a few extreme, rare objects to a mainstream tool for studying galaxy formation out to the highest redshifts. Molecular gas has been observed in close to 200 galaxies at $z > 1$, including numerous AGN host-galaxies out to $z \sim 7$, highly star-forming submillimeter galaxies, and increasing samples of main-sequence color-selected star-forming galaxies at $z \sim 1.5$ to 2.5. Studies have moved well beyond simple detections to dynamical imaging at kiloparsec-scale resolution and multiline, multispecies studies that determine the physical conditions in the ISM in early galaxies. Observations of the cool gas are the required complement to studies of the stellar density and star-formation history of the Universe as they reveal the phase of the ISM that immediately precedes star formation in galaxies. Current observations suggest that the order of magnitude increase in the cosmic star-formation rate density from $z \sim 0$ to 2 is commensurate with a similar increase in the gas-to-stellar mass ratio in star-forming disk galaxies. Progress has been made in determining the CO luminosity to H_2 mass conversion factor at high z, and the dichotomy between high versus low values for main-sequence versus starburst galaxies, respectively, appears to persist with increasing redshift, with a likely dependence on metallicity and other local physical conditions. There may also be two sequences in the relationship between star-formation rate and gas mass: one for starbursts, in which the gas consumption timescale is short (a few 10^7 years), and one for main sequence galaxies, with an order of magnitude longer gas consumption timescale. Studies of atomic FSL emission are rapidly progressing, with some tens of galaxies detected in the exceptionally bright [CII] 158-μm line to date. The [CII] line is proving to be a unique tracer of galaxy dynamics in the early Universe and, together with other atomic FSLs, has the potential to be the most direct means of obtaining spectroscopic redshifts for the first galaxies during cosmic reionization.

1. INTRODUCTION

1.1. Motivation

The past few years have seen remarkable progress in the study of the cool, molecular gas content of galaxies, using centimeter and (sub)millimeter telescopes. The cool gas content is a critical parameter in galaxy evolution, serving as the immediate fuel for star formation in galaxies. The state of the field in 2005 was reviewed by Solomon & vanden Bout (2005; see also Omont 2007). At that point, only a few handfuls of extreme starburst galaxies and luminous AGN host galaxies had been detected in molecular gas emission at significant lookback times, hardly anything was known about the gas excitation, and there were no detections of atomic fine structure lines (FSL). Research in recent years has resulted in an explosion in the number and type of galaxies detected in molecular line emission, as well as in atomic FSL emission, in the distant Universe. Detailed multitransition, multispecies follow-up has determined the physical conditions of the gas in some of the brightest high-redshift systems known. The results are proving extremely telling for our understanding of galaxy formation and evolution and suggest that the molecular gas content of galaxies increases significantly with lookback time.

It is a good time to review the field of molecular line observations of high-redshift galaxies for two reasons. First is the dramatic advance that has been made over the past decade, in both the number of galaxies detected as well as the characterization of the molecular properties of these galaxies through follow-up observations. Second is the imminent full operation of revolutionary telescopes, the Atacama Large Millimeter/Submillimeter Array (ALMA) (Wootten & Thompson 2009), and the Karl J. Jansky Very Large Array (JVLA) (Perley et al. 2011), both of which promise to explore this evolution of the universal molecular gas content to an order-of-magnitude-greater-level of detail and sensitivity than previously possible. This review of the field, at this temporal cusp of knowledge, captures the current state of the field and frames the fundamental questions that will be addressed with the next generation of instruments.

1.2. Galaxy Formation and the Need for Cool Gas Observations

Galaxy evolution has been the subject of many reviews in recent years (e.g., Giavalisco 2002, Renzini 2006, Shapley 2011, Silk & Mamon 2012), and the past decade has seen dramatic advances in our understanding of cosmic structure formation. Cosmic geometry, the mass-energy content of the Universe, and the initial density fluctuation spectrum are now known to better than 10% (Spergel et al. 2007; Komatsu et al. 2011; Planck Collab., Ade et al. 2013). Structure formation through gravitational instabilities has been calculated in exquisite detail through numerical studies (e.g., Springel et al. 2005; Klypin, Trujillo-Gomez & Primack 2011) and observationally verified through studies of galaxy distributions (e.g., Peacock et al. 2001, Reid et al. 2010). And the cosmic star-formation rate (SFR) density (the star formation history of the Universe, SFHU), and stellar mass build-up, have been quantified back to first light and cosmic reionization (e.g., Bouwens et al. 2011a, Coe et al. 2013) within 1 Gyr of the Big Bang. Studies of galaxy formation are now turning attention to the evolution of the cool gas, the fuel for star formation in galaxies. In this section, we briefly summarize some of the general conclusions on galaxy formation that are relevant to our subsequent review of the gaseous evolution of galaxies.

Three main epochs have been identified in the SFHU, starting with a steady rise during cosmic reionization from $z \sim 10$ to 6 (e.g., Bouwens et al. 2011b, 2012a; Coe et al. 2013), corresponding to the epoch when light from the first galaxies reionizes the neutral intergalactic medium (IGM)

that pervaded the Universe (Fan, Carilli & Keating 2006; Finkelstein et al. 2012). The comoving cosmic SFR density then peaks at $z \sim 1$ to 3. This range is known as the epoch of galaxy assembly, during which about half the stars in the present day Universe form (Reddy et al. 2008, Marchesini et al. 2009, Shapley 2011). Last comes the order-of-magnitude decline in the comoving cosmic SFR density from $z \sim 1$ to the present (e.g., Lilly et al. 1996, Madau et al. 1996).

MS: main sequence (of star-forming galaxies)

The study of galaxy formation takes on the challenge to explain this observed SFHU in the context of ΛCDM, the hierarchical dark matter halo model. To understand galaxy formation, we must investigate how stars and star formation are distributed over dark matter halos with different masses as a function of time. The most important feature of our current understanding of the field is that star and galaxy formation is inefficient: only ∼5% of all baryons (i.e., atoms of all kind) are in stars and dark stellar remnants at redshift zero (e.g., Fukugita & Peebles 2004).

Galaxies with a baryonic mass of slightly more than that of the Milky Way are most efficient in converting the available baryons into stars (∼15–20%; e.g., Moster et al. 2010). One key observational result is that this typical galaxy mass has not greatly changed since $z \sim 3$ (e.g., Marchesini et al. 2009, Ilbert et al. 2010). Dark matter halos and their baryon content, however, have grown by two orders of magnitude over that time span (e.g., Springel et al. 2005). It appears that dark matter halos with a total mass of $\sim 10^{12}\,M_\odot$ are, at all cosmic times, the most efficient star-formation factories. For such halos, the SFR at different epochs is observed to roughly follow the cosmological accretion rate as predicted by ΛCDM: SFRs are observed to increase systematically with redshift, in a regular fashion such that a galaxy "main sequence" (defined below) is established, with a relatively small scatter in SFR for a given galaxy stellar mass (e.g., Noeske et al. 2007, Elbaz et al. 2011). At $z \sim 0$, the cosmic SFR density is dominated by galaxies with SFRs $\leq 10\,M_\odot$ year^{-1} [far-infrared (FIR) luminosities $\leq 10^{11}\,L_\odot$]. By $z \sim 2$, the dominant contribution shifts to galaxies forming stars at $\sim 100\,M_\odot$ year^{-1} (Magnelli et al. 2011, Murphy et al. 2011). Once the halo and the galaxy grow beyond this mass, further growth through star formation is marginal (e.g., Peng et al. 2010) and accretion of other galaxies (merging) becomes the dominant evolutionary channel (van der Wel et al. 2009).

Massive galaxies with low star-formation activity, if any, are observed at all redshifts $z \leq 3$ (e.g., Franx et al. 2003, Kriek et al. 2006), and their existence remains a puzzle as there is no trivial mechanism that prevents gas from cooling and forming stars in more massive halos. Many ideas abound: shock heating of in-falling gas (Kereš et al. 2005, Dekel & Birnboim 2006); feedback from AGN (Croton et al. 2006, Bell et al. 2012) as motivated by ubiquitously observed supermassive black holes (SMBHs) in massive galaxies and the coincidence of the peak of quasi-stellar object (QSO, or quasar) and star-formation activity at $z \sim 2$ (Hopkins et al. 2006); and stabilization of gaseous disks as a result of bulge formation (Martig et al. 2009). Feedback by AGN-driven winds appears to be required to explain the evolution of young star-forming galaxies into red, bulge-dominated galaxies at intermediate redshift (e.g., Feruglio et al. 2010), whereas powerful radio jets from AGN may be needed to heat the intercluster gas around massive galaxies at late cosmic epochs, thereby inhibiting further late-time growth of massive galaxies (McNamara & Nulsen 2007, Fabian 2012).

We briefly clarify our use of the terms starburst and main sequence for star-forming galaxies in this review. These classifications have arisen in two, parallel situations. First, studies find that the majority of star-forming galaxies at both high and low redshifts define a main sequence (MS), in which there is a relatively tight distribution (dispersion ∼0.3 dex) in specific SFR (sSFR = SFR/stellar mass) versus stellar mass. The sSFR is typically a slowly decreasing function of increasing stellar mass and, at a given stellar mass, the sSFR increases by a factor 20 from $z = 0$ to 2 for these MS galaxies (Rodighiero et al. 2011, Sargent et al. 2012). However, at all redshifts the distribution function in sSFR requires a second component at a factor 4 to 10 times higher

SFR than the nominal MS. This starburst component constitutes a few percent of the distribution by number, and about 10% in terms of the contribution to the cosmic star-formation rate density.

FSL: fine structure line

Second, as presented in Section 4.5, there also appears to be a dual-sequence in the FIR to CO luminosity ratio, with factor few higher ratios for starburst versus MS galaxies. The implied gas consumption timescales may be an order of magnitude, or more, shorter in starburst systems than in MS galaxies (modulo the conversion factor; see Section 4.2). There is some evidence to support the notion that starbursts are associated with major gas rich mergers, although this remains an area of open investigation. These two sequences of star-forming galaxies are in addition to early-type galaxies discussed above, which are typically of higher stellar mass, and show an sSFR of an order of magnitude, or more, lower.

In order to understand why star-formation efficiency (SFE) peaks at a certain halo mass and then declines for more massive systems, the interplay between gas accretion, cooling, star formation, and feedback must be understood. Most of our current understanding of galaxy formation, as briefly summarized above, is based on studies of the stars, star formation, and ionized gas. There remains a major gap in our knowledge, namely, observations of the cool gas: the fuel for star formation in galaxies. Put simply, current studies probe the products of the process of galaxy formation, but miss the source. If we can trace the presence of cold gas and its distribution in different galaxies and halos over cosmic time, the puzzle of the efficiency of star and galaxy formation can be unraveled. Numerous observational and theoretical papers have pointed out this crucial need for observations of the cool molecular gas feeding star formation in galaxies (Genzel et al. 2008, Dressler et al. 2009, Obreschkow et al. 2009a, Bauermeister et al. 2010). In the sidebar, Galaxy Formation, we summarize some of the highlights from studies of stars and star formation through cosmic time.

We review the current status of observations of the cool gas content of galaxies, as measured via the rotational transitions of common interstellar molecules, and via the atomic FSL transitions, predominantly [CII]. Our focus is on results obtained since the reviews by Solomon & vanden Bout (2005) and Omont (2007). Our review is primarily observational. We present tools and concepts of studying the ISM in distant galaxies (Section 2), then summarize observational results for different galaxy types at high redshift (Section 3). We then discuss implications of the recent observations (Section 4) and what they tell us about conditions in early galaxies and galaxy formation in general (Section 5). We end by raising some of the key questions that can be addressed with new facilities: the JVLA and ALMA (Sections 6 and 7).

We consider only molecular and FSL emission in this review. For a review of the few rotational molecular absorption line systems seen at high redshift to date, see Combes (2008) and Carilli & Menten (2002).

GALAXY FORMATION

Over the past two decades, the star-formation history of the Universe, and the buildup of stellar mass, has been well quantified as a function of galaxy environment and luminosity, back to cosmic reionization ($z \sim 10$). Massive galaxies form most of their stars early, and the majority of star formation occurs at $z > 1$. The dominant contribution to the cosmic star-formation rate density shifts to higher SFR galaxies with redshift. The next major step in the study of galaxy formation is the delineation of the cool gas content of galaxies and, in particular, the molecular ISM out of which stars form as a function of cosmic time.

2. CONCEPTS OF OBSERVING COOL GAS

2.1. Heating and Cooling of the Star-Forming Interstellar Medium in Galaxies

FIR: far-infrared

At high redshift, the ionized ISM can be studied through a combination of optical emission lines (e.g., Lyα, Hα) and FIR atomic FSLs (e.g., [CII], [NII], [OIII]). The neutral medium can be studied with FIR atomic FSLs (e.g., [OI], [CI], [CII]). Unfortunately, HI 21-cm emission from galaxies cannot be studied at redshifts $z > 0.5$ due to limited sensitivity and must await the full square kilometer array (Carilli & Rawlings 2004). The atomic phase in high-redshift systems can also be studied through absorption measurements through individual lines of sight (Wolfe, Gawiser & Prochaska 2005).

In the molecular medium, the high gas densities protect molecules against UV photodissociation because of the shielding by dust and self-shielding of H_2 (Dyson & Williams 1980, Lequeux 2005, Tielens 2005). The molecular gas phase is thought to immediately precede star formation (e.g., Leroy et al. 2008, Schruba et al. 2011), and this phase is thus most relevant to study a galaxy's potential to form new stars. The other phases of the ISM cannot form stars directly (but see, e.g., Glover & Clark 2012) unless they cool sufficiently to form cold and dense molecular gas. The processes in the ISM are highly dynamic, with new gas being accreted [e.g., through mergers or cold mode accretion (CMA); see Section 5.1.2] and gas being lost through both stellar and black hole feedback processes (Section 4.7).

The temperature and density of the ISM are a result of environment and are determined by a balance of heating and cooling. There are several mechanisms that lead to the heating of the molecular gas (e.g., Goldsmith & Langer 1978). Deep within dark molecular clouds, the main heating source is through cosmic rays (i.e., protons and electrons accelerated to gigaelectronvolt energies). Cosmic rays ionize H_2 molecules, and the free electrons then transfer excess kinetic energy to other H_2 molecules.

In molecular clouds associated with active star formation, UV heating is also invoked to explain molecular gas heating. In this picture, O and B stars that dominate the radiation in star-forming regions [mostly in the far-ultraviolet (FUV), $6.0\,\mathrm{eV} < E < 13.6\,\mathrm{eV}$; recall that $1\,\mathrm{eV} \sim 10^4\,\mathrm{K}$ ($1\,\mathrm{eV} = 11605\,\mathrm{K}$)] turn their interface with the molecular clouds into photon-dominated regions [PDRs; also historically known as photodissociation regions (Hollenbach & Tielens 1999)]. On the very surface, the CO is dissociated by UV radiation, and the dominant emission comes from atomic FSLs and H_2 rovibrational lines, as well as dust continuum and polycyclic aromatic hydrocarbon (PAH) emission. Further into the region, dust-shielding and self-shielding allow for the persistence of CO, with the gas heated mainly by electrons that are released from the surfaces of dust grains due to UV absorption.

Related to the UV heating in PDRs is the heating that occurs through X-ray emission (X-ray-dominated region or XDR) emerging from AGN and/or hot plasmas heated by SNe, where the harder input spectrum of the X-rays penetrates further into the molecular clouds than the UV radiation (e.g., Meijerink, Spaans & Israel 2006). Both PDRs and XDRs are discussed in Section 2.6.2. Mechanical shock models have also been invoked to explain the extreme excitation conditions in nuclear starburst or other dense regions (e.g., Flower & Pineau des Forêts 2003, Kristensen et al. 2008, Stacey et al. 2010, Nikola et al. 2011, Meijerink et al. 2013).

In terms of gas cooling, atomic FSLs have long been noted as being the dominant coolant of interstellar gas in star-forming galaxies (Spitzer 1978), in particular, in cooler regions where permitted lines of hydrogen cannot be excited ($<10^4$ K; see Section 2.8). As forbidden transitions, the lines are typically optically thin and, hence, avoid line trapping (resonant scattering) in high column density regions. A few lines have ionization potentials that are higher than hydrogen (13.6 eV) and are thus cooling lines of the ionized medium only (e.g., [NII], [OIII]). Others have

lower ionization potentials and, thus, also trace the neutral ISM (e.g., [CII], [OI], [CI]). Up to a few percent of the FUV energy from star formation in galaxies can go to gas heating via photoelectrons, which is reradiated by FSLs, principally the [CII] 158-μm line (and in some cases [OI]). The majority of the stellar radiation goes into dust heating that is balanced through FIR emission, or is radiated directly into the Universe, in roughly equal proportions (depending on geometry and dust content, e.g., Elbaz 2002).

2.2. Tracing Molecular Gas: Frequencies

The molecular gas mass in galaxies is dominated by molecular hydrogen, H_2. Given the lack of a permanent dipole moment, the lowest rovibrational transitions of H_2 are forbidden, and perhaps more importantly, have high excitation requirements [the first quadrupole line lies 500 K above the ground state, significantly higher than temperatures in giant molecular clouds (GMCs)]. As a consequence, only a very small fraction of the cool molecular gas can be studied through H_2 emission in the IR. This is the reason that, historically, emission from tracer molecules has been used to detect molecular gas in galaxies and from which the total molecular gas mass is then deduced. The molecule of choice has traditionally been carbon monoxide, CO, because it is the most abundant molecule after H_2, has low excitation requirements (~5 K for first excited state; see Section 2.3), and is easily observed from the ground (3-mm band) in its ground transition.

In general, tracer molecules show quantized rotational states populated based on collisions and the radiation field. For a linear polar molecule of moment of inertia, I, the orbital angular momentum is given by $L = n\hbar$ (Townes & Schawlow 1975), and the corresponding rotational energy is $E_{rot} = \frac{L^2}{2I} = \frac{n^2\hbar^2}{2I} = \frac{J(J+1)\hbar^2}{2I}$ with $\Delta J = \pm 1$ (conservation of angular momentum). The energy released from level J to $J-1$ is $\Delta E_{rot} = [J(J+1) - (J-1)J]\frac{\hbar^2}{2I} = \frac{\hbar^2 J}{I} = h\nu_{line}$.

In reality this approximation is not strictly valid, as centrifugal forces will increase with J so that the bond (distance between atoms) will stretch, which in turn changes I. This effect leads to frequencies that are slightly lower than the first harmonic, e.g., for CO, the line-spreading via rotational stretching of higher-order transitions is of order 10 MHz to 15 MHz, or effectively 20 to 30 km s^{-1}, allowing for unique redshift determinations based on just two transitions (e.g., Weiß et al. 2009). Depending on the molecule, there can be other additional fine and hyperfine structures overlaid (i.e., magnetic and electrostatic interactions within the molecule; e.g., Riechers et al. 2007b for the case of CN).

2.3. Gas Temperatures and Critical Density

The kinetic temperature of the H_2 molecules, $T_{\rm kin}$, is determined by the velocity distribution of the molecules following the Maxwell-Boltzmann distribution. The excitation of other tracer molecules, such as CO, is mostly determined by the number of collisions with H_2 molecules as they are very abundant, are massive, and have a high cross section. It is often assumed that this kinetic gas temperature equals the temperature of the dust at high densities. However, it should be noted that the heating and cooling processes of the dust and molecular gas phases are quite different, and therefore thermal balance is not required.

Typically, rotational transitions are expressed as a function of critical density, n_{crit}, i.e., the density at which collisional excitation balances spontaneous radiative deexcitation: $n_{crit} = A/\gamma$, where A is the Einstein coefficient for spontaneous emission, $A \propto \mu^2 \times \nu^3$ in units of s^{-1}, γ is the collision rate coefficient in units of cm^3 s^{-1}, and μ is the dipole moment of the molecular transition under consideration in the $J = 1$ state.

Table 1 Fundamental parameters for frequently observed molecules and fine structure lines

Species	Transition	Excitation potential (K)	λ (μm)	ν (GHz)	Einstein A (s^{-1})	n_{crit} (cm^{-3})
[OI]	$^3P_1 \rightarrow {}^3P_2$	228	63.18	4744.8	9.0×10^{-5}	4.7×10^5
	$^3P_0 \rightarrow {}^3P_1$	329	145.53	2060.1	1.7×10^{-5}	9.4×10^4
[OIII]	$^3P_2 \rightarrow {}^3P_1$	440	51.82	5785.9	9.8×10^{-5}	3.6×10^3 [⋆]
	$^3P_1 \rightarrow {}^3P_0$	163	88.36	3393.0	2.6×10^{-5}	510 [⋆]
[CII]	$^3P_{3/2} \rightarrow {}^3P_{1/2}$	91	157.74	1900.5	2.1×10^{-6}	2.8×10^3
						50 [⋆]
[NII]	$^3P_1 \rightarrow {}^3P_2$	188	121.90	2459.4	7.5×10^{-6}	310 [⋆]
	$^3P_1 \rightarrow {}^3P_0$	70	205.18	1461.1	2.1×10^{-6}	48 [⋆]
[CI]	$^3P_2 \rightarrow {}^3P_1$	63	370.42	809.34	2.7×10^{-7}	1.2×10^3
	$^3P_1 \rightarrow {}^3P_0$	24	609.14	492.16	7.9×10^{-8}	470
CO	$J = 1$–0	5.5	2601	115.27	7.2×10^{-8}	2.1×10^3
	$J = 2$–1	16.6	1300	230.54	6.9×10^{-7}	1.1×10^4
	$J = 3$–2	33.2	867	345.80	2.5×10^{-6}	3.6×10^4
	$J = 4$–3	55.3	650.3	461.04	6.1×10^{-6}	8.7×10^4
	$J = 5$–4	83.0	520.2	576.27	1.2×10^{-5}	1.7×10^5
	$J = 6$–5	116.2	433.6	691.47	2.1×10^{-5}	2.9×10^5
	$J = 7$–6	154.9	371.7	806.65	3.4×10^{-5}	4.5×10^5
	$J = 8$–7	199.1	325.2	921.80	5.1×10^{-5}	6.4×10^5
	$J = 9$–8	248.9	289.1	1036.9	7.3×10^{-5}	8.7×10^5
	$J = 10$–9	304.2	260.2	1152.0	1.0×10^{-4}	1.1×10^6
HCN	$J = 1$–0	4.25	3383	88.63	2.4×10^{-5}	2.6×10^6
	$J = 2$–1	12.76	1691	177.26	2.3×10^{-4}	1.8×10^7
	$J = 3$–2	25.52	1128	265.89	8.4×10^{-4}	6.8×10^7
	$J = 4$–3	42.53	845.7	354.51	2.1×10^{-3}	1.8×10^8
	$J = 5$–4	63.80	676.5	443.12	4.1×10^{-3}	3.8×10^8
	$J = 6$–5	89.32	563.8	531.72	7.2×10^{-3}	7.1×10^8
	$J = 7$–6	119.09	483.3	620.30	1.2×10^{-2}	1.2×10^9
	$J = 8$–7	153.11	422.9	708.88	1.7×10^{-2}	1.8×10^9
	$J = 9$–8	191.38	375.9	797.43	2.5×10^{-2}	2.5×10^9
	$J = 10$–9	233.90	338.4	885.97	3.4×10^{-2}	3.3×10^9

Numbers for the atomic fine structure constants are taken from Stacey (2011). Einstein A coefficients, rest frequencies, and collision rates γ are taken from the Leiden Atomic and Molecular Database (Schöier et al. 2005). The excitation potential is of the upper level above ground. The critcal density is the density at which the rate of the collisional depopulation of a quantum level equals the spontaneous radiative decay rate. We note that definition of the critical density used here is $n_{crit} = A/\gamma$ (Section 2.3). This is not the proper definition that includes the summation of all collisional transitions to the lower level—such a treatment will lower the critical densities presented here. The critical densities also decrease if the lines are optically thick. For species occurring in neutral gas clouds, the collision partners are H and H_2 (assumed $T_{gas} = 100$ K). For species occurring in ionized gas regions, the collision partners are electrons (marked with a [⋆] in the last column). For details see Stacey (2011).

The Einstein coefficient A (see **Table 1**) is determined entirely by the physical properties of the molecule and is proportional to the frequency cubed (i.e., higher J transitions have higher deexcitation rates). The collision rate coefficient γ, however, depends on the temperature of the gas ($\gamma = <\sigma \times \upsilon>$, where σ is the collision cross section and υ is the velocity of the particle). Collision rate coefficients for the excitation of CO by H_2 are given by Flower & Launay (1985)

and Yang et al. (2010), and they are typically ~3 to 10 × 10^{-11} cm^3 s^{-1} for the low-J transitions and temperatures of 40–100 K.

Stars are created in cores of molecular clouds that have much higher densities than the bulk of the gas traced by CO(1–0). Hence, molecules with higher dipole moments (leading to a higher A coefficient as A $\propto \mu^2$ and thus higher critical density) are typically observed only in dense, star-forming cores of GMCs. Typical dense gas tracers and their dipole moments are: CS, 1.958 D (Debye); HCO^+, 3.93 D; HCN, 2.985 D [for comparison, CO has a dipole moment of 0.110 D (Schöier et al. 2005)]. The downside of choosing these high-density tracer molecules is their low abundance and resulting faint line fluxes (as discussed in Section 4.4).

As an example, **Table 1** summarizes the Einstein coefficients for the different transitions of CO and HCN. The critical density for these molecules is given in the last column of the table. It is obvious that higher J transitions need increasingly high critical densities to be visible. Einstein coefficients and collision rates for other molecules are given, e.g., by Schöier et al. (2005).

2.4. Brightness Temperature and Line Luminosities

Historically, radio astronomers express the surface brightness of a source as a Rayleigh-Jeans (RJ) brightness temperature for a blackbody at given temperature through Planck's law. Measurements of brightness temperature and surface brightness are thus equivalent measurements. Rather than expressing the temperature in terms of the Planck temperature, radio astronomers have traditionally used the low-frequency (RJ) limit ($\frac{kT}{h\nu} \gg 1$):

$$B_\nu = \frac{2h\nu^3}{c^2} \times \frac{1}{\exp(\frac{h\nu}{kT}) - 1} \sim \frac{2kT\,\nu^2}{c^2}.$$

In this limit, $T_B^{obs} = \frac{c^2}{2k\nu_{obs}^2} I_\nu$, where I_ν is the surface brightness. The RJ approximation is valid at centimeter wavelengths. However, in the millimeter (and particularly the submillimeter) regime, $\frac{kT}{h\nu} = 0.7[\lambda/1\,\mathrm{mm}][T/10\,\mathrm{K}]$, the RJ approximation is no longer valid in many regions of astrophysical interest, and RJ brightness temperatures can no longer be interpreted as a physical temperature. If one is interested in true temperatures, Planck temperatures should be derived instead.

At high redshift, there are two commonly used ways to express line luminosities. One, L_{line} is expressed as the source luminosity in $L_\odot$ or other rational units. The second, L'_{line}, is expressed via the (areal) integrated source brightness temperature in units of K km s^{-1} pc^2. The following equations can be used to derive these two luminosities (Solomon, Downes & Radford 1992):

$$L'_{line} = 3.25 \times 10^7 \times S_{line}\Delta v \frac{D_L^2}{(1+z)^3 \nu_{obs}^2}\,\mathrm{K\,km\,s^{-1}\,pc^2},$$

$$L_{line} = 1.04 \times 10^{-3} \times S_{line}\Delta v D_L^2 \nu_{obs}\,\mathrm{L_\odot},$$

where $S_{line}\Delta v$ is the measured flux of the line in Janskys kilometers per second, D_L is the luminosity distance in megaparsecs, and ν_{obs} in gigahertz is the observed frequency. Solving for $S\Delta v$ leads to $L_{line} = 3 \times 10^{-11} \nu_r^3 L'_{line}$, where ν_r is the rest frequency of the line. Note that L'_{line} is directly proportional to the surface brightness T_B, i.e., the L'_{line} ratio of two lines gives the ratio of their intrinsic, source-averaged surface brightness temperatures T_B. If the molecular gas emission comes from thermalized, optically thick regions, L'_{line} is constant for all J levels. In the sidebar, Line Luminosities, we outline the different usage of line luminosity definitions in the literature.

LINE LUMINOSITIES

The question often arises as to which quantity should be quoted in a paper, L_{line} or L'_{line}? Both have their justification: for example, if one is interested in comparing the power that is being emitted through a given line to calculate the cooling capability (e.g., in relation to the FIR luminosity, $L_{line}/L_{\rm FIR}$), one uses the L_{line} definition. The L'_{line} is commonly used to translate measured CO luminosities to H_2 masses using the conversion factor α (Section 2.5). Also, for thermalized molecular gas emission, L'_{line} is approximately constant for all transitions. It is good advice to give both quantities in a paper, but in all cases the measured integrated fluxes of the lines $S_{line}\Delta v$ (in units of Jy km s^{-1}) should be included.

2.5. The CO Luminosity–to–Total Molecular Gas Mass Conversion Factor

The conversion factor relating CO(1–0) luminosity to total molecular gas mass (dominated by H_2) in the nearby Universe has been reviewed recently by Bolatto, Leroy & Wolfire (2013). We briefly summarize the main points in this section.

Molecular gas in the Milky Way and nearby galaxies is predominantly in GMCs with overall sizes up to 50 pc. Hence, early work on the conversion factor focused on GMCs. In nearby systems (including the Milky Way), the clouds can typically be spatially resolved, and hence the conversion factor considered, $X_{\rm CO}$, is the ratio of column density (H_2 molecules per centimeter squared) to CO velocity integrated surface brightness (K km s^{-1}), whereas for distant galaxies spatially integrated quantities are usually measured, and the conversion factor $\alpha_{\rm CO}$ is then the ratio of total mass (in $M_\odot$) to total CO line luminosity (K km s^{-1} pc^2). The ratio $X/\alpha = 4.6 \times 10^{10}$ pc^2 cm^{-2} $M_\odot^{-1}$ equals the number of hydrogen molecules per solar mass, converted to the appropriate units and corrected by a factor of 1.36 for helium.

Numerous techniques have been used to determine the conversion factor in GMCs, including (*a*) a comparison of CO columns derived from rare isotopic measurements to H_2 columns derived from optical extinction measurements using a standard dust-to-gas ratio (Dickman 1975, 1978; Dame, Hartmann & Thaddeus 2001), (*b*) a comparison of γ-ray emission to CO surface brightness, where the γ-rays result from the interaction between cosmic rays with H_2 molecules (Bloemen 1989, Strong & Mattox 1996, Hunter et al. 1997), and (*c*) modeling GMCs as self-gravitating clouds. In the latter case, a key discovery was the correlation between line width and cloud size, with line width increasing as the square root of cloud size (the "Larson relations"; Larson 1981). This functional form implies a constant surface density $\sim$100 $M_\odot$ pc^{-2} for GMCs (Solomon et al. 1987), and that the CO luminosity is linearly proportional to cloud virial mass. Indeed, this relationship provides the theoretical underpinning of the use of CO luminosity to derive total gas mass in the case of optically thick emission (Dickman, Snell & Schloerb 1986; Solomon et al. 1987), where luminosity is dictated principally by line width. Bolatto, Leroy & Wolfire (2013) summarize these results and conclude that a value of $X_{\rm CO} = 2 \times 10^{20}$ H_2 molecules cm^{-2} (K km s^{-1})$^{-1}$, or $\alpha_{\rm CO} \sim 4\,M_\odot$ (K km s^{-1} pc^2)$^{-1}$, is appropriate for GMCs in the Milky Way and nearby spiral galaxies, with a factor two (0.3 dex) scatter.

Draine et al. (2007) hypothesized that, if the abundance of the elements can be assumed to be proportional to the oxygen abundance and if a Milky Way fraction of elements tied up in grains is adopted, then $M_{\rm dust}/M_{\rm gas} = 0.010[({\rm O/H})]/[({\rm O/H})_{\rm MW}]$. Using observations of nearby galaxies, they showed that the gas columns derived from the IR thermal dust emission are consistent with $X_{\rm CO} = 4 \times 10^{20}$ cm^{-2} (K km s^{-1})$^{-1}$ and metallicities between 0.3 $M_\odot$ and 1 solar for their galaxy sample. Leroy et al. (2011) use an empirical dust-to-gas ratio approach in nearby galaxies

GMCs: giant molecular clouds

and obtain similar results, showing that the lowest metallicity galaxies clearly have much higher conversion factors. They suggest that decreased dust shielding in low-metallicity environments leads to CO-free, but still H_2-rich, cloud envelopes because H_2 can self-shield (see also Schruba et al. 2012, Sandstrom et al. 2013).

A different picture has emerged for nearby nuclear starburst galaxies, including the nuclei of dwarf starbursts like M82 and NGC 253, corresponding to luminous infrared galaxies, or LIRGs ($L_{IR} > 10^{11}\,L_\odot$), and ultraluminous infrared galaxies (ULIRGs) such as Arp 220 ($L_{IR} > 10^{12}\,L_\odot$). It was noted early on that a Milky Way conversion factor leads to a molecular gas mass larger than the dynamical mass in some of these systems (Bryant & Scoville 1999). In their seminal analysis of CO radiative transfer and gas dynamics in starburst nuclei of ULIRGs on scales <1 kpc, Downes & Solomon (1998) find a characteristic value of $\alpha_{CO} \sim 0.8\,M_\odot\,(K\,km\,s^{-1}\,pc^2)^{-1}$ in these systems. The lower value of α implies more CO emission per unit molecular gas mass. They hypothesize that much of the CO emission is not from virialized GMCs, but from an overall warm, pervasive molecular intercloud medium. In this case, the line width, and hence line luminosity (for optically thick emission), is determined by the total dynamical mass (gas and stars), as well as ISM pressure. Narayanan et al. (2012) show that the lower α value in starbursts can be due to warm gas that is heated by dust (at densities $>10^4$, such energy exchange is efficient), as well as large, nonvirial line widths from the GMCs. More recently, Papadopoulos et al. (2012) suggest that the molecular gas heating processes in nuclear starbursts may be very different than is typically assumed for PDRs, with cosmic rays and turbulence dominating over photons.

In general, the value of α is likely a function of local ISM conditions, including pressure, gas dynamics, and metallicity, and remains an active area of research for nearby galaxies (Glover & Mac Low 2011; Ostriker & Shetty 2011; Feldmann, Gnedin & Kravtsov 2012a; Shetty et al. 2011; Narayanan et al. 2012; Papadopoulos et al. 2012; Schruba et al. 2012; Leroy et al. 2013; Narayanan & Hopkins 2013; Sandstrom et al. 2013).

2.6. Modeling the Line Excitation

Many observations of galaxies at high redshift are unresolved, and studies of the global CO excitation play an important role in constraining their average molecular gas properties. This CO excitation, i.e., the relative strengths of the observed rotational transitions, is sometimes referred to as CO spectral line energy distributions, CO SLEDs, or the CO excitation ladder. We here use the term CO excitation ladder because the measured quantity is the emission of a given rotational transition J. We note that some researchers also chose to plot spectral power distributions (i.e., plotting L instead of $S_v \times dV$ as a function of rotational number J).

The excitation temperature determines the population of the molecular levels through the Boltzmann distribution. Under the assumption of local thermodynamical equilibrium (LTE), this excitation temperature will be equal to the kinetic temperature of the gas. Thermal excitation means that the population of all levels is according to the Boltzmann distribution. The excitation is subthermal if the population of the high levels is less than that given by the kinetic temperature of the gas, as occurs in lower density environments where collisional excitation cannot balance spontaneous emission rates. We briefly discuss the commonly used techniques to model the excitation of the various levels of molecular line emission.

2.6.1. Escape probability/large velocity gradient models. One basic tool commonly used to model the excitation of the molecular gas emission is the large velocity gradient (LVG) method (e.g., Young & Scoville 1991). In the following, we discuss this model for the CO molecule, but

the same modeling can be done for any molecule. The model calculates, for a given temperature T_{kin}, H_2 density, CO abundance ([CO]/[H_2]), and velocity gradient dv/dr, how the various levels of the CO are populated through collisional excitation with H_2. Some models and their dependence on temperature and density are discussed in Section 4.1 (see also figures in van der Tak et al. 2007). Because the CO emission is optically thick (at least in the low-J transitions) the emission would have difficulties escaping the cloud, which is why a velocity gradient that describes how many photons can eventually leave the cloud is introduced in the model. The justification for implementing such a gradient is that in reality the molecular medium is turbulent, which enables CO photons to escape their parental clouds. The LVG codes also take the redshift of the source into account, which dictates the temperature of the cosmic microwave background (CMB; see Section 2.10). Once the occupation numbers of the different levels are calculated, the optical depths τ for the transitions as well as the RJ brightness temperatures T_B (which would be constant in LTE) and the resulting line intensities are derived.

LTE: local thermodynamic equilibrium

In this way, for a given set of parameters, the expected line intensities for any molecule can be derived (assuming certain abundances of the molecule under consideration). In principle, the measurement of the line excitation ladder of a number of different molecules thus puts tight constraints on the temperature and density of the gas. This assumes that these lines probe the same volume, which may not hold for those molecules tracing very high densities (e.g., HCO^+ and HCN). Of particular interest is adding different isotopomers, such as ^{13}CO or $C^{18}O$. These are more optically thin than the $^{12}C^{16}O$ emission and are thought to originate from the same volume as $^{12}C^{16}O$, at least on GMC scales.

2.6.2. Photon-dominated region and X-ray-dominated region models. In PDR and XDR models, a cloud is exposed to a radiation field from which the temperature and density distribution of the H_2 molecules are derived. With the resulting values for T_{ex} and density, a code similar to LVG is then run to calculate the line intensities of the rotational transitions of the molecules under consideration. A difference with respect to the LVG models is that abundances of species are calculated based on the radiation field and the gas column density. The main difference between the PDR and XDR codes is that PDRs only exist at the surface of clouds (where they emit FSLs of [CI], [CII], and [OI], and rotational lines of CO in the submillimeter regime). In the XDR phase (further inside the cloud), the [OI], [CII], and [SiII] lines are main coolants in the submillimeter regime (Meijerink & Spaans 2005). One limitation of most PDR/XDR models is that they are based on (one-dimensional) infinite slabs—i.e., they do not have a confined volume. As a consequence, no mass estimates are typically given by the codes. The gas temperatures calculated in PDR/XDR models are still quite uncertain and depend on the code used, especially in the high-density, high-UV case (e.g., Röllig et al. 2007). Given the high excitation measured in nearby galaxies based on *Herschel Space Observatory* data (up to $J \sim 30$; Hailey-Dunsheath et al. 2012), shock heating is also invoked to explain extreme CO excitation (see also Meijerink et al. 2013).

One complication in all the models above is that it is now established that the high-J rotational transitions of some molecules, e.g., HCN, are not only excited through collisions (as the critical densities of some of the detected high-J lines are extremely high, $\sim 10^9$ cm^{-3}, i.e., they are not even being reached in the cores of GMCs). One potential mechanism to excite the observed high-J HCN rotational modes is through the IR stretching and bending modes of HCN at 3, 5, and 14 μm (this is referred to as IR pumping of the rotational levels, e.g., Weiß et al. 2007a). Similar pumping may be in place even in the case of CO emission and may explain the very high J excitation seen in some local galaxies (see above references, and Harris et al. 1991 for radiative trapping leading to enhanced mid-J CO emission).

2.7. Water Lines

Water is thought to be one of the most abundant molecules in galaxies, present predominantly in icy mantels of dust grains in cold environments (Tielens et al. 1991, Hollenbach et al. 2008). In warmer environments, water in the gas phase is thought to play an important role in cooling (Neufeld & Kaufman 1993; Neufeld, Lepp & Melnick 1995). The rotational transitions of water have high Einstein A values and, thus, very high critical densities ($>10^8$ cm^{-3}), i.e., collisional excitation can only happen in the very centers of dense cloud cores, and other excitation mechanisms, in particular IR pumping, are typically invoked.

Naturally, water lines at low redshift are very difficult to observe from the ground given the Earth's atmosphere. *Herschel* observations enabled the first detections of submillimeter lines of H_2O in nearby galaxies, rather than masers (Mrk 231: González-Alfonso et al. 2010, van der Werf et al. 2010; M82: Weiß et al. 2010). These observations have yielded very different results between the objects: Mrk 231 revealed a rich spectrum of H_2O lines but the ground-state lines remained undetected (van der Werf et al. 2010). In M82, no highly excited emission was found (Panuzzo et al. 2010), but many low-excitation lines were (Weiß et al. 2010). Generally speaking, the water emission line spectrum is very complex and not straightforward to interpret if only one or a few lines are measured (González-Alfonso et al. 2010). We discuss recent high-redshift detections of water lines in Section 4.4.

2.8. Atomic Fine Structure Lines

The atomic FSLs are major coolants of the cool interstellar gas (Section 2.1). **Table 1** summarizes key parameters of important submillimeter atomic FSLs.

2.8.1. Singly ionized carbon. [CII] is the strongest line from star-forming galaxies at radio through FIR wavelengths [e.g., [CII] line fluxes are typically $>10^3$ times stronger than CO(1–0) in star-forming galaxies], and in particular, [CII] 158 μm is the strongest line from the cool gas in galaxies ($<10^4$ K).

The ratio of [CII]/FIR luminosity for the Milky Way is 0.003, and this value holds in nearby disk galaxies, with a relatively large scatter (factor of three; e.g., Malhotra et al. 1997, 2001). However, the ratio appears to drop significantly at FIR luminosities above 10^{11} $L_\odot$. One explanation for this drop is a reduction in the heating efficiency by photoelectric emission from dust grains in high-radiation environments due to highly charged grains. This explanation is supported by the fact that the [CII]/FIR ratio is also a decreasing function of increasing dust temperature (e.g., Malhotra et al. 2001, Luhman et al. 2003). High dust opacity/absorption at 158 μm may also decrease the [CII]/FIR ratio in high-luminosity systems.

[CII] has a lower ionization potential than HI (11.3 eV versus 13.6 eV), hence [CII] traces both the cold neutral medium and ionized gas. This makes [CII] less easy to interpret, in particular if the emission cannot be resolved spatially. The [CII] luminosity is not a simple function of SFR, nor is there a simple dependence between [CII] luminosity and the total mass of the ISM. In an early study, Stacey et al. (1991) argue that roughly 70% of the total [CII] emission from nearby spiral galaxies comes from PDRs, and recent *Herschel* observations show a possible correlation between the [CII] luminosity and the 11.3-μm PAH feature, suggesting a close correlation between PDRs and [CII] emission (Sargsyan et al. 2012). *Herschel* imaging has also shown significant differences in the spatial distribution of the [CII] emission and CO emission on scales ≤300 pc in nearby galaxies (Rodriguez-Fernandez et al. 2006, Mookerjea et al. 2011; see also Cormier et al. 2010).

A clear trend for increasing [CII]/FIR ratio with decreasing metallicity has been established (Cormier et al. 2010, Israel & Maloney 2011). Lower metallicity leads to less dust and higher

UV mean free paths. In this picture, the decreased dust-shielding in PDRs leads to deeper photo-dissociation into the molecular clouds and increased photo-electric heating efficiencies, leading to higher [CII] luminosities relative to the FIR. High-redshift observations of [CII] are discussed in Section 4.3.2.

2.8.2. Atomic carbon: [CI]. Because the ^{3}P fine structure system of atomic carbon forms a simple three-level system, detection of both optically thin carbon lines, CI ($^3P_1 \rightarrow {}^3P_0$) and CI ($^3P_2 \rightarrow {}^3P_1$), enables one to derive the excitation temperature, neutral carbon column density, and mass independent of any other information (e.g., Ojha et al. 2001, Weiß et al. 2003, Walter et al. 2011). A combination of this method (using [CI]) with the aforementioned CO excitation ladder is particularly powerful as it eliminates some of the degeneracy frequently found in CO radiative transfer models under the assumption that [CI] traces the same regions as CO (see discussion in Section 4.1).

Studies of atomic carbon in the local Universe have been carried out in molecular clouds of the galactic disk, the galactic center, *M*82, and other nearby galaxies (e.g., White et al. 1994, Stutzki et al. 1997, Gerin & Phillips 2000, Ojha et al. 2001, Israel & Baas 2002, Israel 2005). These studies have shown that [CI] is closely associated with the CO emission independent of environment. Because the critical density for the CI ($^3P_1 \rightarrow {}^3P_0$) and CO(1–0) lines are both $n_{cr} \approx 10^3$ cm^{-3}, the transitions arise from the same volume and share similar excitation temperatures (e.g., Ikeda et al. 2002). We discuss high-redshift detections of [CI] in Section 4.3.1.

2.8.3. Other fine structure lines: [NII], [OI], [OIII]. Beyond [CII] and [CI], there are a number of other FIR FSLs that are potentially important physical diagnostics for the ISM, in particular the lines from [OI] 63 μm, [OIII] 52 μm and 88 μm, and [NII] 122 μm and 205 μm. Although typically 10 times weaker than [CII], the oxygen line strengths increase dramatically with the hardness of the radiation field, such that in AGN environments the [OIII] 88 μm can be stronger than [CII] (Spinoglio & Malkan 1992, Genzel & Cesarsky 2000, Stacey et al. 2010, Spinoglio et al. 2012). Most of these lines are at even higher frequencies than [CII] and are thus difficult to observe even when galaxies are observed at high redshifts.

The ionization potentials of carbon, oxygen, and nitrogen are 11.3 eV, 13.6 eV, and 14.5 eV, respectively. Hence, [CII] traces both the neutral and ionized medium, whereas oxygen and nitrogen trace the ionized medium only (except for [OI]). The [NII] 122-μm /[OIII] 88-μm ratio is a sensitive measure of hardness of the radiation field because these two lines have similar critical densities for excitation (∼300 to 500 cm^{-3}) but very different ionization potentials (35 eV for [OII]). [CII] 158 μm and [NII] 205 μm have essentially the same critical density for thermal excitation (∼45 cm^{-3}), hence the ratio of $[CII]_{158}/[NII]_{205}$ indicates the fraction of [CII] emission from ionized gas, assuming only a gas phase C/N abundance (Oberst et al. 2006; Walter et al. 2009b; Ferkinhoff et al. 2010, 2011; Decarli et al. 2012). In this case, the $[CII]_{158}/[NII]_{205}$ ratio for ionized gas ranges between 3 and 4 (figure 2 in Oberst et al. 2006). Oberst and colleagues show that the $[NII]_{122}/[NII]_{205}$ ratio is a densitometer, with a value of ∼0.5 for densities below 10^2 cm^{-3} and rising to 10 for densities greater than 10^3 cm^{-3}.

2.9. Relation to Far-Infrared Emission and Star-Formation Rates

In this review, we concentrate on the molecular gas properties of high-redshift galaxies. To put the physical properties of the ISM into perspective, we also use the FIR emission and SFRs in galaxies. For reference we here give the equations that are commonly used to derive IR/FIR luminosities and SFRs from single-band FIR continuum measurements. We stress that the numbers that follow are appropriate for dusty spectral energy distributions (SEDs) typically found in highly star-forming

CMB: cosmic microwave background

galaxies at high redshift, but that the relations are a strong function of galaxy properties, such as the star-formation activity and dust optical depth. The following equations are to first order independent of redshift for $z > 1$, given the inverse K-correction in the submillimeter regime (e.g., Blain et al. 2002, Kennicutt & Evans 2012).

The IR luminosity $L_{\rm IR}$ is defined from 8–1,000 μm, whereas the FIR luminosity $L_{\rm FIR}$ is commonly defined from 40–400 μm (Sanders et al. 2003). $L_{\rm IR}$ is typically ∼30% higher than $L_{\rm FIR}$ for dusty SEDs. Some researchers also define FIR from 42–122 μm (Helou, Soifer & Rowan-Robinson 1985)—this latter definition gives $L_{\rm FIR}$ values that are 20–30% smaller than the $L_{\rm FIR}$ definition above.

In measured flux densities at 250 GHz and 350 GHz (850 μm), the following relations are commonly used: $L_{\rm FIR}[{\rm L}_\odot] \sim 1.2 \times 10^{12} S_{350\,{\rm GHz}}[{\rm mJy}]$ (e.g., Pope et al. 2006, Genzel et al. 2010, Magnelli et al. 2010), $L_{\rm FIR}[{\rm L}_\odot] \sim 2.5 \times 10^{12} S_{250\,{\rm GHz}}[{\rm mJy}]$ (e.g., Omont et al. 2001, Bertoldi et al. 2003), with significant dependencies on the actual shape of the SED. As Scoville (2012) points out, a continuum measurement around 1-mm wavelengths (observed frame) is not suited to give good estimates of $L_{\rm IR}$ given the unknown intrinsic dust SED, at least for redshifts $z < 4$. However, it gives a good estimate of the dust mass (given that the dust is optically thin in that regime and that the dust temperatures are not found to vary greatly).

The SFR can be calculated from the IR luminosities according to the relation $SFR \sim \delta_{MF} \times 1.0 \times 10^{-10}\, L_{\rm IR}$, where δ_{MF} depends on the stellar population (this assumes that the galaxy is dusty, i.e., that most of the power radiated by young stars is absorbed by dust and re-emitted in the IR; also that there is no contribution of a possible AGN to the FIR emission). For a range of metallicities, starburst ages (<100 Myr), and initial mass functions (IMFs), Omont et al. (2001) find $0.8 < \delta_{MF} < 2$. Typically $\delta_{MF} = 1.8$ is appropriate for a Salpeter IMF (e.g., Kennicutt et al. 1998a), and $\delta_{MF} \sim 1.0$ for a Chabrier IMF.

Supplemental Material

We adopted FIR luminosities for all high-redshift sources in which line emission has been detected (see the **Supplemental Table**; follow the **Supplemental Material link** from the Annual Reviews home page at **http://www.annualreviews.org**). These FIR luminosities have been derived using various methodologies and therefore should be treated with caution. Wherever available, we adopted the FIR luminosities given by individual studies but caution that not all researchers have adopted the same FIR definition, e.g., $L_{\rm FIR}$ is frequently assumed to go from 8–1,000 μm, whereas strictly speaking this is the definition of the IR luminosity (see above). For the purpose of this review we simply set $L_{\rm FIR} \sim L_{\rm IR}$. For each source in the **Supplemental Table** we have computed the FIR luminosities as follows: (*a*) if an $L_{\rm FIR}$ value is already reported in the literature (e.g., based on dust SED fitting of multiple photometric information), we use the most up-to-date estimate available; (*b*) for a number of color-selected star-forming galaxies (CSGs), only an estimate of the SFR is available—in this case, we convert it into dust luminosity using the relation $\log L_{\rm FIR} = \log SFR - \log(1.3) + 10$, where $L_{\rm FIR}$ is in solar units and SFR is in solar masses per year (see Genzel et al. 2010); or (*c*) if only a continuum estimate is available, we use the 850-μm flux to infer continuum luminosity, assuming the Arp 220 template by Silva et al. (1998) and integrating from 8 to 1,000 μm, using the equations above.

2.10. Role of the Cosmic Microwave Background

The temperature of the CMB at redshift z is given by: $T_{\rm CMB}(z) = 2.73 \times (1 + z)$. For example, at a redshift of $z = 6$, $T_{\rm CMB} = 19.1$ K, meaning it is warmer than the dust temperature of the Milky Way at present. As the dust will always be heated by photons of the CMB, the minimum dust temperature will be that of the CMB (and the kinetic temperature of the gas will equal the thermal dust temperature at high enough densities; da Cunha et al. 2013). As brightness temperature

CO AND THE COSMIC MICROWAVE BACKGROUND

It should be noted that all CO detections at very high redshift ($z > 5$), i.e., where T_{CMB} is significant compared to typical ISM temperatures, are to date from galaxies that harbor hyper-star-forming environments [e.g., the $z \sim 6$ quasars and the few known submillimeter galaxies at $z > 5$ have SFRs of $\sim$1,000 $M_\odot$ year^{-1}] with accompanying high temperatures of the ISM, ranging from 35–50 K, i.e., at least a factor two warmer than the CMB. However, it is clear that in lower temperature environments, more typical of lower luminosity star-forming galaxies, the consequences of the CMB will be significant: the lowest J lines will be faint at $z > 4$, and other cool ISM tracers may be required, such as [CII].

measurements are by definition always done with respect to the background (i.e., the CMB), it will be increasingly difficult to detect cold dust emission at high redshift.

The molecular gas is affected in two ways by the CMB: First, the higher temperature of the CMB leads to an increase of the line excitation (e.g., Obreschkow et al. 2009b, da Cunha et al. 2013). Second, the observing background against which the line is measured also increases. The relative effect of the CMB will depend on the intrinsic excitation temperature of the gas (Combes, Maoli & Omont 1999; Obreschkow et al. 2009b; da Cunha et al. 2013). For example, for molecular gas at a temperature much higher than the CMB, the relative decrease in line flux will be much lower than in a case where the molecular gas temperature is almost equal to the CMB. As a result of this, the shape of the observed CO ladder for a source with given temperature and density will also change as a function of redshift: The peak of the SED will shift to higher J values as the lower J transitions are most easily affected by the effects of the CMB (da Cunha et al. 2013). A suppressed measurement of the CO lines also implies that the conversion factor α will change as a function of CMB temperature. In the sidebar, CO and the Cosmic Microwave Background, we summarize the general impact of the CMB on CO measurements at the very highest redshifts.

3. MOLECULAR GAS AT HIGH REDSHIFT

3.1. Introduction

Historically, different groups have been focusing on different selection techniques in their searches for molecular gas in high-redshift systems. This has led to different source categories and types that we broadly follow for consistency. But it is important to point out that there is major overlap in the properties of the sources discussed. Many high-redshift quasars are found to be bright in the submillimeter regime, but they are classified as quasars rather than submillimeter galaxies (SMGs) because they were originally identified as quasars. Likewise, SMGs have typically been identified in blind submillimeter surveys of the sky, but some show signatures of a quasar. However, they are still typically referred to as SMGs because they were originally identified as such (e.g., Ivison et al. 1998, Alexander et al. 2005).

Observationally, most work has been done using the IRAM Plateau de Bure interferometer (PdBI); the Very Large Array (VLA) and its successor [the Expanded Very Large Array/JVLA]; the Owen's Valley Radio Observatory (OVRO) and its successor CARMA (Combined Array for Research in Millimeter Astronomy); the Australia Telescope Compact Array; and the IRAM 30-m, James Clerk Maxwell Telescope (JCMT), the 100-m MPIfR Effelsberg, the NRAO Green Bank Telescope (GBT), and Nobeyama Radio Observatory single-dish telescopes. These facilities have undergone a series of improvements in receiver and antenna performance, as well as correlator

SMGs: submillimeter galaxies

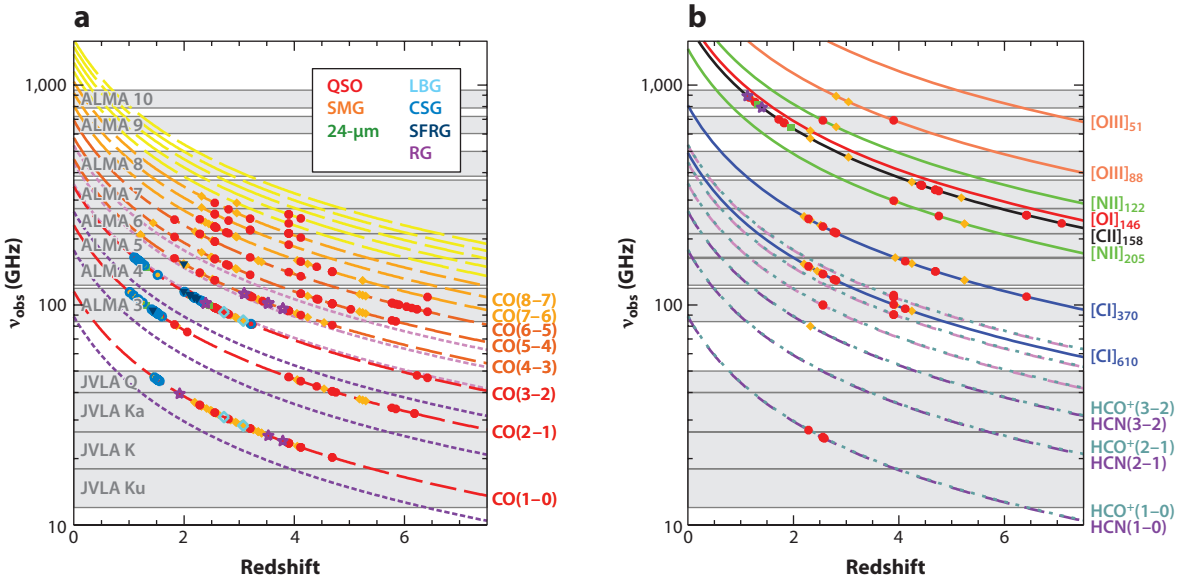

Figure 1

(*a*) Redshifted frequencies ν_{obs} of CO transitions and (*b*) other key tracers of the star-forming ISM as a function of redshift z, following $\nu_{obs} = \nu_{rest}/(1 + z)$. The shaded areas indicate the frequency bands covered by various telescopes. Highlighted are the Atacama Large Millimeter/Submillimeter Array (ALMA) frequency bands as well as the high-frequency bands of the Jansky Very Large Array (JVLA). We note that other telescopes cover these bands: The Green Bank Telescope and the Australia Telescope Compact Array cover the JVLA bands as well as an expanded range of the lowest band of ALMA, whereas the IRAM telescopes cover the lowest five ALMA bands. The colored points indicate detection of all high-redshift ($z > 1$) lines. The color of the points refer to the different source types, as explained in the legend in panel *a*. Abbreviations: 24-μm, 24-μm galaxy; CSG, color-selected star-forming galaxy; LBG, Lyman-break galaxy; QSO, quasi-stellar object; RG, radio galaxy; SFRG, star-forming radio galaxy; SMG, submillimeter galaxy.

upgrades leading to dramatic improvements in bandwidth. The improved bandwidth has been particularly important in detecting the often broad lines seen in high-redshift galaxies in the absence of precise redshifts. Also, customized receivers on single-dish telescopes have been built with very large bandwidths to blindly detect CO emission in high-redshift galaxies (e.g., Gromke et al. 2002, Harris et al. 2010). These systems have led to successful blind searches, aided in part by strong lensing of galaxies discovered in recent very wide-field *Herschel* surveys.

Figure 1 shows a plot of the frequency coverage for CO and other molecules for some available telescopes, with all actual measurements superposed. This plot emphasizes the complementarity of centimeter and millimeter telescopes to probe a broad range in molecular gas and atomic fine structure transitions, providing a detailed diagnostic suite to study the ISM in early galaxies.

3.2. Quasars

Quasars were the first targets for submillimeter continuum observations at high redshift (e.g., Omont et al. 1996). Extensive subsequent work has shown that 1/3 of optically selected quasars are detected in submillimeter continuum observations with milliJansky sensitivity, and this fraction remains roughly constant from $z \sim 1$ to 6 (e.g., Priddey et al. 2003; Beelen et al. 2006; Wang et al. 2008a,b). Searches for CO emission have systematically detected CO in submillimeter-detected quasar samples. More recently, [CII] is now being detected in quasar host galaxies (Maiolino et al.

2005; Wang et al. 2013; Willott, Omont & Bergeron 2013), including the most distant quasar known with a spectroscopic redshift at $z = 7.1$ (Venemans et al. 2012).

As we shall see below (Section 4.1), of all objects detected at high redshifts, quasar host galaxies show the highest excitation for the molecular gas (Barvainis et al. 1997, Weiß et al. 2007b, Riechers et al. 2009a) and, in the few cases where the emission could be resolved, the CO is distributed in compact (less than a few kiloparsecs) gas reservoirs (Walter et al. 2004; Riechers et al. 2008a,b, 2009b, 2011a; Carilli et al. 2002; Wang et al. 2013; Willott, Omont & Bergeron 2013). The resulting SFR surface densities can thus be very high ($\sim$1,000 $M_\odot$ year^{-1} kpc^{-2}; Walter et al. 2009a). This suggests the presence of a coeval starburst with the SMBH growth (Walter et al. 2004, Coppin et al. 2008, Wang et al. 2010). Typically the gas excitation in the quasar host galaxies can be modeled with one gas component only, and there is no evidence for extended molecular gas reservoirs around these objects (Weiß et al. 2007a,b, Riechers et al. 2009a, Riechers 2011a).

SMBH: supermassive black hole

The molecular medium in quasar host galaxies is among the best studied at high redshift, and typical molecular gas masses are a few $\times 10^{10}(\alpha/0.8)\,M_\odot$, with resulting short implied gas consumption times $\sim 10^7$ years (Section 4.5). Evidence for molecular outflows in quasars has recently been presented in two cases (Section 4.7).

3.3. Submillimeter Galaxies

SMGs were classically selected from the (sub)millimeter maps obtained at 850 μm by the Submillimetre Common-User Bolometer Array (SCUBA) at the JCMT and at 1.2 mm with the Max Planck Millimetre Bolometer Array (MAMBO) at the IRAM 30-m telescope (e.g., Smail, Ivison & Blain 1997; Hughes et al. 1998; Ivison et al. 2000, 2007; Blain et al. 2002; Dannerbauer et al. 2004). Given the sensitivities of the submillimeter cameras of typically $\geq$1 mJy, detections are by definition hyperluminous infrared galaxies (HyLIRGs), with $L_{\rm FIR} \sim 10^{13}\,L_\odot$, implying SFRs of $\sim$1,000 $M_\odot$ year^{-1}. Early searches for molecular gas emission then revealed large gas reservoirs (Frayer et al. 1998, 1999 using OVRO), and extensive campaigns at the PdBI (Neri et al. 2003; Greve et al. 2005; Tacconi et al. 2006, 2008; Engel et al. 2010; Bothwell et al. 2010, 2013) have characterized the molecular ISM in exquisite detail. In a few cases, the molecular reservoirs could be resolved (Ivison et al. 2010a, 2011; Carilli et al. 2011; Riechers et al. 2011c; Hodge et al. 2012), leading to substantial sizes of $\sim$10 kpc in a number of galaxies, although compact CO emission has been seen in a few cases as well (Carilli et al. 2002, Tacconi et al. 2008). In all cases, a common trait for SMGs is extremely high optical extinction in the main regions of star formation traced by CO and thermal dust emission. This trait is accentuated by the case of the first SMG discovered in a submillimeter deep field, HDF 850.1 (Hughes et al. 1998), which still remains unidentified in the deepest optical and near-IR images even though a precise position and redshift exist (Walter et al. 2012a).

The average excitation of the molecular gas in SMGs is less extreme than in the quasars (e.g., Weiß et al. 2007b; see Section 4.1), which may be attributed to the fact that the star formation in some SMGs proceeds on more extended scales than in the compact quasar hosts. Typical gas reservoir masses are of order a few $\times 10^{10}(\alpha/0.8)\,M_\odot$, which implies that the gas consumption times are short, of order $\sim 10^7$ years (similar to the quasars). Determining the redshift distribution for SMGs has been difficult due to the high dust obscuration in the optical (Carilli & Yun 1999, 2000; Yun & Carilli 2002; Schinnerer et al. 2008; Coppin et al. 2009; Daddi et al. 2009b; Riechers et al. 2010a, 2013; Walter et al. 2012a; Yun et al. 2012). Using optical follow-up spectroscopy of a radio-detected sample of SMGs, Chapman et al. (2003) find a median redshift of $z \sim 2.3$. However, this selection technique suffers from a low-redshift bias. More recently, observations of strongly lensed SMGs from the South Pole Telescope (SPT) millimeter survey yield a median redshift of $z \sim 3.2$, with redshifts obtained directly from molecular and FSLs. Roughly 20% of

the sources are at $z > 4.5$ (Vieira et al. 2013; Weiß et al. 2013). In this case, the lensing selection may lead to a high-redshift bias in the sample.

QSO: quasi-stellar object or quasar

FIR-bright galaxies have recently also been blindly detected by large areal mapping with *Herschel* (sometimes referred to as *Herschel*-selected galaxies or HSGs) at shorter wavelengths than in the original SCUBA/MAMBO selection (Negrello et al. 2010) and thus have a different selection function (either warmer dust temperatures or lower redshifts) than the traditional SMG selection (see also Greve et al. 2008). The HSGs are also typically a few factors lower in FIR luminosity than classical (SCUBA-selected) SMGs. These galaxies have also been shown to harbor massive reservoirs of gas (Cox et al. 2011, Riechers et al. 2011b, Combes et al. 2012, Harris et al. 2012). A significant fraction of the brightest HSGs are gravitationally lensed, as has been accentuated by the recent ALMA imaging survey of the brightest sources from the SPT millimeter survey, showing ubiquitous cases of strong lensing (Vieira et al. 2013, Hezaveh et al. 2013).

The SMG surveys and related work showed a 1,000-fold increase in the space density of ULIRGs from $z = 0$ to $z \sim 2.5$ (Hughes et al. 1998, Blain et al. 2002). Like in the case of the quasar host galaxies, it has been proposed that the SMGs pinpoint the formation of a massive galaxy at high redshift (Swinbank et al. 2006; Daddi et al. 2009a,b; Hickox et al. 2012).

Like low-z ULIRGs, QSOs and SMGs lie significantly above the so-called SFR-$M_\star$ MS (Sections 1.2 and 4.5); however, they have other properties that are often dissimilar to nearby nuclear starbursts, such as more extended gas disks in many cases (Section 4.6), cooler average dust and gas temperatures, and disk-like FSL ratios (Section 4.3). Overall, SMGs are certainly extreme starbursts, but they are likely a heterogeneous population, including compact starbursts in gas-rich major mergers, massively accreting disk galaxies, and enhanced star formation likely due to gravitational harassment in dense protocluster regions (Hayward et al. 2012, Hodge et al. 2012).

3.4. Radio Galaxies

RGs are identified in wide-field radio surveys at centimeter wavelengths, and the radio emission is related to AGN jet activity, typically on scales >10 kpc. RGs were the first very high-redshift galaxies discovered, and they remain the best beacons to massive, clustered galaxy formation at high redshift (Miley & De Breuck 2008). In the standard AGN unification model, radio galaxies (RGs) are simply radio-loud quasars seen with the jets closer to the sky plane, such that the broadline region is obscured by the accreting dusty torus (so-called type-II AGN).

RGs were also among the first high-redshift sources in which molecular gas was detected (Scoville et al. 1997; Papadopoulos et al. 2000; De Breuck, Neri & Omont 2003; De Breuck et al. 2003, 2005; Greve, Ivison & Papadopoulos 2004). Like some quasars, RGs are often bright in (sub)millimeter continuum emission and have similar gas masses to the quasars and SMGs. CO imaging of radio galaxies often reveals multiple components on tens of kiloparsec scales, likely indicating major gas-rich mergers (De Breuck, Neri & Omont 2003; De Breuck et al. 2003, 2005; Emonts et al. 2011; Ivison et al. 2012).

3.5. Color-Selected Star-Forming Galaxies

Major progress has been achieved in recent years in identifying star-forming galaxies at $z \sim 1.5$ to 3 selected via their optical or near-IR colors. These galaxies have been selected in multiple ways, although the resulting samples show substantial overlap, depending on redshift.

One strategy involves near-IR BzK color selection, which selects galaxies by their 4,000-Å break (Daddi et al. 2004). Daddi et al. (2008) demonstrated that this color selection successfully selects gas-rich, active star-forming galaxies at $z \sim 1$ to 2. Daddi et al. (2010a) then used this selection technique to target 6 sBzK galaxies with stellar masses $>10^{10}\,M_\odot$, that were also detected in the

radio (but not the submillimeter) band. All galaxies were detected in CO emission, implying large reservoirs of molecular gas in galaxies that are not forming stars at the extreme rates seen in quasars and SMGs (Daddi et al. 2008, 2010a).

CSG: color-selected star-forming galaxy

A second technique involves rest-frame UV color selection, known as the BM/BX selection (Steidel et al. 2004). Tacconi et al. (2010, 2013) used this technique to identify samples of CSGs at $z \sim 1$ to 3 for CO observations. They also detected large gas reservoirs in the majority of their sample.

A third color-selected sample is the star-forming radio-selected galaxies (SFRGs). These objects are rest-frame UV-color selected to be $z > 1$ galaxies, and then further identified as 20-cm radio continuum sources of ~50 to 100 μJy but are not detected in the submillimeter band. Chapman et al. (2008) and Casey et al. (2011) detected large molecular gas reservoirs in about half of their sample [which includes a few BzK galaxies studied by Daddi et al. (2008)].

It has been found that there is significant overlap in samples selected via the various color-selection techniques (Grazian et al. 2007). In the following, we use the term CSGs (color-selected galaxies) for the BzK and BM/BX samples. The term "normal star-forming galaxies" at high redshift is often used for these CSGs. The intrinsic SFRs are between 10 to 100 $M_\odot$ year^{-1} (Daddi et al. 2010, Tacconi et al. 2010), with stellar masses $\sim 10^{10}$ to $\sim 10^{11}$ $M_\odot$. These galaxies correspond to the galaxies that dominate the cosmic star-formation rate density during the epoch of galaxy assembly (see Section 1.2). The samples studied in CO emission to date are typically at the higher mass/luminosity end of the distribution. However, they follow a similar CO-to-FIR luminosity ratio as low-redshift spirals (Section 4.5), and they lie on the specific SFR MS (as described in Section 1.2).

Extensive studies of CSGs have shown that they are extended on 10-kpc scales in gas and stars, appearing as clumpy, turbulent, but clearly rotating disks (Daddi et al. 2010a; Tacconi et al. 2010, 2013) (Section 4.6). Their gas excitation is lower than that found in quasar hosts or SMGs (Dannerbauer et al. 2009, Aravena et al. 2010) (Section 4.1).

3.6. MIPS/24-Micron-Selected Galaxies

Spitzer 24-μm-selected galaxies at $z \sim 2$ have been studied in molecular gas emission by Yan et al. (2010). At the typical redshift of the sample, the 8-μm PAH feature, a tracer for star formation, is shifted into the 24-μm band. Even though these sources are bright at 24 μm and are thus forming stars at high rates, they are mostly undetected at 1.2 mm using MAMBO. Still they often have CO luminosities comparable to SMGs. These sources often show evidence for mergers, and some host dust-obscured AGNs (Yan et al. 2010; see also Iono et al. 2006a). This population is likely a hodgepodge of sources, including type 2 quasars, SMGs, and hot dust sources.

3.7. Lyman-Break Galaxies, Lyα Emitters, and Lyα Blobs

Progress has been made on detecting CO emission from strongly lensed Lyman-break galaxies (LBGs), corresponding to CSGs at $z \geq 3$. Baker et al. (2004) and Coppin et al. (2007) detected CO(3–2) emission in two LBGs at $z \sim 3$ that are lensed by a factor of 30. Riechers et al. (2010b) detected CO(1–0) emission in these two systems, finding relatively low excitation, and gas masses $\sim 4 \times 10^9 (\alpha/4)\, M_\odot$ after correcting for lensing. The first detection of a more massive, unlensed LBG at $z = 3.2$ has been reported by Magdis et al. (2012a).

CO emission has also been searched for in high-z Lyα-emitting galaxies (LAE) and Lyα-emitting blobs. Observations of one strongly lensed LAE at $z = 6.5$ resulted in a stringent upper limit to the gas mass of $4.9 \times 10^9 (\alpha/0.8)\, M_\odot$ (Wagg, Kanekar & Carilli 2009). Lyα blobs are typically large (tens of kiloparsecs), and their exact origin remains uncertain, possibly being the

remnants of radio-mode feedback as seen in the Lyα halos around powerful RGs (Miley & De Breuck 2008) or even representing cooling gas in dense filaments from the IGM (Dekel et al. 2009). Searches for CO emission have led to nondetections at $z \sim 3$ (Yang et al. 2012) and $z = 6.6$ (Wagg & Kanekar 2012), with gas mass limits on the order of $10^{10}(\alpha/0.8)\,M_\odot$.

The advent of ALMA early science has opened the very real and exciting prospect of detecting [CII] 158-μm emission from typical LBGs and LAEs at very high ($z > 6$) redshift. Even with limited capabilities (one-third of the final array and short integrations), ALMA is now systematically detecting star-forming galaxies in the distant Universe. In their study of an SMG-quasar host galaxy pair at $z = 4.7$, Wagg et al. (2012) and Carilli et al. (2013) detected [CII] emission from two typical LAEs in this merging group of galaxies. Likewise, in their study of the $z = 5.3$ protocluster, Aztec 3 in the Cosmos field, Riechers et al. (2013) detected three LBGs, plus two previously unidentified galaxies, in [CII] emission. Note that in most of these cases, the dust continuum emission has not been detected.

3.8. Table of All High-z Interstellar Medium Detections

Supplemental Material

We have compiled a table (see **Supplemental Table**) of all high-redshift ($z > 1$) detections of the molecular ISM. Most of the detections are of the CO line, but there are also detections of higher-density molecular gas tracers (observed only in quasar hosts), such as CN, HCN, HNC and HCO^+, and the CO isotopomer ^{13}CO. For many sources, multiple J CO detections are available. The table also includes measurements of the atomic FSLs, most notably [CII], but also [NII], [OIII], and [CI]. For convenience, we have also added the FIR luminosities of these sources, derived through heterogeneous ways (see footnotes in the **Supplemental Table**), following the equations in Section 2.9.

In total, the cool ISM has now been detected in close to 200 sources at $z > 1$. Below, we summarize the basic observational parameter space (CO line luminosities and excitation, full width half maximum, submillimeter continuum emission, and redshift distribution) through some key plots to interpret this rich set of observational data. In all plots, we use the same color coding for different groups of galaxies (as defined in Section 3). These are the QSOs (quasars), SMGs [including one extremely red object and HSGs], CSGs (selected through BzK and BM/BX selection techniques), RGs, SFRGs, *Spitzer* 24-μm-selected galaxies, and LBGs. The classification is therefore entirely based on the selection technique, not on the actual physical properties.

3.9. Historical Note

Since the earliest detection of molecular gas in the $z = 2.28$ quasar IRAS F 10214 by Brown & Vanden Bout (1991) and Solomon, Downes & Radford (1992), there has been a steady increase in the number of line detections at high redshift. This is illustrated in **Figure 2*a***, where the cumulative number of detections is presented as a function of discovery year. From this plot, it is clear that over the first decade or so, the detections were dominated by quasars, with SMGs picking up in larger numbers around the turn of the millennium. Only recently have CSGs been added to the list in significant numbers. **Figure 2*b*** shows the redshift distribution of all galaxies with a line detection.

4. OBSERVATIONAL DIAGNOSIS OF THE COOL ISM IN DISTANT GALAXIES

4.1. Molecular Gas Excitation

As noted in Section 2.6, the excitation of molecular gas in high-redshift galaxies provides important information regarding the average physical properties of the gas, in particular its temperature and

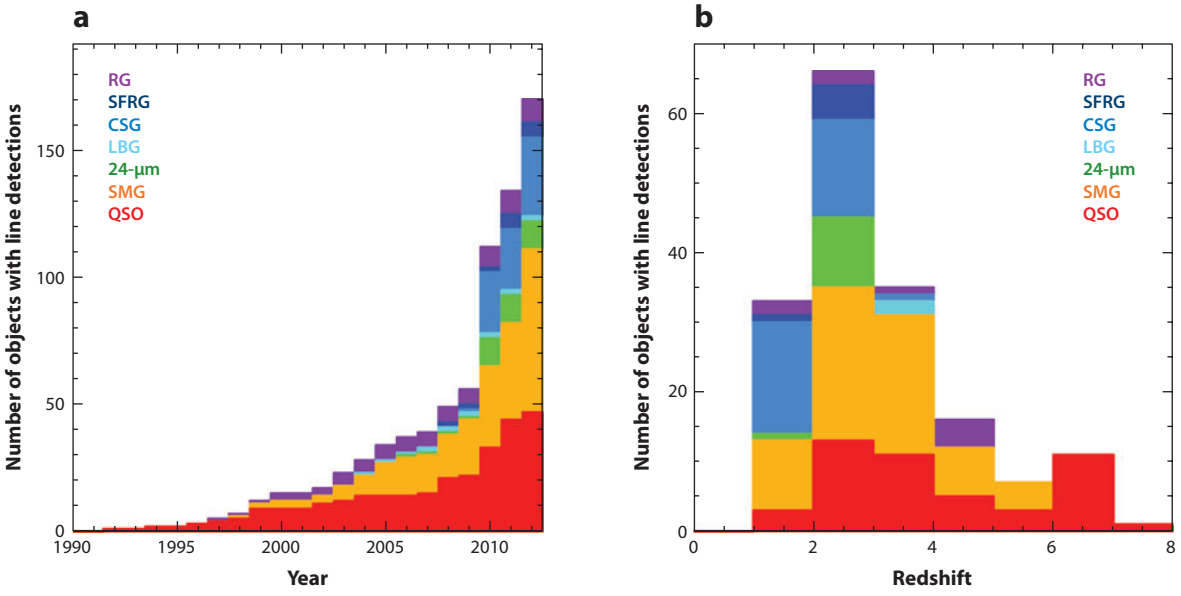

Figure 2

(*a*) Discovery history of high-redshift ($z > 1$) line detections. The cumulative number of detections is shown, and the different colors indicate the different galaxies populations. Historically, QSOs (quasi-stellar objects; Section 3.2), submillimeter galaxies (SMGs; Section 3.3), and radio galaxies (RGs; Section 3.4) have been the focus of most studies. In recent years, these have been complemented by observations of color-selected star-forming galaxies (CSGs; Section 3.5). To date, close to 200 galaxies have been detected in line emission at $z > 1$. (*b*) Redshift distribution of all sources for all $z > 1$ line detections. The highest-redshift sources $z > 5$ detected are the QSOs, with a growing contribution from SMGs. Abbreviations: 24-μm, 24-μm galaxy; LBG, Lyman-break galaxy; SFRG, star-forming radio galaxy.

density. This is illustrated in **Figure 3**, where the expected CO excitation is shown as a function of density and temperature. One important caveat is that typically only galaxy-integrated line fluxes can be measured at high redshift. These measurements are then fed into LVG (Section 2.6.1) or PDR/XDR (Section 2.6.2) models that assume that the line emission is emerging from the same cloud/volume (i.e., that they share the same physical conditions). The validity of this assumption is questionable, as it is known that the different rotational transitions have different critical densities: the higher-*J* transitions need much higher densities than the low-*J* ones to be excited. This situation is further complicated if unresolved measurements of high-density tracers (e.g., HCN, HCO^+) are added to the single component models. Another caveat is that the molecular gas excitation measurements in high-redshift galaxies are typically restricted to the mid-*J* levels of CO emission.

With these caveats in mind, there are a number of important results emerging from high-redshift CO excitation analyses. The main result is that the different source populations at high redshift show distinctly different excitation (see the compilation of all high-redshift CO excitation in **Figure 4**). The CO excitation of quasar host galaxies can in essentially all cases be modeled by a simple model with one temperature and density out to the currently measured highest *J* CO transition with a typical gas density of $\log(n_{H_2})[\mathrm{cm}^{-3}]) = 3.6–4.3$, and temperatures of $T_{kin} = 40–60$ K. A prominent example is the highly excited quasar host APM 08279+5255 (Weiß et al. 2007a). Measurements of the CO ground transition in a number of quasar host galaxies have shown that the measured CO(1–0) flux is what was expected based on a single-component extrapolation from higher *J* CO transitions, i.e., there is no excess of CO(1–0) emission in these

LVG: large velocity gradient

PDR: photon-dominated region or photodissociation region

XDR: X-ray-dominated region

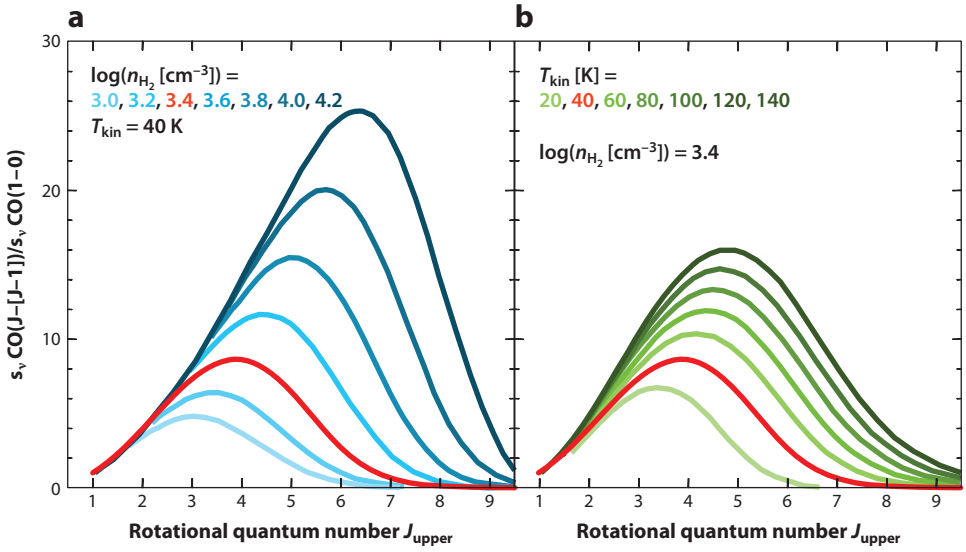

Figure 3

This figure illustrates how the measured CO excitation ladder changes as a function of temperature and density (adapted from Weiß et al. 2007b). (*a*) The effect of changing density at fixed temperature (T_{kin} = 40 K). (*b*) The effect of varying kinetic temperatures for a fixed density [log(n_{H_2}) = 3.4]. Both panels have been normalized to the CO(1–0) transition. High CO excitation is achieved through a combination of high kinetic temperature and high density. Given the typically sparsely sampled CO excitation and large error bars in high-redshift observations, this degeneracy cannot be easily broken observationally. Additional information, such as independent estimates of the kinetic temperature through [CI] or dust measurements, can help to break this degeneracy. Note that increased temperatures lead to a broader CO excitation ladder, as more and more high-*J* levels are populated following the Boltzmann distribution.

sources (Riechers et al. 2006a, 2011a). One interpretation of this finding is that the molecular gas emission comes from a very compact region in the center of the quasar host, which is confirmed by the few (barely) resolved measurements of quasar hosts (Section 4.6). It should be noted, though, that there is recent evidence that an additional high-excitation component, likely related to the AGN itself, is needed to explain the elevated high-*J* line fluxes in some sources, e.g., PSS 2322+1944 (A. Weiß and colleagues, private communication) and J 1148+5251 (D. A. Riechers and colleagues, private communication).

The SMGs, however, show (*a*) less excited molecular gas, and (*b*) excess emission in the CO(1–0) ground transition. This is again illustrated in **Figure 4**, where the orange symbols of the SMGs are on average at lower fluxes compared to the quasars (*red dots*). On average, the typical density of SMGs is log(n_{H_2})[cm^{-3}]) = 2.7–3.5, and temperatures are in the range of T_{kin} = 30–50 K. Observations in the CO(1–0) line of a few SMGs have furthermore demonstrated that an additional cold component is needed to explain the observed excitation (Ivison et al. 2011, Carilli et al. 2011, Riechers et al. 2011c, Bothwell et al. 2013). This implies that the total gas mass of the SMGs is underestimated if mid-*J* CO transitions are used to calculate masses assuming constant brightness temperature (see Section 4.2). A few SMGs have been resolved spatially and show more extended emission in the ground transition than in higher transitions (Ivison et al. 2011; although cf. Hodge et al. 2012).

Up to the mid-*J* measurements available for high-redshift sources, the CO excitation of the SMGs and QSOs roughly follows those of the centers of nearby starburst galaxies (e.g., M82: Mao

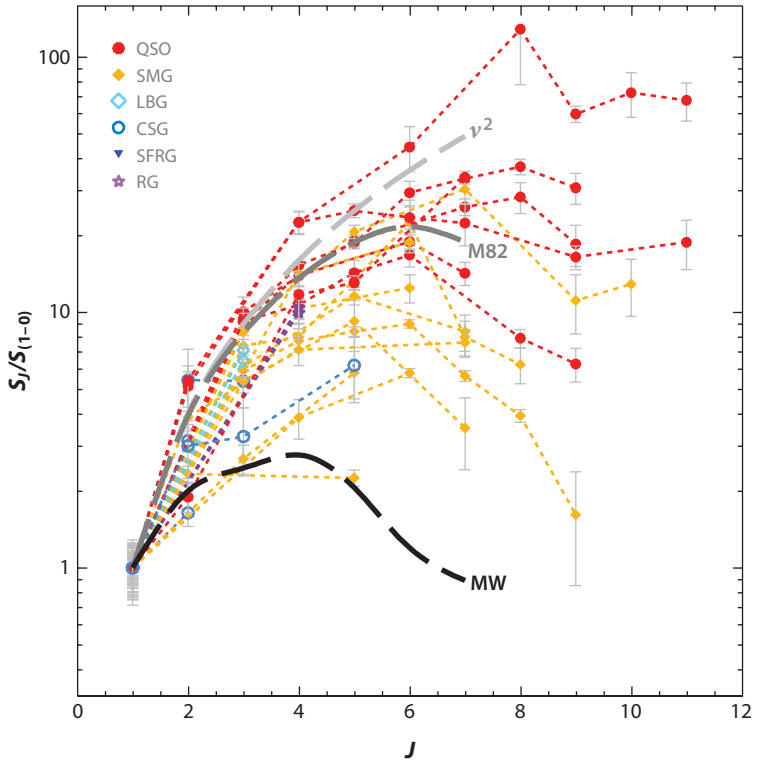

Figure 4

CO excitation ladder of all sources where the CO(1–0) line has been measured. The CO line flux is shown as a function of rotational quantum number, and the colors indicate the different source types. Measurements for individual sources are connected by a dashed line. The line fluxes have been normalized to the CO(1–0) line. The quasi-stellar objects (QSOs) are the most excited systems found, with an average peak of the CO ladder at around $J \sim 6$. This is consistent with the high star-formation rate and compact emission regions in their host galaxies. The submillimeter galaxies (SMGs) are slightly less excited on average, and their CO excitation ladders peak around $J \sim 5$. The dashed thick lines indicate template CO excitation ladders for the Milky Way (MW; *black*) and M82 (*gray*). The few multitransition measurements of color-selected galaxies (CSGs) show CO excitation lower than SMGs on average, but higher than the Milky Way (E. Daddi, private communication). The dashed dark gray line shows constant brightness temperature on the Rayleigh-Jeans scale, i.e., $S \sim \nu^2$ (note that this approximation is not valid for high J). Abbreviations: LBG, Lyman-break galaxy; RG, radio galaxy.

et al. 2000, Ward et al. 2003, and see *dashed line* in **Figure 4**; NGC 253: Bradford et al. 2003, Bayet et al. 2004; and Henize 2–10: Bayet et al. 2004). It should be noted that the excitation in Galactic molecular cloud cores can be equally high (e.g., Habart et al. 2010, van Kempen et al. 2010, Leurini et al. 2013, Manoj et al. 2013). However, in Galactic clouds such very high excitation is only seen on parsec scales in cloud cores, whereas in nearby starburst nuclei high excitation is seen on scales on the order of 100 pc, and for high-redshift galaxies the scale can extend to a few kiloparsecs.

As stated in Section 3, the separation between SMGs and QSO host galaxies is largely due to historical selection effects, and there are sources that fulfill both definitions. The different excitation conditions in the two groups, however, can be used to make the argument that, broadly speaking, gas-rich quasars and SMGs represent different stages of galaxy evolution, with the

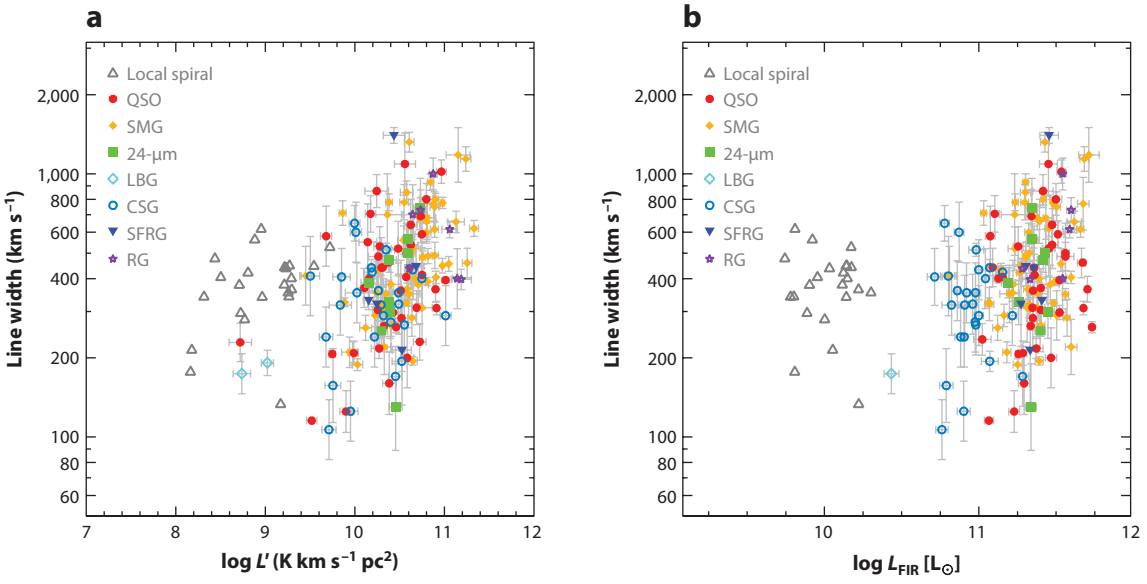

Figure 5

The CO line width (FWHM) (*a*) versus CO line luminosity and (*b*) versus the far-IR luminosity. Note that the color-selected star-forming galaxies (CSGs) show systematically lower line widths for a given CO line luminosity than the hyperstarburst quasar hosts and submillimeter galaxies (SMGs) [we have corrected the $v_{rot,max}$ values from Tacconi et al. (2010) to FWHM values]. The gray data points show local spiral galaxies, with stellar masses $>10^{10}$ $M_\odot$ from the HERACLES/THINGS surveys (Walter et al. 2008, Leroy et al. 2009). The local FWHM values are corrected for inclination, the high-z values are not (in the absence of unknown inclinations). Abbreviations: 24-μm, 24-μm galaxy; LBG, Lyman-break galaxy; QSO, quasi-stellar object; RG, radio galaxy; SFRG, star-forming radio galaxy.

quasars being more compact and harboring more highly excited gas than the SMGs. In a simplistic picture, the quasars could be the result of a merger, in which the molecular gas concentrates in the center of the potential well, whereas the SMGs would then constitute merging systems that have not fully coalesced. The latter is supported by the fact that high-resolution observations of many SMGs show multiple emission components (e.g., Engel et al. 2010, Tacconi et al. 2010). SMGs and quasars also show similar clustering properties (Hickox et al. 2012).

To date, only a few excitation measurements exist for the CSGs (Dannerbauer et al. 2009, Aravena et al. 2010; also E. Daddi and colleagues, private communication). The best studied case is that of BzK-21000 at $z = 1.5$. Early work by Dannerbauer et al. (2009) showed that the $J = 3$ emission is significantly subthermally excited, resembling that of the Milky Way. The latest measurements including CO(5–4) show an excitation higher than that seen for the Milky Way, but lower than typical SMGs and quasars (**Figure 4**). CSGs have lower SFRs than those found in the FIR-luminous quasar hosts and SMGs and have large (~10 kpc) sizes. The combination of these characteristics apparently leads to a less extreme gas excitation than that found in the hyperstarburst galaxies at high redshift. Further observations of the CO excitation are clearly required in these systems.

Bothwell et al. (2013) suggest that there is a correlation between CO luminosity and line width in high-redshift starbursts, likely relating to baryon-dominated gas dynamics within the regions probed. In **Figure 5**, we plot the CO line widths (FWHM) versus CO luminosity for a broader range of CO-detected distant galaxy types. Considering only the hyperstarbursts (SMGs and

quasar hosts), both occupy similar regions in this diagram, and there is no significant correlation between CO luminosity and line width. However, the CSGs clearly segregate to smaller line widths relative to SMGs, by about a factor of two and, while the scatter is large, the median CO luminosity for CSGs is smaller by a similar factor.

4.2. CO Luminosity–to–Total Molecular Gas Mass Conversion

Until a few years ago, the standard practice for high-redshift galaxies was to use the starburst conversion factor to derive gas masses. This practice was justified in part because of the extreme luminosities, the high inferred gas densities based on CO excitation, and in some cases the direct observation of compact star-forming regions (scales ~2–4 kpc) (Carilli et al. 2002; Momjian et al. 2007; Tacconi et al. 2008; Walter et al. 2009a; Ivison et al. 2010a, 2012). Also, in some cases it appeared that, like nearby nuclear starbursts, the gas mass exceeded the dynamical mass when a Milky Way conversion factor was used (Solomon et al. 1997; Walter et al. 2004; Riechers et al. 2009b; Tacconi et al. 2008; Carilli et al. 2011).

As other populations of galaxies are now being detected in CO emission at high redshift, such as CSGs (Section 3.5), the question of the conversion factor has become paramount. The past few years have seen a few attempts at the first direct measurements of the CO luminosity–to–gas mass conversion factor.

A minimum α can be derived assuming optically thin emission and adopting a Boltzmann distribution for the population of states. In this case, the CO(1–0) luminosity, $L_{CO(1-0)}$, simply counts the number of molecules in the $J = 1$ state via $N_{J=1} = L_{CO(1-0)}/(A \times h\nu)$, where A is the Einstein A coefficient (6×10^{-8} s^{-1}), and $\nu = 115$ GHz. The total number of CO molecules is then determined by the partition function, i.e., the relative fraction in the $J = 1$ state, which we designate as f. For example at $T = 10$, 20, and 40 K, $f = 0.47$, 0.31, and 0.19, respectively. One can then perform a conversion to the total number of H_2 molecules assuming a CO/H_2 abundance ratio, which for Galactic GMCs is 10^{-4}. Multiplying by the mass of an H_2 molecule, and including a factor of 1.36 for the helium abundance, leads to the total gas mass. Converting to the relevant units leads to $\alpha = (0.09/f)\,M_\odot$ [K km s^{-1} pc^2]$^{-1}$, at $z = 0$. [Including a correction for the relative contribution of the CMB increases these values by about 35% at $z = 2.5$ (Ivison et al. 2011).]

Tacconi et al. (2008, 2010) use spatially resolved spectral imaging to derive either virial or Keplerian rotational masses for a sample of SMGs and CSGs. Galaxy sizes are estimated from the CO imaging and/or optical or near-IR imaging (see also Neri et al. 2003, Thomson et al. 2012). Tacconi et al. compare the dynamical masses with the sum of the gas mass (modulo α) and stellar mass (derived from near-IR photometry), including a small correction (10% to 20%) for dark matter. They conclude that for the SMGs, the value of α is most likely close to the starburst value ($\alpha \sim 1$), whereas for the CSG a value $\alpha \sim 4.8$ is favored.

Daddi et al. (2010b) have performed a similar analysis on CSGs, based on (marginally) spatially resolved imaging with the PdBI of CO(2–1) emission of a sample of three $z \sim 1.5$ sBzK galaxies. Their dynamical analysis is guided by numerical simulations of clumpy, turbulent disks to allow for significant noncircular motions (Bournaud, Elmegren & Martig 2009). They find that the measurements are consistent with $\alpha_{CO} = 3.6 \pm 0.8\,M_\odot$ (K km s^{-1} pc^2)$^{-1}$.

The best rotational dynamical analysis of an SMG to date is the JVLA observation of GN20 at $z = 4.0$ by Hodge et al. (2012) (see Section 4.6). They show that the CO(2–1) emission is well characterized by a rotating disk of radius 7 kpc with a large rotation velocity of 575 $\pm$ 100 km s^{-1} and an internal velocity dispersion of 100 km s^{-1}. They derive a dynamical mass of $5.4 \pm 2.4 \times 10^{11}\,M_\odot$. Subtracting the stellar mass, including a 15% dark matter contribution, leads to $\alpha \sim 1\,M_\odot$ (K km s^{-1} pc^2)$^{-1}$.

The main uncertainties in the dynamical analysis are the current crude estimates of the dynamical masses based on marginally resolved imaging data, and the standard pitfalls in estimating the stellar masses based on SED fitting, in particular for starburst-type systems (Ivison et al. 2011).

Magdis et al. (2011) use a metallicity-dependent dust-to-gas ratio approach to estimate α_{CO}. They analyze two galaxies in the GOODS-N deep field with excellent rest-frame IR SEDs: one SMG (GN20) and one CSG (BzK-21000). From these, and using the Draine & Li (2007) dust models, they derive a dust mass for each source. Metallicities are derived from the stellar mass–metallicity relation for the CSG (Erb et al. 2006) and from a starburst model for GN20. They then use the Solomon et al. (1997) metallicity-dependent dust-to-gas relation to obtain estimates of the gas masses, $9 \times 10^{10}\,M_\odot$ for the CSG and $1.5 \times 10^{11}\,M_\odot$ for the SMG. Comparing these masses to the CO(1–0) luminosities leads to $\alpha \leq 1.0$ for the SMG, whereas for the CSG they find $\alpha \sim 4$, consistent with earlier estimates. These results have been generalized in the more comprehensive study by Magdis et al. (2012b).

Ivison et al. (2011) take two different approaches to deriving molecular gas masses and, hence, infer α in SMGs. First, they propose a model in which some fraction of the CO emission occurs at the Eddington limit in dense star-forming regions (a maximal starburst), i.e., a self-gravitating disk supported by starburst-driven radiation pressure on the dust grains (Thompson, Quataert & Murray 2005; Thompson 2009; Krumholz & Thompson 2012). Thompson (2009) derives a maximum SFE of $SFE_{\rm max} \equiv L_{\rm IR}/M_{\rm gas} < 500\,L_\odot\,M_\odot^{-1}$, and an areal SFR density of $1{,}000\,M_\odot\,{\rm year}^{-1}\,{\rm kpc}^{-2}$. This maximum surface density is seen to hold on scales from star-forming cloud cores in GMCs ($\sim$1 pc) to the nuclear starburst regions of low-z ULIRGs.

Ivison et al. then make a correction to the total gas for the fraction of cold, quiescent gas not involved in active star formation based on the CO excitation. Under these assumptions, the molecular gas mass can be estimated from the IR luminosity. For 4 of their 5 SMGs, the values are between $\alpha = 0.4$ and 0.7, whereas for the last source the value is 3.7. This latter source also has by far the lowest CO excitation.

Second, Ivison et al. (2011) use radiative transfer modeling to derive physical conditions within the clouds and infer gas masses in a manner analogous to the low-redshift ULIRG analysis of Downes & Solomon (1998). Unfortunately, LVG models have a fundamental degeneracy between density, temperature, and nonvirial gas kinematics when using just CO excitation (Section 2.6.1). They find the CO SEDs are consistent with either $\alpha \sim 4.5$ in cold, dense gas with large nonvirial motions or $\alpha \sim 1$ in warm, more diffuse gas closer to virial dynamics.

Genzel et al. (2012) consider the effect of metallicity on the conversion factor α in a sample of CSG at $z \sim 1$ to 2. They have obtained estimates for the metallicities from optical [NII]/Hα measurements. They find that galaxies having similar sizes, SFRs, and dynamical masses, but different metallicities (and stellar masses; Erb et al. 2006) show very different SFEs, with the CO–to–FIR luminosity ratio decreasing dramatically with decreasing metallicity, at fixed FIR luminosity. If α is the same in each system, then this would imply a much shorter gas consumption timescale (gas mass/SFR) in low-metallicity galaxies versus high-metallicity galaxies.

Alternatively, Genzel et al. (2012) propose adopting a standard SFE (SFE = SFR/gas mass) relating gas mass to SFR (Section 4.5). In this case, the decrease in CO luminosity is not due to a lower gas mass but rather an increase in α at low metallicity. Such a trend is expected and observed at low metallicity in nearby galaxies (Section 2.5), because dust shielding becomes less efficient, and CO in molecular cloud envelopes is photodissociated deeper into the cloud (Leroy et al. 2011; Schruba et al. 2012; Bolatto, Leroy & Wolfire 2013). Genzel et al. (2012) and Stacey et al. (1991) derive the empirical relationship $\log(\alpha_{CO}) = 12\text{–}1.3 \times [12 + \log({\rm O/H})]$. The implication is that stars can form in CO-poor molecular gas, and that the expected CO

CO CONVERSION FACTOR

Many conclusions in astronomy are based not on a single, absolutely compelling direct measurement, but on a series of measurements and modeling as well as on a consistency of arguments from which the weight of evidence leads to a "concordance model." This approach applies to the CO-to-gas mass conversion factor in distant galaxies. The current measurements of α_{CO} are principally based on dynamical imaging and modeling, dust-to-gas measurements, radiative transfer modeling, and most recently, on SFEs. These measurements suggest a nuclear starburst value $\sim 0.8\,M_\odot\,(K\,km\,s^{-1}\,pc^2)^{-1}$ for SMGs and quasar hosts, and a Milky Way GMC value of $\alpha_{CO} \sim 4\,M_\odot\,(K\,km\,s^{-1}\,pc^2)^{-1}$ in CSG, with a likely further increase in low-metallicity galaxies. These values are consistent with the generally extended, clumpy disk-like CO distribution, lower CO excitation, and Milky Way CO/FIR (FIR derived from SFR) ratios in CSG, compared to the often (although not exclusively) more compact, merger-like morphologies, higher excitation, and starburst CO/FIR ratios in SMGs and quasars.

luminosities of low-metallicity galaxies at high redshift are lower than previously predicted based on standard α values (Papadopoulos & Pelupessy 2010, Glover & Clark 2012).

Magnelli et al. (2012) perform a similar analysis of the conversion factor based on dust-to-gas ratios for a mixed sample of SMGs and CSGs at $z = 1$ to 4. They adopt a similar dust mass calculation based on the FIR luminosity and a metallicity-dependent dust-to-gas ratio as in Genzel et al. (2012). Their results are consistent with a low value of α for starbursts, and a factor five higher value for CSGs. They also find a trend of decreasing α with increasing dust temperature, and though the trend may be continuous, they recommend that for dust temperatures <30 K, a Milky Way conversion factor is appropriate, whereas for higher dust temperatures the starburst value should be used, at least for solar metallicity systems. The sidebar, CO Conversion Factor, describes our current knowledge of α_{CO} in high-redshift galaxies.

4.3. Atomic Fine Structure Lines

In addition to spectral lines emitted by molecules there are a number of atomic FSLs that provide key diagnostics of the conditions of the ISM. We discuss the most important ones in the following sections.

4.3.1. Atomic carbon: [CI]. In a recent study, Walter et al. (2011) summarize the [CI] observations of 13 high-redshift galaxies [this compilation included work by Barvainis et al. (1997), Weiß et al. (2003, 2005a), Pety et al. (2004), Wagg et al. (2006), Ao et al. (2008), Riechers et al. (2009a), Casey et al. (2009), Lestrade et al. (2010), Danielson et al. (2011)]. These systems studied in [CI] are among the brightest emitters both in the submillimeter regime and in CO line emission, and many of them are lensed. The main finding was that the [CI] properties of high-redshift systems do not differ significantly compared to those found in low-redshift systems, including the Milky Way. In addition, there are no major differences in [CI] properties between the QSO- and SMG-selected samples. The $L'_{CI(1-0)}/L'_{CO}$ ratios (0.29 ± 0.12) are similar to low-z galaxies (e.g., 0.2 ± 0.2; Gerin & Phillips 2000).

As argued in Section 2.8, measurements of both [CI] lines can constrain gas excitation temperatures of the molecular gas, independent of radiative transfer modeling. For the available sample, a carbon excitation temperature of 29.1 ± 6.3 K was derived (Walter et al. 2011). This temperature is lower than that typically found in star-forming regions in the local Universe despite the fact

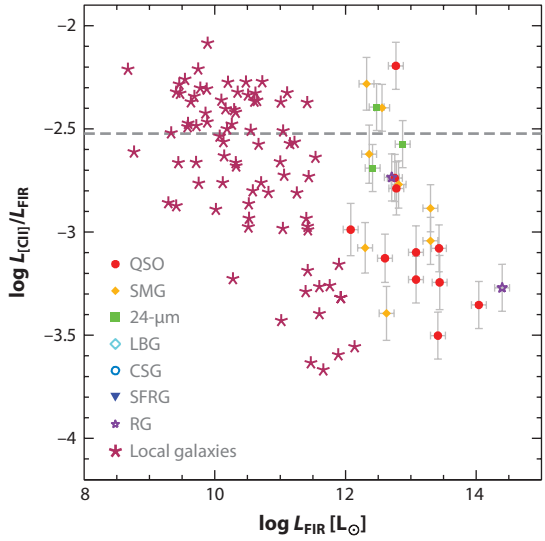

Figure 6

Supplemental Material

The ratio $L_{[CII]}/L_{FIR}$ as a function of L_{FIR} (data can be found in the **Supplemental Table**). The dashed horizontal line indicates a value of 3×10^{-3}. This value is approximately the Milky Way value.

that the sample galaxies have SFR surface densities on kiloparsec scales of hundreds of solar mass per year per kiloparsec squared. However, the temperatures are roughly consistent with published dust temperatures of high-redshift star-forming galaxies (Beelen et al. 2006; Kovács et al. 2006, 2010; Harris et al. 2012). Low carbon excitation as well as low dust temperatures could indicate that the measurements include a significant amount of gas/dust unaffected by star formation.

The [CI] abundances in the current high-z galaxy sample of $X[CI]/X[H_2] = (8.4 \pm 3.5) \times 10^{-5}$ are comparable, within the uncertainties, to those found in local star-forming environments (Walter et al. 2011). The [CI] lines are a negligible coolant [average $L_{CI}/L_{FIR} = (7.7 \pm 4.6) \times 10^{-6}$]. There is tentative evidence that this ratio may be elevated in the SMGs by a factor of a few compared to the QSOs (Walter et al. 2011).

4.3.2. Ionized carbon: [CII]. The [CII] 158-μm line is rapidly becoming a workhorse line for the study of the cool atomic gas in distant galaxies. The number of [CII] detections at high redshift has increased substantially in the past few years using the Caltech Submillimeter Observatory, PdBI, Atacama Pathfinder EXperiment, and the Submillimeter Array (Iono et al. 2006b, Maiolino et al. 2009, Hailey-Dunsheath et al. 2010, Stacey et al. 2010, Wagg et al. 2010, Cox et al. 2011, De Breuck et al. 2011, Walter et al. 2012a, Gallerani et al. 2012), as well as a few detections in strongly lensed galaxies with *Herschel* (Ivison et al. 2010b, Valtchanov et al. 2011). To date, there have been about two dozen [CII] detections from galaxies at $z > 1$, including several at $z > 6$ (see Section 5.2).

Figure 6 shows a broad scatter in the [CII]/FIR ratio at $z > 1$. Note that the high-z galaxy samples all have FIR luminosities $\geq 10^{12}$ $L_\odot$. However, there is a trend for luminous AGN to have the lowest ratios and for star-formation-dominated galaxies (e.g., SMGs) to have ratios closer to that of the Milky Way (e.g., Stacey et al. 2010).

Stacey et al. (2010) use the CO, FIR, and [CII] emission to argue that the [CII] emission is dominated by PDRs in the star-forming galaxies. From these observations, they derive the physical conditions in the PDRs in high-redshift galaxies, finding gas densities of order a few

$\times 10^4$ cm^{-3}, and the strength of the FUV radiation field: $G \sim 10^3 \times 1.6 \times 10^{-3}$ erg cm^{-2} s^{-1}, where 1.6×10^{-3} erg cm^{-2} s^{-1} is the local Galactic interstellar radiation field (ISRF, or Habing field). They find a further factor 10 higher G for the AGN-dominated systems. Their modeling also implies that the scale of the PDRs is greater than a few kiloparsecs, much larger than for GMCs or nuclear starburst galaxies at low redshift. The fraction of molecular gas mass associated with PDRs is between 20% and 100% in their sample.

Swinbank et al. (2012a) detect likely [CII] 158-μm emission in two SMGs using ALMA, from which they derive redshifts of $z \sim 4.4$ and 4.2. They suggest that the bright-end of the [CII] luminosity function increases dramatically with redshift, with close to a thousand-fold increase in the number density of galaxies with L[CII] $>10^9$ L$_\odot$ from $z = 0$ to 4. We discuss [CII] detections in a number of $z > 6$ galaxies in Section 5.2. Early ALMA results on [CII] imaging at high redshift are changing the field. Imaging of the well-known quasar-SMG pair, BRI1202-0725 at $z = 4.7$, has revealed a major gas-rich merger, including a rotating disk for the SMG, a tidal bridge between the quasar and the SMG, possible quasar outflow, and [CII] emission from two LAEs in the field (Wagg et al. 2012, Carilli et al. 2013). Similarly, imaging of the $z = 5.3$ protocluster, Aztec 3 in the Cosmos field, detects at least five galaxies in a 1-arcmin field in [CII] emission, including two dusty starbursts and an interacting group of three LBGs (D. A. Riechers, private communication). These observations demonstrate the ease with which ALMA can image the atomic gas in distant galaxies using the [CII] in normal star-forming galaxies at high redshift. We note that in many of these sources the dust continuum was not detected in the submillimeter band, and yet the [CII] remained strong. In these cases, the [CII]/FIR luminosity ratio is at least that of the Milky Way, and perhaps higher.

4.3.3. Other fine structure lines. There have been only a few detections of FSLs other than [CII] at high redshift to date, mostly in strongly lensed systems using principally the PdBI and *Herschel*. We summarize some of the physical diagnostics that have been achieved with such observations.

In their *Herschel* study of SMGs at $z \sim 1.4$, Coppin et al. (2012) find that the [OI] 63-μm/FIR ratio is comparable to spiral galaxies nearby, and much higher than that seen in low-z nuclear starbursts. Similar results were found by Ferkinhoff et al. (2010) and Sturm et al. (2010) in their [OI] 63-μm, [OIII] 52-μm, and [CII] 158-μm studies of a strongly lensed ULIRG at $z = 1.3$ (see also Hailey-Dunsheath et al. 2010). The interesting conclusion is that, although these systems are intrinsically ULIRGs or HyLIRGs, they do not show a deficit in the major PDR cooling lines as seen in nearby ULIRGs. A similar conclusion has been reached based on [CII] and [NII] observations of lensed SMGs (De Breuck et al. 2011, Nagao et al. 2012). In particular, the compilation by Decarli et al. (2012) shows a mean value for [NII] 122-μm/FIR $\sim 3 \times 10^{-4}$, close to that seen in low-z disk galaxies, although admittedly the scatter is large.

Conversely, Valtchanov et al. (2011) and Ferkinhoff et al. (2010, 2011) perform PDR analyses of lensed SMGs at $z \sim 3$, using FIR, CO, [OIII], [NII], and/or [CII] measurements. They find mean densities of order 2,000 cm^{-3}, FUV radiation fields of $G = 200$, and sizes for the emitting region ~0.6 kpc. The relatively strong [OIII] implies that the radiation field must be very hot (35,000 K), dominated by either O9.5 stars or an AGN NLR-like radiation field. Lastly, the combination of [CII], [CI], and molecular lines is providing multiple spectral transitions for blind redshift surveys in the millimeter and submillimeter bands (Weiß et al. 2013, Vieira et al. 2013). In the sidebar, Fine Structure Lines, we discuss the increasing role of atomic FSLs in the study of galaxy formation.

4.4. Dense Gas Tracers and Other Molecules at High Redshift

Emission from high-dipole molecules, such as HCN and HCO$^+$, comes only from the highest density regions in molecular clouds ($n_{CR} > 10^4$ cm^{-3}), corresponding to regions directly

FINE STRUCTURE LINES

The [CII] 158-μm line is realizing its potential in the study of the cooler atomic gas in distant galaxies. This strong line will be a workhorse-line for redshift determinations in the first galaxies and in the study of galaxy dynamics at the highest redshifts. However, the interpretation of [CII] emission is not straightforward because [CII] traces both the neutral as well as the ionized medium, and it appears to be suppressed in high-density regions. Likewise, multi-FSL diagnostics at high redshift have tremendous potential to probe the physical conditions in the ISM in high-z galaxies, but studies are in their infancy. The current observations reflect the heterogeneous nature of SMGs, with many showing spiral galaxy-like FSL properties and a few showing evidence for an AGN-like component.

associated with active star formation. These lines are typically an order of magnitude weaker than the integrated CO emission from star-forming galaxies, although the higher dense gas fraction in nuclear starbursts can lead to line strengths up to 25% of CO (Riechers et al. 2011d). To date, there remain just a handful of detections at high redshift, mostly from strongly lensed hyperstarbursts (García-Burillo et al. 2006; Riechers et al. 2006b, 2010c, 2011d; Danielson et al. 2011). The two strongly lensed hyperstarburst/AGN, APM 0827+5255 at $z = 3.91$ and the Cloverleaf quasar (H1413+117; Barvainis et al. 1994) at $z = 2.56$, play an analogous role to the Galactic molecular cloud SgrB2 as high-z molecule factories. These are the only sources with multiple transitions detected from molecules and isotopes other than ^{12}CO, including HCN, HNC, HCO^+, H_2O, CN, and ^{13}CO. We briefly review the recent results on these sources.

For APM 0827+5255, strong emission from very high-order transitions is seen (Weiß et al. 2007a, Riechers et al. 2010c). Formally, the critical densities for excitation for the higher-order HCN and HCO^+ transitions are $>10^8$ cm^{-3}. The excitation suggests emission from a region with a radius of ∼200 pc around the AGN, where IR pumping (Section 2.6.2) plays a dominant role in molecular excitation. The $J = 6$ isomer ratio of HNC/HCN = 0.5 is consistent with the IR pumping model (Riechers et al. 2010c).

For the Cloverleaf quasar, low- and high-order emission, from HCN and HCO^+, and CN, have been detected (Wilner, Zhao & Ho 1995; Barvainis et al. 1997; Solomon et al. 2003; Riechers et al. 2006b, 2007b, 2011d). Modeling including the multiple CO transitions implies collisional excitation by gas with a mean kinetic temperature of 50 K and density of $10^{4.8}$ cm^{-3} in a molecular region with a radius of ∼0.8 kpc (Riechers et al. 2011d). Hence, in contrast to APM 0827+5255, the Cloverleaf is consistent with collisional excitation in a hyperstarburst region with a radius of order 1 kpc.

The only detection of rare isotopic emission at high redshift is ^{13}CO(3–2) emission from the Cloverleaf (Henkel et al. 2010). The isotopic luminosity ratio for the $J = 3$ emission is 40, eight times larger than that seen in Milky Way GMCs. The only nearby galaxy with a ratio approaching that of the Cloverleaf is the merging ULIRG NGC 6240, where Greve et al. (2009) obtain a lower limit of 30. Henkel et al. (2010) conclude that the large isotope ratio in the Cloverleaf likely reflects a real ^{13}C abundance deficit, by a factor of about four, relative to a Milky Way GMC value of 40 to 90 (Henkel et al. 1993).

Progress has recently been made on detecting thermal emission from (rest frame) FIR rovibrational transitions of water at high redshift (Omont et al. 2011, van der Werf et al. 2011, Combes et al. 2012). In APM 0827+5255, van der Werf et al. show that the lower-level transitions (rest frame frequencies below 1 THz) likely arise in collisionally excited gas with kinetic temperatures of 100 K and clump densities of order 3×10^6 cm^{-3}. The higher-order transitions require radiative excitation by IR radiation on a scale of a few hundred parsecs around the AGN, with conditions

DENSE GAS TRACERS

Progress on dense gas tracers at high redshift has been limited to strongly lensed, extremely luminous systems, due to the limited sensitivity of existing telescopes. The results thus far indicate a mixture of PDR/XDR heating and collisional excitation in compact extreme starburst regions. Given the very high average densities in dense starbursts at high redshift, cosmic ray heating and related modeling will play an increasingly important role. In the future, much progress is expected from much broader receiver bandwidths, as they will in almost all cases yield "involuntary line surveys" of dense gas tracers.

similar to the nuclear regions of the low-redshift starburst/AGN galaxy, Mrk 231 (van der Werf et al. 2010). They argue for distributed gas heating, as expected for a star-formation-heated PDR, and not an AGN-dominated XDR.

We note that a linear relation between $L'_{\rm HCN(1-0)}$ and $L_{\rm FIR}$ has been found for local galaxies, including spirals and ULIRGs (Gao & Solomon 2004a,b), unlike the nonlinear relationship between $L'_{\rm CO(1-0)}$ and $L_{\rm FIR}$. This relation extends even to the dense cores of galactic clouds (Wu et al. 2005). One interpretation of this finding is that the dense molecular phase traced by HCN immediately precedes the onset of star formation. However, Riechers et al. (2007a) have shown that this linear relationship appears to break down in the high-redshift systems studied to date, i.e., that they have lower HCN luminosities than expected based on a linear extrapolation from the low-redshift (and Galactic) measurements. This finding may indicate even higher average gas densities in the highest redshift systems compared to dense environments found locally. It may also hint at an increased SFE (or both) (Riechers et al. 2007a).

The most spectacular example of dense gas tracers in distant galaxies is the recent spectroscopic study of a $z = 6.3$ SMG by Riechers et al. (2013), who find multiple species and transitions of ammonia, water, CO, and other molecules (see Section 5.2). In the sidebar, Dense Gas Tracers, we summarize the potential for the study of dense gas tracers in distant galaxies.

4.5. Star-Formation Laws and Gas Consumption

Quantifying the relationship between SFR and gas density (the so-called star-formation law, Schmidt law, Schmidt-Kennicutt law or K-S law) has been a key goal in observational astrophysics over the past 50 years, starting with Schmidt (1959). Any relationship between SFR and gas surface densities has important implications for our understanding of galaxy formation and evolution as it describes how efficiently galaxies turn their gas into stars. Such a "law" would also serve as essential input to hydrodynamical simulations (and other models) of galaxy evolution that start with dark matter halos that are being fed by gas infall. It should be noted that the term "law" (in the sense of a physical law) is not appropriate to describe an empirical relationship. However, we stick to this nomenclature as it is now common practice to refer to the SFR-gas relationship. This relationship has been reviewed recently for nearby galaxies by Kennicutt & Evans (2012). Herein, we focus on $z > 1$ galaxies.

The relation between SFR and gas density is typically expressed in terms of surface densities ($\Sigma_{\rm SFR} \sim \Sigma^n_{\rm gas}$). One complication is that the measurement of surface densities requires resolved measurements of galaxies. In the compilation by Kennicutt (1998a,b) the integrated SFRs and gas masses were averaged over entire galaxy disks to derive an average surface density for a given galaxy. Observational capabilities have improved since then, and spatially resolved measurements

Table 2 Factors to calculate $L'_{CO(1-0)}$ from higher J transitions up to $J = 5$[a]

Source	SMG	QSO	CSG	MW	M82
$L'_{CO(2-1)}/L'_{CO(1-0)}$	0.85	0.99	∼0.9	0.5	0.98
$L'_{CO(3-2)}/L'_{CO(1-0)}$	0.66	0.97	∼0.6	0.27	0.93
$L'_{CO(4-3)}/L'_{CO(1-0)}$	0.46	0.87	–	0.17	0.85
$L'_{CO(5-4)}/L'_{CO(1-0)}$	0.39	0.69	–	0.08	0.75

[a]For the submillimeter galaxies (SMGs) and quasi-stellar objects (QSOs), average values are quoted based on all available literature estimates. For the color-selected star-forming galaxies (CSGs), the ratio is taken from Dannerbauer et al. (2009) and Aravena et al. (2010, their LVG model 1). The values for the Milky Way (MW) and the center of M82 are from Weiß et al. (2005b). "–" indicates that no well-constrained value is available. We assume the same excitation for the CSGs as for the Lyman-break galaxies and star-forming radio galaxies. We adopt QSO excitation for the radio galaxies and SMG excitation for the 24-μm and ERO sources.

of the SFR and gas surface densities are now available for a number of nearby galaxies (e.g., Kennicutt et al. 2007; Bigiel et al. 2008, 2011; Leroy et al. 2008, 2013; Liu et al. 2011; Rahman et al. 2011, 2012). These spatially resolved measurements typically have resolutions of 1 kpc or slightly better, i.e., they still average over many individual GMCs that are typically ∼50 pc in size. It is clear from Galactic studies that the relationship $\Sigma_{SFR} \sim \Sigma^n_{gas}$ must break down on very small scales: e.g., a star-forming region will ionize its immediate surrounding, thus destroying any relationship that may be present on a larger scale. This has been quantified observationally by Schruba et al. (2010) and Onodera et al. (2010), who have shown that in the case of M33 the star-formation law on large/galactic scales breaks down on scales below ∼500 pc (for a theoretical approach, see Feldmann, Gnedin & Kravtsov 2011, 2012b). There is now largely consensus that the star-formation law is molecular, i.e., that the equation above becomes: $\Sigma_{SFR} \sim \Sigma^n_{H_2}$. HI does not appear to be intimately linked to the star-formation process through such a simple description, even though it is clear that HI is initially needed to form H_2 (Kennicutt & Evans 2012).

Measuring the star-formation law at high redshift is complicated by the fact that few resolved CO measurements exist, and dust and/or AGN emission confuses determination of optical sizes. The recent comprehensive study by Tacconi et al. (2013) shows that, where both the size of the star-forming disk as well as the size of the CO emission could be measured, reasonable agreement between the quantities was found (see also Daddi et al. 2010a). However, typically only global measurements of SFR and molecular gas are plotted in high-redshift research.

Unlike in the local Universe, where L'_{CO} luminosities and H_2 masses can be calculated from the low-J CO transitions (Section 2.5), the majority of high-redshift measurements are performed using higher J transitions. To put all high-redshift systems on the same plot, the L'_{CO} luminosity of the CO(1–0) transition needs to be estimated, assuming the typical excitation of the galaxy under consideration. Narayanan et al. (2010a) discuss how the slope of the star-formation law could change if different transitions of CO are used and if the different line ratios are not accounted for properly. We consider the CO excitation ladder in Section 4.1, and in the analysis below, we adopt a set of canonical values for different galaxy types, based on the available data (**Table 2**).

Two further complications are involved when comparing derived quantities, such as gas mass and SFR. First is the CO luminosity–to–gas mass conversion factor, α. As discussed in detail in Section 4.2, different source populations likely have different values of α. The second complication is derivation of the SFR from observed SEDs. Methods include SED fitting of UV/optical/IR data for CSGs, FIR luminosities for SMGs and AGN after correction for hot dust heated by the AGN (Genzel et al. 2010; Jiang et al. 2010; Leipski et al. 2010, 2013; Riechers 2011), and radio luminosities assuming the radio-FIR correlation (Condon 1992).

To avoid some of the above complications, we focus on the empirical relationship between $L_{\rm FIR}$ and $L'_{\rm CO(1-0)}$, for all high-redshift galaxies detected to date in **Figure 7** (see caption for the derivation of $L'_{\rm CO(1-0)}$). Most of the galaxies detected at high redshift have luminosities (both FIR and CO) that are much higher than typical systems seen in the local Universe (**Figure 7**, *gray/black* data points). At the highest luminosities, the SMGs and quasar host galaxies dominate. The entire distribution can be fit with a power law of the form

$$\log(L_{\rm IR}) = 1.37(\pm 0.04) \times (\log L'_{\rm CO}) - 1.74(\pm 0.40),$$

with a slope that is consistent with the power law found when looking at the integrated properties of nearby galaxies only (including ULIRGs; Kennicutt 1998a). However, it is also apparent that the CSGs have higher CO luminosities for a given $L_{\rm FIR}$ (or SFR) compared to the QSO/SMG population (Daddi et al. 2008, 2010a; Tacconi et al. 2010, 2013). Genzel et al. (2010) and Daddi et al. (2010b) argue that there are in fact two sequences visible in this plot, one starburst sequence (*red dashed line*) and one MS/CSG relation (*gray dashed line*). For the latter, Daddi et al. (2010b) and Genzel et al. (2010) derived

$$\log(L_{\rm IR}) = 1.13 \times (\log L'_{\rm CO}) + 0.53,$$

with $L'_{\rm CO}$ in units of K km s^{-1} pc^2 and $L_{\rm IR}$ in units of $L_\odot$. The values given here are from Daddi et al. (2010b), but the relation derived by Genzel et al. (2010) is very similar.

Both Genzel et al. (2010) and Daddi et al. (2010b) proceed to calculate molecular gas masses from the CO luminosities using a molecular gas conversion factor α that is about five times higher in the case of the CSGs relative to SMGs, based on the arguments in Section 4.2. This then leads to an increased gap between the CSG population and the SMGs/QSOs with an offset of roughly 1 dex in $L_{\rm FIR}$. This strengthens the presence of two different star-formation regimes, one highly efficient star-formation mode for starbursts (presumably triggered by mergers and/or other interactions) and one less efficient and thus longer-lasting mode for the CSGs (MS galaxies).

The different ratios of $L_{\rm FIR}/L'_{\rm CO}$ are further highlighted in **Figure 7*b***. It is immediately obvious from this plot that this ratio for the CSG is lower compared to the high-redshift quasars and SMGs by a factor of a few and that the CSGs reach values that are similar to that found in local galaxies. The offset between the two sequences becomes even more pronounced when different α conversion factors are used for the two high-redshift galaxy populations.

The gas consumption timescale is defined simply as $\tau_{\rm consumption} = M_{\rm gas}/SFR$, i.e., the time it would take to use up the available molecular gas reservoir given the current SFR. The right hand axis of **Figure 7*b*** shows these timescales, assuming the two different conversion factors relevant to SMGs and CSGs (Section 4.2). The gas consumption timescale in CSGs is of order 10^8 to 10^9 years (Daddi et al. 2008, 2010a,b; Genzel et al. 2010; Tacconi et al. 2010, 2013), comparable to that in low-redshift disk galaxies (Bolatto, Leroy & Wolfire 2013). For comparison, the SMGs and other HyLIRGs have extremely short consumption timescales of $\leq 10^7$ years.

In the local Universe, Kennicutt (1998a,b) has shown that if the dynamical timescale is taken into account (i.e., $\Sigma_{\rm SFR}$ is plotted as a function of $\Sigma_{\rm gas}/\tau_{\rm dyn}$ and not only as a function of $\Sigma_{\rm gas}$), all galaxies fit on one relation with slope $\sim$1. Both Genzel et al. (2010) and Daddi et al. (2010a) showed that this trend also continues at high redshift, i.e., that a universal star-formation law is obtained, with no separation between the two star-forming sequences. The dynamical timescale $\tau_{\rm dyn}$ is here defined to be the rotational period at the last measured point in a galaxy (typically taken to be the half-light radius). We note that the latter is not easily determined given current observations at high redshift and that a physical interpretation of this finding is not straightforward. In a sense, it is puzzling that the global properties of a galaxy ($\tau_{\rm dyn}$) appear to be related to local star-formation

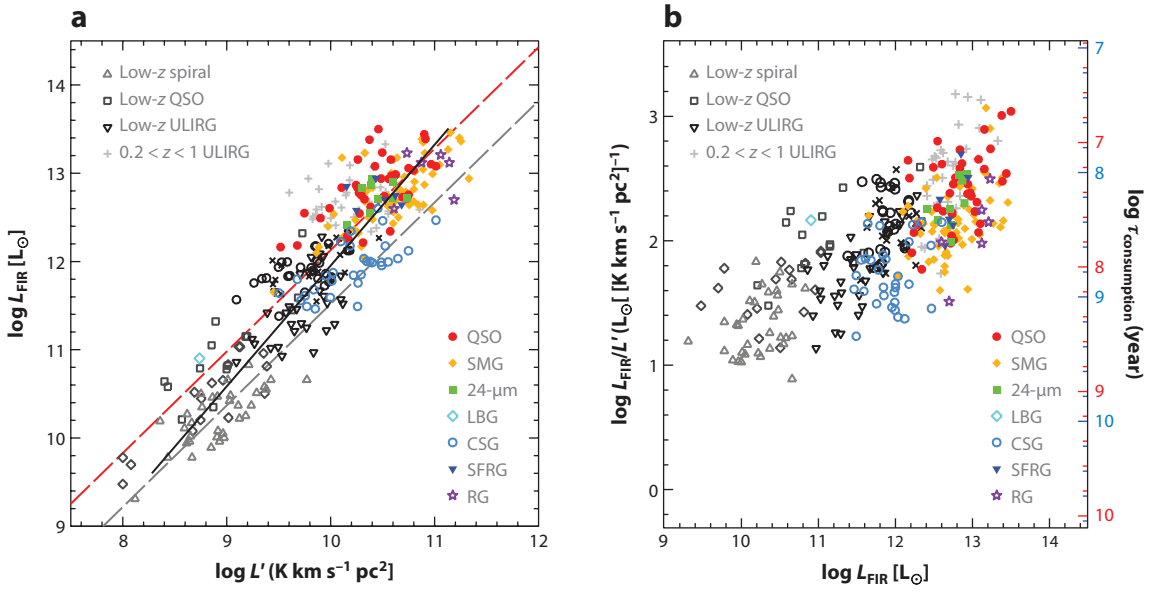

Figure 7

(*a*) L'_{CO} as a function of L_{FIR} for all systems detected at $z > 1$ (*colored points*). L'_{CO} was calculated using the lowest available *J* measurement and assuming the excitation correction tabulated in **Table 2** (see table caption for details on different source populations). The gray symbols represent $z < 1$ measurements: the $0.2 < z < 1$ ultraluminous infrared galaxy (ULIRG) sample (Combes et al. 2011, 2013; *crosses*); low-*z* quasars from the Hamburg-ESO quasi-stellar object (QSO) survey (Bertram et al. 2007; *diamonds*); Palomar-Green quasars (Evans et al. 2001, Scoville et al. 2003, Evans 2006; *squares*); low-*z* spirals, starburst galaxies, and ULIRGs (Gao & Solomon 2004a,b; *downward* and *upward triangles*); and the $z < 0.2$ IR QSO sample (Xia et al. 2012) and the $0.04 < z < 0.11$ ULIRG sample (Chung et al. 2009; *open circles*). The full line is a fit to all data points, which gives a slope of 1.35 ± 0.04. The dashed lines indicate the best fits for the main sequence galaxies (*gray dashed line*) and starburst galaxies (*red dashed line*) derived by Genzel et al. (2010) and Daddi et al. (2010a). (*b*) The logarithmic ratio L_{FIR}/L'_{CO} as a function of L_{FIR}. L_{FIR}/L'_{CO} is a measure for the star-formation efficiency in an object, and under the assumption of a conversion factor is the inverse of the consumption time $\tau_{consumption}$. The consumption time is plotted on the right-hand side of the panel for two different values of α, Galactic (*blue labels*) and ULIRG (*red labels*). The consumption times for nearby galaxies and the color-selected star-forming galaxies (CSGs) are ~1 Gyr, assuming a Galactic α. The consumption times for the most actively star-forming systems are only a few $\times 10^7$ years under the typical assumption of a ULIRG α. Abbreviations: 24-μm, 24-μm galaxy; LBG, Lyman-break galaxy; RG, radio galaxy; SFRG, star-forming radio galaxy.

processes. Krumholz, Dekel & McKee (2011) perform a similar analysis, but only using an estimate of the local gas free-fall time, and conclude that all systems, from local molecular clouds to distant galaxies (starburst and MS), fall on a single star-formation law in which the SFR is simply ~1% of the molecular gas mass per local free-fall time.

It should be kept in mind that there are significant selection effects that may contribute to the apparent functional behavior in the star-formation law plot. For example, as essentially all galaxies have been preselected based on their star-formation activity, it is conceivable that large molecular gas reservoirs exist at low L_{FIR}; they simply have not yet been looked at. We summarize star-formation laws for high-redshift galaxies in the sidebar, Star-Formation Laws.

4.6. Imaging of the Molecular Gas in Early Galaxies

The past few years have seen tremendous progress in high-resolution imaging of the molecular gas in high-redshift galaxies, mainly by the VLA and the IRAM PdBI. Imaging of CO emission

STAR-FORMATION LAWS

Constraining the star formation law, i.e., relating the SFR to the available gas reservoir, has been the focus of many studies at low- and high-redshift in the past decade. Even though it is not a law in a physical sense, this empirical relation has the potential power to predict one quantity from the other, sheds light on the star-formation process, and serves as vital input in numerical simulations and galaxy-formation models. At high redshift, there is a clear relation between the main observables, $\log(L_{IR})$ and $\log(L'_{CO})$. Once translated into physical quantities (SFR and H_2 mass), there is now good evidence for two sequences of star formation, one starburst sequence with very short consumption times of 10^7–10^8 years (local ULIRGs, SMGs and QSOs) and a normal, quiescent sequence of $\sim 10^9$ years (local spirals, CSGs, MS galaxies).

has been performed on the brighter sources with a spatial resolution comparable to that of the HST (~0.15 arcsec or roughly 1 kpc at $z > 1$). Below, we highlight a few of the best examples to date (see **Figure 8**).

4.6.1. A typical color-selected star-forming galaxy. In their groundbreaking studies of CSGs, Tacconi et al. (2010) and Daddi et al. (2010a) find gas-rich disks without extreme starbursts (see also Tacconi et al. 2013) (Section 3.5). One of the best imaging studies to date of a CSG is that of the CO(3–2) emission from EGS 1305123 using the PdBI at 0.6 arcsec resolution by Tacconi et al. (2010) (**Figure 8**). The H_2 mass is $1.3 \times 10^{11}(\alpha/3.2)\,M_\odot$, distributed in a rotating disk with a radius of 8 kpc and a terminal rotation velocity of 200 km s^{-1}. Although clearly rotating, the disk also has a high internal velocity dispersion $\geq$20 km s^{-1}, implying substantial disk turbulence.

The disk is punctuated by high brightness temperature clumps with radii $\leq$2 kpc and masses $\sim 5 \times 10^9\,M_\odot$. The gas surface densities are $\sim 500\,M_\odot$ pc^{-2}, a factor of a few larger than that for Galactic GMCs, and Tacconi et al. hypothesize that these clumps are conglomerates of a number of Galactic-type GMCs rather than a single giant GMC, owing to the relatively low internal velocity dispersions (~20 km s^{-1}). Daddi et al. (2010a) obtain similar imaging results for a few CSGs at $z \sim 1.5$, although at somewhat lower spatial resolution.

These imaging observations of CO in $z \sim 1$ to 3 CSGs have been critical to the interpretation that the CSGs are gas-dominated, rotating disk galaxies undergoing steady, high levels of star formation (see Section 3.5). They also helped to constrain the conversion factor α for these systems through dynamical arguments (Section 4.2).

4.6.2. BRI 1335-0417: tidally disturbed gas surrounding a luminous quasar. BRI 1335-0417 at $z = 4.4$ was among the first optically selected, very high-z quasars to be identified with a hyperluminous FIR host galaxy, implying an accreting SMBH with mass $\sim 10^9\,M_\odot$ coeval with an extreme starburst (SFR $\sim$1,000 $M_\odot$ year^{-1}) (Guilloteau et al. 1997). The host galaxy has been detected in CO line emission, with an implied $M(H_2) \sim 8 \times 10^{10}(\alpha/0.8)\,M_\odot$ (Carilli et al. 2002), as well as strong [CII] emission (Wagg et al. 2010). BRI 1335-417 is a broad absorption-line quasar, indicating AGN outflow. **Figure 8*b*** shows the CO images of BRI 1335-0417 from the VLA (Riechers et al. 2008b). This is one of the highest-quality CO images of any nonlensed high-z quasar to date. The system shows complex morphology in the gas on a scale of ~1 arcsec. The molecular gas shows multiple components distributed over ~7 kpc, with a pronounced tail extending to the north, peaking in a major CO clump ~0.7 arcsec from the quasar and with a few other streams connecting to the quasar from other directions. Although there is an overall north-south velocity gradient, the general velocity field appears chaotic.

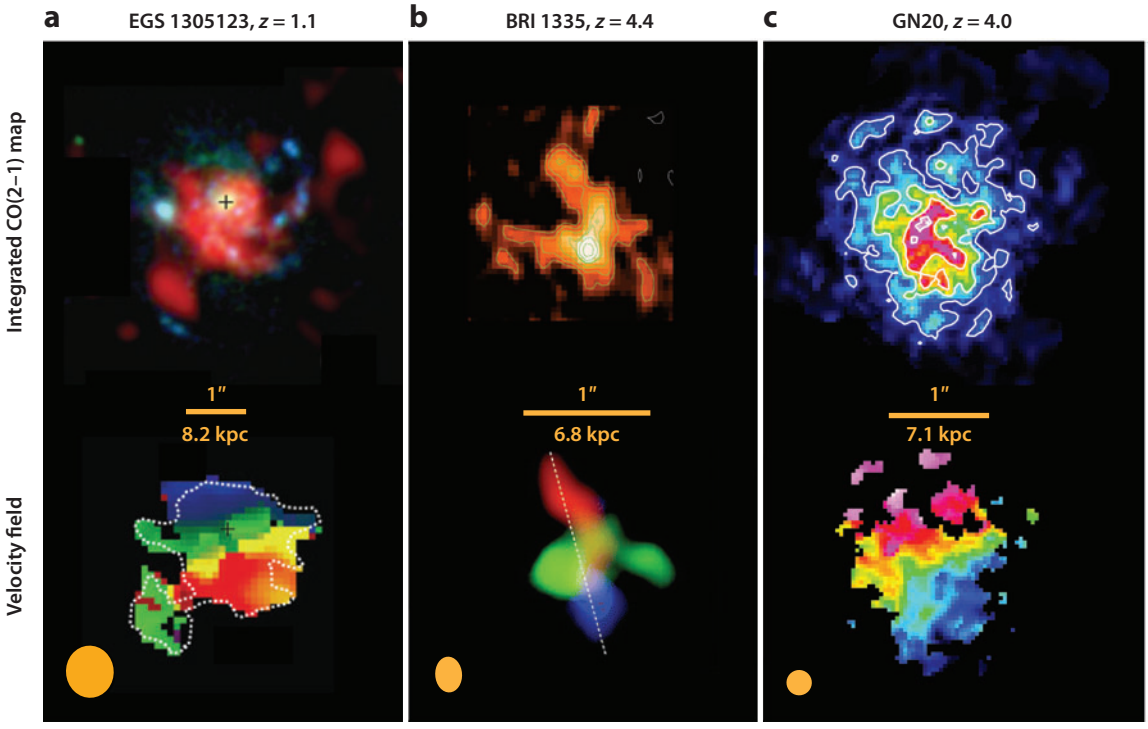

Figure 8

Best examples of resolved molecular line emission at high redshift from which gas kinematics can be derived. These are (*a*) the color-selected star-forming galaxy EGS 1305123 (Tacconi et al. 2010), (*b*) the quasi-stellar object BRI 1335 (Riechers et al. 2008b), and (*c*) the submillimeter galaxy GN20 (Hodge et al. 2012). The top images show the integrated CO(2–1) maps of the targets. The bottom images show the velocity fields of the targets; here the color indicates the velocity at which gas is moving in a given position on the sky. The velocity scale ranges from (*blue* to *red*) -65 to $+100$ km s^{-1}, -154 to $+154$ km s^{-1}, and -300 to 300 km s^{-1}, respectively. The beam sizes are given in the bottom left of each galaxy; the bar indicates 1 arcsec on the sky (the size in kiloparsecs at the respective redshift is also given).

Riechers et al. interpret the complex gas structure in BRI 1335-0417 as tidal remnants from a late-stage, gas-rich (wet) merger. The merger drives gas accretion onto the main galaxy, fueling the hyperstarburst and the luminous AGN, which is generally consistent with the high molecular excitation seen in quasar hosts (Section 4.1).

4.6.3. GN20: a submillimeter galaxy with a gas-rich disk. The galaxy GN20 is the brightest SMG in the GOODS-North field (Pope et al. 2006), and the host galaxy is heavily obscured at optical wavelengths. Daddi et al. (2009a) made a serendipitous redshift determination of $z = 4.05$ from CO emission using the PdBI. Two other SMGs at this redshift have been detected in CO and dust continuum emission about 20 arcsec to the west (Carilli et al. 2011), and there is a clear over-density of galaxies in this field, with 15 LBGs with $z_{\rm phot} \sim 4$ within a radius or 25 arcsec of GN20 (Daddi et al. 2009b).

A long observation using the JVLA in early science of the CO(2–1) emission (Hodge et al. 2012) shows that the CO is distributed in a disk with a diameter ~14 kpc (**Figure 8*c***). The regions emitting in CO and dust continuum are mostly obscured in the HST I-band image. The only

CO IMAGING

Spatially resolving the molecular gas emission in high-redshift galaxies is to date restricted to very few bright sources. Imaging the molecular and cool atomic gas of a few selected high-redshift galaxies has revealed 10-kpc-scale, clumpy and turbulent, but apparently rotating disks in CSGs and some SMGs, as well as tidally disturbed gas distributions in some SMGs and quasar hosts.

optical emission is seen at the edges of the source (Hodge et al. 2012). Such heavy obscuration in the optical is characteristic of SMGs.

The GN20 disk dynamics are consistent with a standard tilted-ring gas rotation model, with a dynamical mass of $5.4 \pm 2.4\ 10^{11}\,M_\odot$. Observations at 1-kpc resolution reveal that 30% to 50% of the gas is in giant clumps with gas masses of a few $\times 10^9(\alpha/0.8)\,M_\odot$, brightness temperatures between 16 K and 31 K, and line widths of order 100 km s^{-1} (Hodge et al. 2012). A dynamical analysis suggests the clumps could be self-gravitating. The gas surface densities of the clumps are $\sim$4,000$(\alpha/0.8)\,M_\odot$ pc^{-2}, more than an order of magnitude larger than typical GMCs. An analysis of the overall galaxy dynamics has been used to determine the value of α in GN20 (see Section 4.2).

The apparent disk in GN20 suggests that not all HyLIRGs at very high redshift result from an ongoing major merger. This conclusion has also been reached for a few other SMGs at lower redshift, where low-order CO observations show large, disk-like gas reservoirs similar to GN20 (Greve, Ivison & Papadopoulos 2004; Ivison et al. 2010a,b; Ivison et al. 2011; Riechers et al. 2011b).

In GN20, the clumpy disk is consistent with that expected in the CMA model (e.g., Kereš et al. 2005, Dekel & Birnboim 2006, Dekel et al. 2009), only now scaled up by almost an order of magnitude in FIR luminosity relative to typical CSGs (see Section 5.1.2). It is possible that the star formation in this gas-rich disk has been enhanced due to gravitational harassment by the other SMGs and smaller galaxies in the protocluster. In the sidebar, CO Imaging, we summarize results from CO imaging of distant galaxies.

4.7. Outflows

Theoretical models without negative feedback (negative feedback = ejection of material due to either star formation or AGN activity) predict both a higher gas content in massive galaxies in the nearby Universe and a larger population of star-forming massive galaxies today than has been observed. At high galactic masses, including AGN feedback mitigates these problems in simulations, both driving gas out of the immediate ISM of the host galaxy via AGN winds and suppressing further gas accretion from the IGM via large-scale radio jets (Fabian 2012). Direct evidence for feedback has been seen in nearby galaxies, including outflows seen in OH FIR lines, molecular emission lines, optical lines, and atomic FSLs (Martin 1998; Walter, Weiss & Scoville 2002; Veilleux, Cecil & Bland-Hawthorn 2005; Strickland & Heckman 2009). The fact that old, gas-poor massive galaxies have now been seen at redshifts of 2 and beyond suggest that feedback must be an important process at even earlier times.

Recent observations have detected evidence for feedback on kiloparsec-scales in very early galaxies. One of the best examples of AGN feedback are the broad line wings of the [CII] emission from the $z = 6.4$ quasar J1148+5251 by Maiolino et al. (2012). They derive an outflow velocity of 1,300 km s^{-1}, an outflow rate of $\dot{M}_{\rm outfl} \sim 3{,}500\,M_\odot$ year^{-1}, and kinetic power of $P_{\rm K} \sim 1.9 \times 10^{45}$ erg s^{-1}. This is roughly 0.6% of the quasar bolometric luminosity, well below the theoretical

CMA: cold mode accretion

OUTFLOWS

Molecular outflows have only very recently been detected in a few high-redshift systems. Given that they feature (by definition) broad and faint line wings, they remained undetected by past observations, due to both missing sensitivity and insufficient bandwidth. Quantifying the kinetic energy and masses associated with such outflows will provide important input in galaxy simulations in which feedback by stellar (or AGN) activity is a key driver for galaxy evolution.

upper limit to a radiatively driven quasar outflow of 5% of the bolometric luminosity (Lapi, Cavaliere & Menci 2005), but it is barely consistent with the maximum kinetic power that can be driven by the associated starburst in the quasar host (Veilleux et al. 2005). Likewise, theoretical models indicate that star-formation driven winds reach a maximum velocity of ∼600 km s^{-1} (Thacker, Scannapieco & Couchman 2006). Maiolino et al. (2012) argue that the outflow is most likely AGN driven. The gas consumption timescale for the outflow is comparable to that due to star formation, of order 10^7 years.

Other systems show varying degrees of feedback in the cooler gas. The BRI 1202-0725 quasar-SMG galaxy pair does show evidence for a broad wing in the quasar host galaxy [CII] 158-μm spectrum, but the outflow kinetic energy is well below that of J1148+5251, and star formation likely dominates gas depletion in the galaxy (Wagg et al. 2012, Carilli et al. 2013). Weiß et al. (2012) detect a 250-km-s^{-1} outflow signature in a $z = 2.8$ quasar in both CO and [CI]. They derive a lower limit to the mass outflow rate of 180 $M_\odot$ $year^{-1}$, which is slightly larger than the SFR in the host galaxy. The sidebar, Outflows, describes the importance of studies of outflows in galaxy formation.

5. DENSE GAS HISTORY OF THE UNIVERSE

5.1. Gas-Dominated Disks During the Epoch of Galaxy Assembly

The increasing sample sizes of CO detections in distant galaxies have allowed for general studies of the properties of galaxy populations. We herein consider the key question of the baryon fraction of gas in forming galaxies.

5.1.1. Gas fraction. One of the most striking results from the study of CSGs is the remarkably high detection rate (between 50% and 100%) in CO emission (Daddi et al. 2010a; Tacconi et al. 2010, 2013). The line strengths are comparable to those seen in the hyperstarbursts, but the SFRs are almost an order of magnitude smaller (Section 4.5). Moreover, these galaxies have a space density more than an order of magnitude larger than SMGs (10^{-4} Mpc^{-3} down to $M_{stars} = 10^{10}$ $M_\odot$), and they represent the galaxies that dominate the integrated cosmic SFR during the "epoch of galaxy assembly" (see Section 1.2).

A series of measurements and consistency arguments lead to a value of $\alpha_{CO} \sim 4$ in CSGs (Section 3.5). The implied H_2 masses range from 3×10^{10} $M_\odot$ to 10^{11} $M_\odot$. Interestingly, these gas masses are comparable to, or even larger than, the stellar masses in these galaxies, as first pointed out by Daddi et al. (2010a) and Tacconi et al. (2010). This ratio is very different with respect to large disk galaxies at low redshift, where the stellar masses are close to an order of magnitude larger than the cool gas masses.

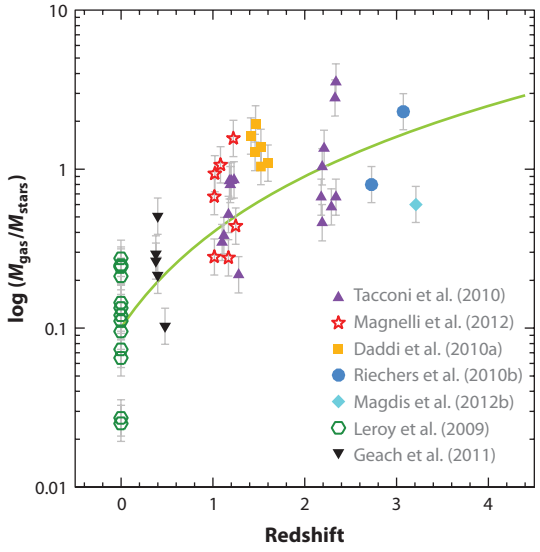

Figure 9

The ratio of gas mass to stellar mass ($M_{\rm gas}/M_{\rm stars}$) for various galaxy samples. The green circles are from the $z = 0$ HERACLES nearby galaxy sample (Leroy et al. 2009), where we only include galaxies with stellar masses $>10^{10}\,{\rm M}_\odot$, to be consistent with the high-z samples plotted. All the points plotted assume $\alpha \sim 4$. The green curve follows $M_{\rm gas}/M_{\rm stars} = 0.1 \times (1+z)^2$ (e.g., Geach et al. 2011).

In **Figure 9** we plot a compilation of the latest measurements of the gas fraction, here defined as $f_{\rm gas} \equiv M_{\rm gas}/M_{\rm stars}$, out to $z \sim 4$, where $M_{\rm gas}$ corresponds to the molecular component, including a 1.36 factor for helium. At all redshifts, the galaxies were selected to be star-forming disk galaxies with stellar masses $>10^{10}\,{\rm M}_\odot$.

Although the scatter in **Figure 9** at any given redshift is large, there is a clear trend for increasing gas fraction with redshift in massive disk galaxies. The mean value at $z \sim 0$ is $M_{\rm gas}/M_{\rm stars} \sim 0.1$, which increases to $M_{\rm gas}/M_{\rm stars} \sim 1$ at $z > 2$. A functional form of $f_{gas} \sim 0.1 \times (1+z)^2$ fits the data reasonably (see also Geach et al. 2011, Magdis et al. 2012b). Note that the high-z CSG CO samples tend to be at the upper end of the mass range for CSGs, but are typical of MS galaxies in all other respects (e.g., Daddi et al. 2010a). Moreover, the recent large study by Tacconi et al. (2013) suggests that the gas fraction in CSGs may increase with decreasing galaxy mass, thereby accentuating the results in **Figure 9**.

We note that all points in **Figure 9** are for large disk galaxies (stellar masses $>10^{10}\,{\rm M}_\odot$) and that the same value of $\alpha \sim 4\,{\rm M}_\odot\ ({\rm K\ km\ s^{-1}\ pc^2})^{-1}$ was used for all sources. Moreover, though stellar masses are nominally based on full SED-fitting, the outcome is predominantly dictated by the observed near-IR data, corresponding to roughly rest frame R band (E. Daddi, private communication). Hence, the ratio on the ordinate of **Figure 9** can be considered to be approximately empirical and $\propto L'_{\rm CO1-0}/R^{\rm rest}_{\rm mag}$.

Narayanan et al. (2012) consider the question of how the conversion factor could affect these conclusions on the increasing gas fraction with redshift. Using numerical models of galaxy formation including molecular gas, they conclude that the conversion factor may be lower in high-redshift galaxies due to higher velocity dispersions and gas temperatures. They predict a typical reduction in inferred gas mass of about 50% in CSGs due to a lower conversion factor relative to the Milky Way value. Although this reduces the overall effect, the fact remains that galaxies in the

GAS FRACTION

The gas fraction of molecular gas versus stars in massive disk galaxies increases by an order of magnitude from $z = 0$ to $z \sim 2$. Hence, the peak epoch of cosmic star formation ($z \sim 2$) corresponds to the epoch when typical star-forming disk galaxies appear to be dominated by cool gas, not stars.

distant Universe are considerably more gas rich than their low-z counterparts by a factor of five to twenty. Bauermeister et al. (2013) analyze a more heterogeneous sample of galaxies, including SMGs, but reach a similar conclusion as inferred from **Figure 9**.

Overall, the CO measurements of CSGs suggest that the peak epoch of cosmic star formation also corresponds to an epoch when molecular gas masses dominate over stellar masses in common star-forming galaxies (see also Geach et al. 2011, Magdis et al. 2012b, Swinbank et al. 2012b). This fundamental change in the baryon content of disk galaxies with redshift likely has definitive consequences for the nature of star formation in early galaxies (see Section 5.2).

Of course, we must keep in mind that the CSGs at high redshift may not evolve into low-redshift disk galaxies, and demographics suggest that subsequent mergers can lead to substantial morphological evolution. For instance, the space density and clustering of the CSGs at $z \sim 2$ are consistent with their evolution into early-type galaxies at $z \sim 0$ (Tacconi et al. 2008, Shapley 2011). The evolution of the gas fraction in galaxies is summarized in the sidebar, Gas Fraction.

5.1.2. Gas accretion. Gas resupply for star formation in galaxies has become an important issue at both low and high redshift. The most extreme situations are the gas consumption times in QSO host galaxies and SMGs, which are always extremely short, in some cases as short as 10 million years (Section 4.5). However, even CSGs have gas consumption timescales substantially shorter than the Hubble time (Tacconi et al. 2013). This point is emphasized by Bauermeister et al. (2010), where they conclude, based on the short molecular gas consumption timescales in high-z galaxies and the lack of evolution of the cosmic HI mass density (from study of damped Lyα absorption systems), that ultimately the gas must be accreted from the IGM.

The clear need for rapid gas resupply over cosmic time has led to a change in thinking on the gas supply to early galaxies. As opposed to either cooling of virialized, hot halo gas (White & Rees 1978) or major, gas-rich mergers (Robertson et al. 2006), the dominant mode of star formation during the epoch of galaxy assembly may have been driven by CMA, also known as stream-fed galaxy formation. A convergence of observations, simulations, and analytic studies suggests that gas accretion in early galaxies occurs along cold streams ($T \sim 10^4$ K) from the filamentary IGM that never shock-heat, but stream onto the galaxy at close to the free-fall time (Kereš et al. 2005, 2009; Bournaud, Elmegren & Martig 2009; Dekel, Sari & Ceverino 2009; Dekel et al. 2009; Elmegreen & Burkert 2010). This cool gas may form a thick, turbulent, rotating disk (Genzel et al. 2006, 2008, 2011; Daddi et al. 2010a). The disks are marginally Toomre-unstable (Tacconi et al. 2010, Swinbank et al. 2011), leading to rapid fragmentation into a few kiloparsec-scale clumps that very efficiently form stars. These clumps can be 100 times larger than Galactic GMCs, and 10^7 times more luminous (Swinbank et al. 2010). The star-forming regions could then migrate to the galaxy center via dynamical friction and viscosity, forming compact stellar bulges (Genzel et al. 2008; Dekel, Sari & Ceverino 2009; Kereš et al. 2009). The process leads to relatively steady, active ($\sim 100\,M_\odot$ year^{-1}) star formation in galaxies over timescales of order 1 Gyr, and has been termed "rapid secular galaxy evolution" (Genzel et al. 2008).

GAS ACCRETION

The current evidence for gas accretion through CMA at $z > 1$ is circumstantial, based on the similarity between the predicted and observed morphologies of gas-dominated disks in CSGs. Low-ionization quasar absorption lines may provide the best means by which to prove the existence of these flows.

In these models, the process slows down dramatically as gas supply decreases, and the halo mass increases, generating a virial shock in the accreting gas. Subsequent dry (gas-poor) mergers at $z < 2$ lead to continued total mass build up, and morphological evolution, but little star formation in such models (Kereš et al. 2009; Naab, Johansson & Ostriker 2009; Hopkins et al. 2010). In this scenario, the majority of stars in spheroidal galaxies are thought to form via CMA at $z \sim 2$ to 3.

Davé et al. (2010) suggest that the CMA phenomenon may even scale up to HyLIRGs, and that a substantial fraction of high-z SMGs could be fed primarily by CMA and not major mergers. Hydrodynamical simulations show that quite high gas accretion rates can be achieved in large halos at early epochs, and SFRs can be elevated over the average accretion rate by a factor 2 to 3 via (common) minor mergers and general gravitational harassment in the dense environments of SMGs (see also Finlator et al. 2006, Narayanan et al. 2010b).

Physically, there may be a continuum of accretion processes, from relatively continuous CMA, through "clumpy" accretion of small satellites, to the rare major gas-rich merger. However, current modeling and observations favor a model in which most of the accretion occurs relatively continuously over timescales $\geq 10^9$ years (Guo & White 2008, Dekel et al. 2009).

We emphasize that clumpy, turbulent but rotating gas disks are simply a consistency argument for CMA (Shapiro et al. 2008), and they do not conclusively rule out gas-rich mergers. Robertson & Bullock (2008) have shown that ordered rotation of an extended gas disk can be reestablished shortly after a major merger. Some recent observations detected low-metallicity gas near high-redshift galaxies; the properties of this gas are argued to be consistent with a CMA scenario (e.g., Ribaudo et al. 2011, Kacprzak et al. 2012). The few single detections to date are, however, not sufficient to conclusively prove the existence of CMA from an observational perspective. Open issues concerning gas accretion are summarized in the sidebar, Gas Accretion.

5.2. First Galaxies

Deep fields at near-IR wavelengths, and narrow band near-IR surveys, are now systematically detecting galaxies at $z \sim 6$ to 10, corresponding to the tail end of cosmic reionization when the Universe was less than 1 Gyr old (Pentericci et al. 2011; Bouwens et al. 2012a,b; Bradač et al. 2012; Coe et al. 2013). Reionization represents the epoch when light from the first galaxies acted to reionize the neutral IGM that pervaded the Universe after recombination (e.g., Fan, Carilli & Keating 2006). Current studies suggest that the typical star-forming galaxies at these redshifts have lower dust content than similar luminosity galaxies at lower redshift (Bouwens et al. 2010).

The search for dust and cool gas into cosmic reionization has focused predominantly on the host galaxies of luminous quasars with good spectroscopic redshifts. One of the most distant, and best studied, of the molecular gas detections remains the quasar SDSS J1148+5251 at $z = 6.42$ (Walter et al. 2003, 2004, 2009a; Riechers et al. 2009a; Wang et al. 2013). This and similar systems represent the coeval formation of massive galaxies and SMBHs within 1 Gyr of the Big Bang. Large-scale cosmological simulations show that massive galaxies and SMBHs can form at

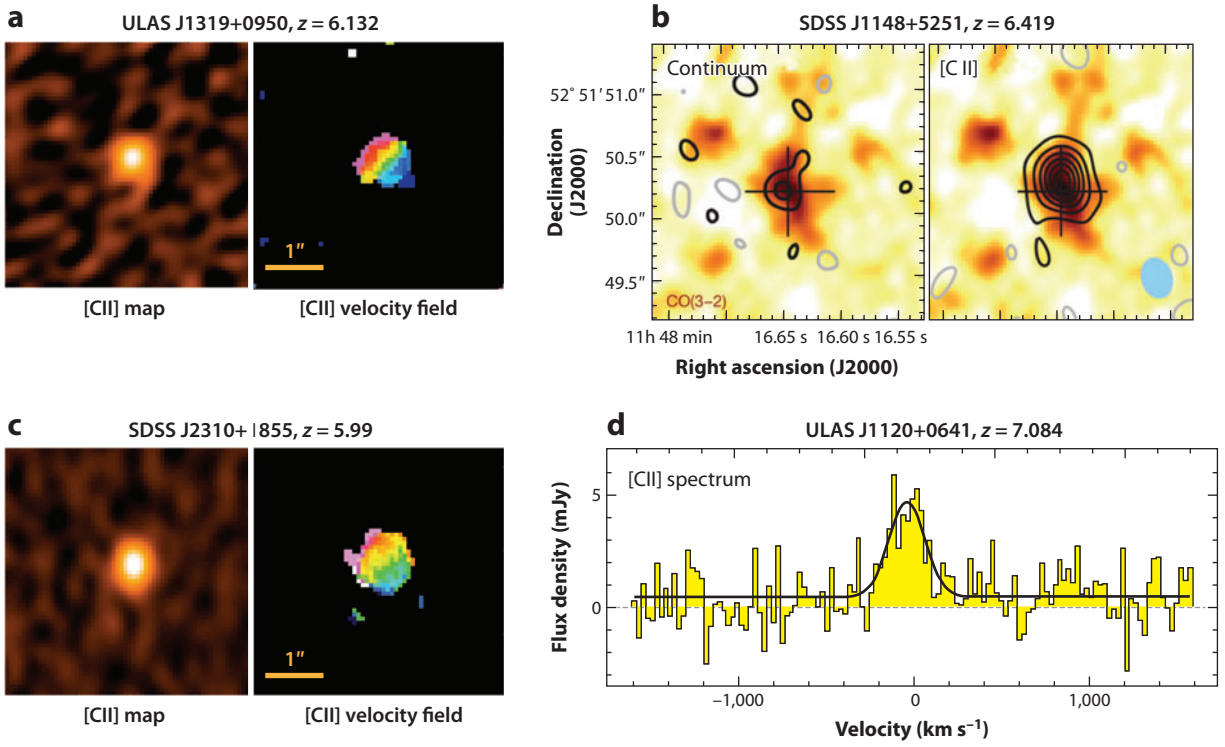

Figure 10

Results from observations of [CII] 158-μm emission from $z \geq 6$ quasars. (*a*,*c*) Atacama Large Millimeter/Submillimeter Array images of the total intensity plus the intensity-weighted mean gas velocity for two SDSS quasars (Wang et al. 2013). The velocity range in panel *a* is ± 300 km s^{-1} (*red* to *blue*), whereas that in panel *c* is ± 100 km s^{-1}. Note the clear velocity gradients, consistent with gas rotation on scales of ∼7 kpc (∼1 arcsec at $z \sim 6$). (*b*) The Very Large Array CO images of the $z = 6.42$ SDSS quasar, J1148+5251, as color scale in both frames. The contours on the left show the 250-GHz continuum emission, and those on the right show the [CII] 158-μm emission imaged by the Plateau de Bure interferometer (PdBI) (from Walter et al. 2009b). (*d*) The PdBI [CII] 158-μm spectrum of the most distant spectroscopic redshift quasar known, a quasar at $z = 7.08$ (Venemans et al. 2012). Abbreviation: ULAS, UKIDSS (UK Infrared Deep Sky Survey) Large Area Survey.

$z \sim 6$ via gas-rich mergers, driving extreme starbursts, and rapid accretion onto the black holes, with subsequent black hole mergers (Li et al. 2007). Such systems are thought to evolve into large galaxies in rich clusters at low z. More recent simulations suggest that cold accretion from the IGM may also play a role in, and possibly even dominate, the gas resupply (Khandai et al. 2012). As the SMBH builds, feedback from the AGN expels gas from the galaxy and hinders further accretion, thereby terminating star formation in the galaxy (Maiolino et al. 2012).

Exciting results have been obtained via imaging of the [CII] 158-μm line in $z > 6$ galaxies, as demonstrated in **Figure 10**. Imaging of [CII] emission from the highest redshift SDSS quasars ($z \sim 6$) shows velocity gradients indicative of rotation, with disk scales of order a few kiloparsecs (Wang et al. 2013). In a number of cases, the [CII] emission indicates "maximal starburst disks" on scales ∼1 kpc (Walter et al. 2009a; Wang et al. 2013; and see Section 4.2). [CII] has also been detected in the most distant quasar known, at $z = 7.08$ (Venemans et al. 2012). From the dust continuum emission for this system, Venemans et al. derive a SFR ~ 300 $M_\odot$ year^{-1}.

The gas dynamics in distant quasar host galaxies allows for a study of the evolution of the black hole–bulge mass relation. Wang et al. (2010) present the most detailed analysis to date

FIRST GALAXIES

The presence of detectable CO and [CII] (and dust) emission at redshifts out to $z = 7$ was almost inconceivable a little more than 10 years ago. At these redshifts, the age of the Universe was <1 Gyr, and there has been little time to enrich the ISM with carbon and oxygen, and then cool to form dust and molecules. The detection of molecular emission and FSL emission at $z > 6$ currently remains limited to HyLIRGs. These results reveal the coeval formation of massive galaxies and SMBHs in extreme starburst events within 1 Gyr of the Big Bang. Given the difficulties of detecting CO at the highest redshifts, [CII] and other FSLs will likely play the dominant role in the study of the star-forming ISM at the earliest epochs.

out to $z \sim 6$. In this study, the black hole masses are based on standard line-width relations of ionized gas and are consistent with simple Eddington arguments. They find that the median black hole–bulge mass ratio is 15 times higher at $z \sim 6$ than typically seen in nearby galaxies, although the scatter is close to an order of magnitude (see also Shields et al. 2006, Coppin et al. 2008). These results suggest that SMBHs may assemble before the mass in their host galaxies. Such a deviation has been predicted in hydrodynamical simulations of very early SMBHs and massive galaxy formation (Khandai et al. 2012). Most recently, Riechers et al. (2013) have discovered an SMG at $z = 6.3$ through red FIR color selection. They obtained a spectroscopic redshift via molecular and atomic FSL. They present numerous centimeter through submillimeter line detections, including multiple transitions of CO, water, ammonia, and FSLs. This system provides a clear demonstration of the detailed studies that can be performed on the cool ISM in very early galaxies.

As pointed out in Section 4.3.2, the [CII]/FIR ratio increases with decreasing metallicity. Hence, even if the dust content of star-forming galaxies at the highest redshifts were indeed to decrease (Bouwens et al. 2010b, 2011a; Walter et al. 2012b), the [CII] line might remain strong, and would be a key redshift determinant, and a primary means to image gas dynamics in the first galaxies because it traces both PDRs and the cold neutral medium. Early ALMA results have already demonstrated the ease with which LBGs and LAEs are detected in [CII] emission at $z \sim 5$ (see Section 4.3.2). The sidebar, First Galaxies, summarizes the progress and potential for studies of the cool gas in the first galaxies.

5.3. Spectral Deep Fields and the Dense Gas History of the Universe

Most observations of the molecular gas phase in the Universe have been restricted to galaxy populations that were preselected in the UV/optical/IR/FIR bands, i.e., based on their star-formation properties. However, in order to obtain an unbiased census of the molecular gas content in primeval galaxies, there is a clear need for a blind search of molecular gas down to mass limits characteristic of the normal star-forming galaxy population, i.e., a CO deep field. Such a CO deep field has been out of reach given past instrumentation, in terms both of sensitivity and instantaneous bandwidth. However, this situation is now dramatically changing with the advent of new observational facilities. Clearly, fields with the best photometric supporting data are preferred for rapid follow-up identification, as well as dense spectroscopic coverage, for possible "3D-stacking."

We note that a number of researchers have successfully used frequency scans to obtain redshifts from CO emission for sources that were very bright in the FIR but that had no easily identifiable counterpart in the optical, and therefore no redshift determination (Weiß et al. 2009, Lestrade

et al. 2010, Cox et al. 2011, Riechers 2011, Scott et al. 2011, Combes et al. 2012, Walter et al. 2012a). A good example of such a redshift search using CO is the recent GBT spectroscopic survey of Herschel-discovered SMGs, for which redshifts were determined for 11 of 24 galaxies observed (Harris et al. 2012). Likewise the ALMA survey of bright millimeter sources in the SPT survey has established millimeter scans as an efficient method by which to determine redshifts of dusty, distant galaxies (Weiß et al. 2013). Recent ALMA observations by Swinbank et al. (2012a) have shown the power of the [CII] 158-μm line as a redshift determinant at $z \geq 4$.

Cosmological simulations have been used to predict the cosmic evolution of the dense gas history of the Universe. Most of these models and simulations start with dark matter simulations, such as the Millennium simulations (Springel et al. 2005). The dark matter halos are then populated with model galaxies, and these evolve according to simple rules (semi-analytical modeling). In this modeling, each galaxy today has a well-defined history of growing and merging galaxies. Obreschkow et al. (2009b) applied post-processing to these galaxies to subdivide their cold gas masses into the atomic and molecular gas phases by assuming that the ISM pressure (Leroy et al. 2008, 2013) sets the phase balance between these two phases. As discussed in Section 4.2, an important complication is the CO luminosity–to–gas mass conversion factor. In a follow-up paper, Obreschkow et al. (2009a) predicted the CO luminosity functions for the various transitions of CO, including a number of effects, such as heating by starbursts and CMB, and metallicity dependence. Power, Baugh & Lacey (2010) compared a number of currently favored semianalytical galaxy models (again applying them to the Millennium simulation). Lagos et al. (2011) used a similar methodology, but with a different galaxy-formation model to separate the atomic and molecular gas phases of the ISM. Lagos et al. (2012) then refined their model through modeling the various rotational transitions of CO using a PDR code. All these models are scaled such that the CO(1–0) luminosity function at $z = 0$ is matched (Kereš et al. 2003).

An independent approach to predicting CO and H_2 luminosity functions as well as the cosmic evolution of the H_2/CO density is presented by M. T. Sargent and colleagues (in preparation). They separate the contributions of MS and starburst galaxies to the IR luminosity functions of galaxies at various redshifts and use the relation between CO luminosities and IR luminosities for these two populations to predict CO luminosities (see Section 4.5). They also use a metallicity-dependent conversion factor to go from predicted CO luminosities to H_2 masses (see Section 4.2). Other calculations of this type include those by Geach & Papadopoulos (2012) and Carilli & Blain (2002).

Figure 11 summarizes the various predictions put forward to date. **Figure 11*a*,*b*,*c*** shows the predicted CO luminosities in five redshift bins, including $z = 0$. The CO luminosity function has to date only been measured at $z = 0$ (see data points in **Figure 11*a*** by Kereš et al. 2003). The luminosity functions for all other redshift bins are essentially unconstrained.

The integral under each of the luminosity curves gives the total CO luminosity, which can then, under the assumption of a given conversion factor α, be translated to total molecular gas for each galaxy population. The summed density of this quantity is plotted in **Figure 12** for the models discussed above. We note that the cosmic density in HI, determined through studies of damped Lyα absorption line systems, appears to show little evolution at least through the epoch of galaxy assembly (Wolfe, Gawiser & Prochaska 2005).

The number of high-z detections of molecular gas in CSGs remains limited, and to date no truly deep, wide-field spectral search has been performed. However, we are reaching a point where it may be possible to set limits on the evolution of the cosmic density of molecular gas. We here take a very simple approach, based on the measured stellar-to-gas mass ratios in existing [admittedly limited, e.g., Aravena et al. (2012)] samples and the cosmic stellar mass densities of these populations.

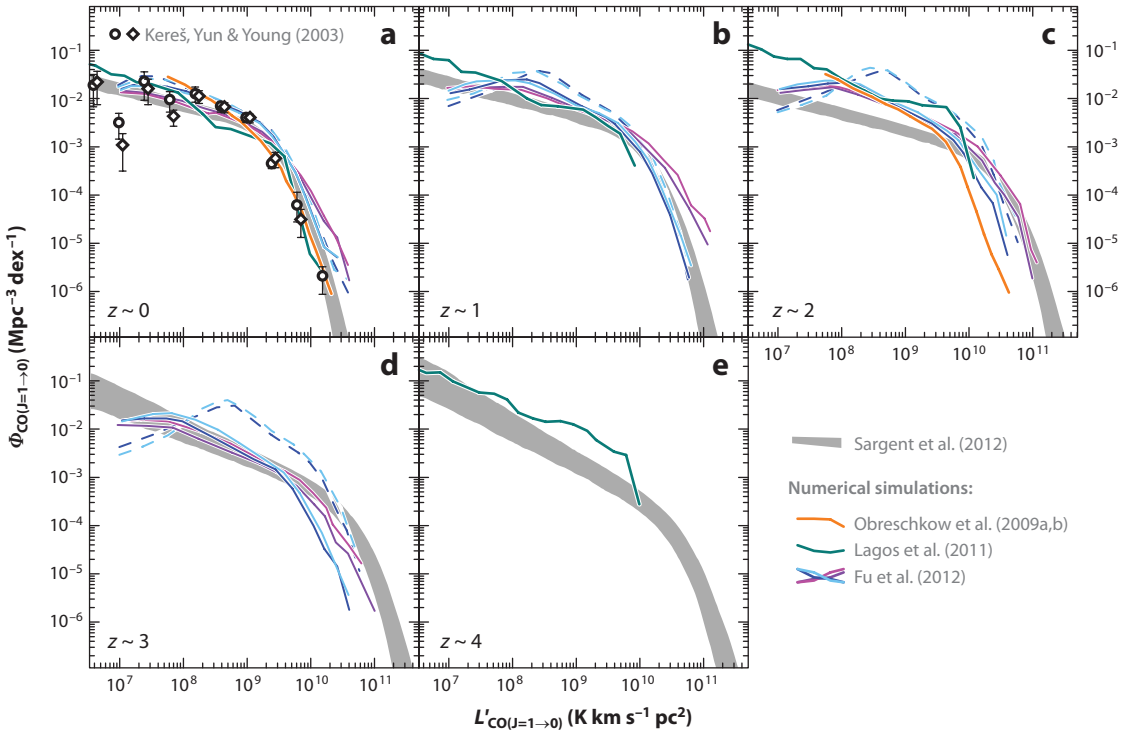

Figure 11

Models for the evolution of the CO luminosity function based on semianalytical cosmological models plus "recipes" to relate gas mass to CO luminosity (*colored lines*). The gray shading is from M. T. Sargent and colleagues (in preparation) and shows the indirectly inferred redshift evolution of the CO(1–0) luminosity function based on (1) the evolution of the stellar mass function of star-forming galaxies, (2) the redshift evolution of the specific star-formation rate (SFR) of main-sequence (MS) galaxies, (3) the distribution of MS and starbursting galaxies in the SFR-$M_\star$ plane (Sargent et al. 2012), (4) distinct prescriptions of the star-formation efficiency (SFE) of MS and starbursting galaxies, and (5) a metallicity-dependent conversion factor α_{CO}. The CO luminosity function includes contributions from both the MS galaxies and starbursts, where the latter is characterized by a more than 10-fold increase of the SFE. In panel *a* the observational constraints on the local CO luminosity function reported by Kereš, Yun & Young (2003) are also shown (M. T. Sargent and colleagues, in preparation).

For five sBzK galaxies at $z \sim 1.5$ to 2, Daddi et al. (2010a) find a mean value of $M_{gas}/M_{stars} = 1.15$. For ten BX/BM galaxies at $z \sim 2$ to 2.5, Tacconi et al. (2010) find $M_{gas}/M_{stars} = 0.79$. Tacconi et al. (2013) reach similar conclusions for CSGs at $z = 1.2$ and 2.2. Riechers et al. (2010b) measure a mean of $M_{gas}/M_{stars} = 1.4$ for two lensed LBGs at $z \sim 3$. At all redshifts, a value of $\alpha \sim 4 \pm 0.4$ was assumed (see also Magdis et al. 2012b). In all cases, the scatter in the ratio is close to a factor of two, and so for simplicity, we adopt $M_{gas}/M_{stars} = 1$ in all cases. Note that we focus on CSGs because their space density is more than an order of magnitude higher than for HyLIRGs, such as quasar hosts and SMGs, and their gas masses appear comparable (although there is a question of duty cycle in the latter samples). In this sense, these calculations represent lower limits.

Grazian et al. (2007) tabulate the total cosmic stellar mass density in different types of galaxies at different redshifts. They also quantify the substantial overlap between populations selected with the different techniques. At $z \sim 1.8$, they find the sBzK galaxies dominate the stellar mass density of the star-forming galaxy population (we assume only star-forming galaxies contribute

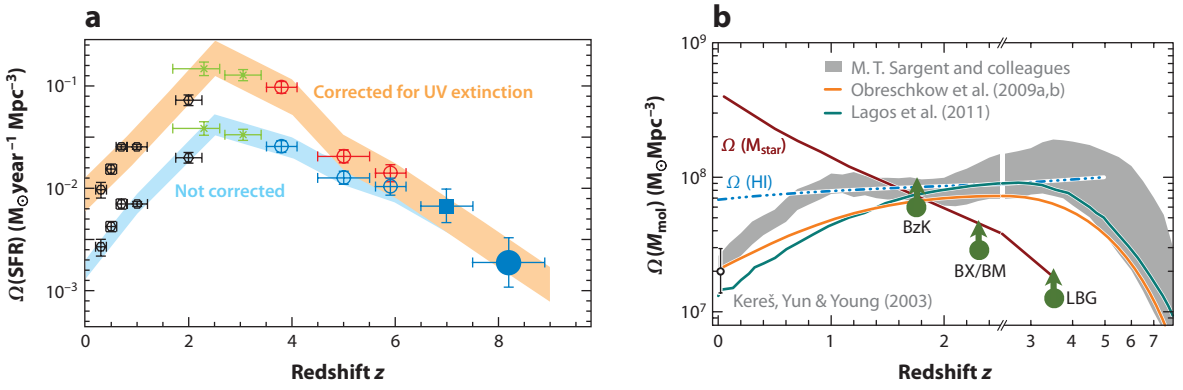

Figure 12

(*a*) Representation of the evolution of the cosmic star-formation rate density [adapted from the compilation by Bouwens et al. (2010)]. (*b*) The evolution of the cosmic cool gas mass density (M. T. Sargent and colleagues, in preparation), including predictions from semianalytical cosmological models (Obreschkow et al. 2009a,b; Lagos et al. 2011) as well as the models by M. T. Sargent and colleagues (in preparation). The latter shows the evolution inferred from the integration of the indirectly inferred molecular gas mass functions underlying the CO luminosity distributions of **Figure 11**. Also included are some admittedly extremely rough limits based on what is known about known galaxy populations at $z > 1$. These points illustrate the potential impact of molecular deep-field (blind) surveys.

to the cosmic gas density), with comoving stellar mass density of $\rho_{\rm stars} = 5.9 \times 10^7\,{\rm M}_\odot\,{\rm Mpc}^{-3}$. Likewise for BX/BM/LBG at $z \sim 2.5$, they find $\rho_{\rm stars} = 2.8 \times 10^7\,{\rm M}_\odot\,{\rm Mpc}^{-3}$, and at $z \sim 3.3$, $\rho_{\rm stars} = 1.2 \times 10^7\,{\rm M}_\odot\,{\rm Mpc}^{-3}$.

Assuming unity ratio with the gas mass, we can then establish lower limits to the cosmic gas mass density at the respective epochs, plotted in **Figure 12**. We also include the $z = 0$ measurement of Kereš, Yun & Young (2003). Interestingly, the sBzK limit is already pushing the cosmic density into the modeled regime based on, e.g., the SFHU and star-formation laws.

We emphasize that this analysis is mainly illustrative, with very substantial uncertainties. First, we assume the unity gas–to–stellar mass ratios hold for galaxies well below the masses of those currently observed in CO. In particular, the galaxies in the Daddi et al. (2010a) and Tacconi et al. (2010) samples were typically at the high-mass end of the CSG distribution, although having MS galaxy properties otherwise (e.g., sSFR, gas consumption timescales). Interestingly, the larger sample studied by Tacconi et al. (2013) shows a trend for increasing gas fraction with decreasing stellar mass, which would increase the cosmic gas densities in **Figure 12**. Second, we adopt a standard GMC value of α, when in fact this value could increase dramatically with, e.g., decreasing metallicity, such that the GMC value radically underestimates the total gas mass (e.g., Genzel et al. 2012). And third, we currently cannot rule out a population of lower-mass, gas-rich galaxies that do not appear in any optical survey. The sidebar, Molecular Deep Fields, discusses the potential for deep and large bandwidth observations to trace out the dense gas history of the Universe.

6. CONCLUDING REMARKS

Over the past decade, observations of the cool ISM in distant galaxies via molecular line and atomic FSL emission has gone from a curious look into a few extreme, rare objects to a mainstream tool in the study of galaxy formation, out to the highest redshifts ($z \sim 7$). Molecular gas has now

MOLECULAR DEEP FIELDS

Studies of the molecular medium at high redshift have been restricted to galaxies that have been preselected in the optical or IR wavebands through their star-formation activity. This could potentially lead to a biased view of the molecular gas properties of high-redshift galaxies. A promising way forward is through observations of molecular deep fields, i.e., complete frequency scans toward regions in the sky that have superb multiwavelength observations available. Such observations were prohibitive given the sensitivity and bandwidth of past facilities; this is a situation that will be changing with ALMA and the JVLA. The principal remaining uncertainty in determining the cosmic space density of molecular gas [$\Omega_{H2}(z)$] will be the calibration of the conversion factor, α.

been observed in close to 200 galaxies, including numerous AGN host-galaxies, extreme starburst SMGs, and increasing samples of main-sequence galaxies selected via their optical or near-IR colors. Studies have moved well beyond simple detection to dynamical imaging at kiloparsec-scale resolution and multiline, multispecies studies of the ISM in early galaxies. Study of atomic FSL emission is also rapidly accelerating, with some tens of galaxies detected in [CII] 158-μm emission, and other species, at $z > 1$, including detection of the most distant quasar with a spectroscopic redshift ($z = 7.08$).

The results of these studies are extremely telling for models of galaxy formation, providing the required complement to studies of the stars and star formation in early galaxies. One of the most exciting empirical results is the discovery that CSGs have CO luminosities approaching those of SMGs and quasar hosts, but FIR luminosities that are close to an order of magnitude lower than SMGs. The higher space density of the CSGs provides a rich hunting ground for molecular line studies of distant galaxies. Observations suggest that the gas fraction (M_{gas}/M_{stars}) in massive disk galaxies increases by an order of magnitude from $z \sim 0$ to $z \geq 1.5$. Hence, the epoch of peak cosmic star-formation density corresponds to an epoch of gas-dominated disks.

For the rarer, hyperstarburst galaxies, the quasar hosts and powerful radio galaxies show the most extreme gas properties, in terms of gas excitation, SFE, and compact, although complex, gas morphologies. These results indicate compact, hyperstarbursts coeval with Eddington-limited AGN accretion. SMGs are a mixed bag of gas-rich mergers and extended, gas-rich disks.

Current measurements suggest that the hyperstarbursts have a low CO luminosity–to–gas mass conversion factor, $\alpha \sim 0.8$, consistent with the extreme dense ISM conditions seen in nearby nuclear starbursts. The CSGs are consistent with an MW GMC value of $\alpha \sim 4$. There is increasing evidence that α increases with decreasing metallicity in galaxies, and in general, there may be a continuum of values of α, depending on ISM pressure, dynamics, and metallicity. The correlation between CO and FIR luminosity suggests two populations: starburst galaxies with rapid gas consumption timescales of a few $\times 10^7$ years, and MS galaxies with gas consumption timescales an order of magnitude longer.

The strong ISM gas cooling line from [CII] is proving to be a key tool in the study of the dynamics of the earliest galaxies. [CII] imaging of $z > 4$ galaxies has already revealed a maximal starburst disk on subkiloparsec scales, likely rotating disks on a few to 10-kpc scales, and possible tidal structures on even larger scales. ALMA has already demonstrated the ability to detect [CII] emission from LAEs and LBGs at high redshift.

We have made a first attempt at quantifying the dense gas history of the Universe, based on current observations. Although admittedly gross, these measurements are consistent with

modeling based on large-scale cosmological simulations and on empirical models based on assumed star-formation laws.

7. FUTURE DIRECTIONS

We stand at a cusp in knowledge, with the breathtaking promise of the ALMA and JVLA poised to revolutionize the study of the cool gas in early galaxies, and we have presented some of the early science results from these telescopes. Later in the decade, telescopes such as Cerro Chajnantor Atacama Telescope and the Northern Extended Millimeter Array will also make important contributions through their wide-field and wide-bandwidth imaging capabilities.

We are no longer limited by numbers of high-z sources to study—there are thousands of CSGs, quasars, and SMGs from cosmological deep fields. These populations have been delineated in terms of their space density, cosmic environment, and redshift distribution in remarkable detail. At this stage, we feel it is the high-resolution imaging capabilities of ALMA and the JVLA that will be most incisive for unraveling the complex processes involved in early galaxy formation. Some of the key questions that need to be addressed include:

- For interpreting CO observations, the key uncertainty remains the conversion factor, especially in low-metallicity systems where lack of dust shielding may dramatically reduce the CO content. We expect calibrating this relationship will follow the current path using multiple methods, including dynamics, radiative transfer modeling, and dust-to-gas modeling, leading to a concordance of estimates, and likely multiparameter models involving, e.g., metallicity.
- Spatially resolved (subkiloparsec) imaging of multiple CO transitions, as well as of the thermal dust continuum emission, is needed to study the relative distribution and excitation of the fuel for star formation with respect to regions of active star formation. Such imaging also allows for a study of star-formation laws as a function of surface brightness, and not integrated quantities.
- Observations of high-dipole-moment molecules, and other complex molecules, will allow for detailed astrochemical modeling of the dense gas immediately involved in active star formation in distant galaxies.
- An inventory of FSLs is required to set the ISM gas cooling budget, the AGN versus star-formation indicators, and metallicity determinations.
- Studies of the [CII] 158-μm line will play an increasingly important role in the determination of redshifts and dynamics of the first galaxies, well into cosmic reionization.

The new telescopes coming on line open up the very real possibility of performing blind, deep-field surveys for molecular gas, and atomic FSL emission, from distant galaxies. Over the next few years, we expect that the dense gas history of the Universe diagram will be fully populated, as the CO luminosity functions and conversion factors are quantified out to the highest redshifts. Coupled with the near-IR through X-ray studies of stars, star formation, and AGN, such panchromatic deep fields will provide a complete picture of the conversion of gas into stars over the history of the Cosmos.

DISCLOSURE STATEMENT

The authors are not aware of any affiliations, memberships, funding, or financial holdings that might be perceived as affecting the objectivity of this review.

ACKNOWLEDGMENTS

The authors are indebted to their many long-term collaborators who have all greatly contributed to the field of high-redshift molecular gas emission. They include M. Aravena, F. Bertoldi, P. Cox, E. Daddi, R. Decarli, J. Hodge, K. Menten, R. Neri, D. Riechers, J. Wagg, R. Wang, and A. Weiss. We thank E. da Cunha, R. Decarli, D. Narayanan, D. Riechers, M. Sargent, G. Stacey, L. Tacconi, A. van der Wel, E. van Dishoeck, and A. Weiss for their valuable detailed input regarding this manuscript. We thank R. Bouwens, J. Hodge, D. Riechers, M. Sargent, L. Tacconi, B. Venemans, and R. Wang for permission to reproduce some of their figures, and we thank R. Decarli in particular for his help with preparing the figures. F.W. thanks the Aspen Center for Physics, where part of this work was conducted. C.L.C. thanks the Astrophysics Group, Cavendish Laboratory, Cambridge, for support while much of this manuscript was written.

LITERATURE CITED

Alexander DM, Bauer F, Chapman SC, Smail I, Blain AW, et al. 2005. *Ap. J.* 632:736–50
Ao Y, Weiß A, Downes D, Walter F, Henkel C, Menten KM. 2008. *Astron. Astrophys.* 491:747–54
Aravena M, Carilli C, Daddi E, Wagg J, Walter F, et al. 2010. *Ap. J.* 718:177–83
Aravena M, Carilli CL, Salvato M, Tanaka M, Lentati L, et al. 2012. *MNRAS* 426:258
Baker AJ, Tacconi LJ, Genzel R, Lehnert MD, Lutz D. 2004. *Ap. J.* 604:125–40
Barvainis R, Maloney P, Antonucci R, Alloin D. 1997. *Ap. J.* 484:695
Barvainis R, Tacconi L, Antonnucci R, Alloin D, Coleman P. 1994. 371:586–88
Bauermeister A, Blitz L, Bollato AD, Bureau M, Leroy A, et al. 2013. *Ap. J.* 768:132
Bauermeister A, Blitz L, Ma C-P. 2010. *Ap. J.* 717:323–32
Bayet E, Gerin M, Phillips T, Contursi A. 2004. *Nature* 427:45–59
Beelen A, Cox P, Benford D, Dowell C, Kovacs A, et al. 2006. *Ap. J.* 642:694–701
Bell EF, van der Wel A, Papovich C, Kocevski D, Lotz J, et al. 2012. *Ap. J.* 753:167
Bertoldi F, Carilli CL, Cox P, Fan X, Strauss M, et al. 2003. *Astron. Astrophys.* 406:L55–58
Bertram T, Eckart A, Fischer S, Zuther J, Straubmeier C, et al. 2007. *Astron. Astrophys.* 470:571
Bigiel F, Leroy A, Walter F, Brinks E, de Blok WJG, et al. 2008. *Astron. J.* 136:2846–71
Bigiel F, Leroy AK, Walter F, Brinks E, de Blok WJG, et al. 2011. *Ap. J.* 730:L13
Blain A, Smail I, Ivison R, Kneib J-P, Frayer DT, et al. 2002. *Phys. Rep.* 369:111–76
Bloemen H. 1989. *Annu. Rev. Astron. Astrophys.* 27:469–516
Bolatto AD, Leroy AK, Wolfire M. 2013. *Annu. Rev. Astron. Astrophys.* 51:207–68
Bothwell M, Chapman SC, Tacconi L, Smail I, Ivison RJ, et al. 2010. *MNRAS* 405:219–33
Bothwell M, Smail I, Chapman SC, Genzel R, Ivison RJ, et al. 2013. *MNRAS*. 429:3047
Bournaud F, Elmegreen BG, Martig M. 2009. *Ap. J.* 707:L1–5
Bouwens R, Illingworth G, Labbé I, Oesch P, Trenti M, et al. 2011b. *Nature* 469:504–7
Bouwens R, Illingworth G, Oesch P, Franx M, Labbé I, et al. 2012b. *Ap. J.* 754:83
Bouwens R, Illingworth G, Oesch P, Labbé I, Trenti M, et al. 2011a. *Ap. J.* 737:90
Bouwens R, Illingworth G, Oesch P, Trenti M, Labbé I, et al. 2012a. *Ap. J.* 752:L5
Bouwens RJ, Illingworth GD, Oesch PA, Trenti M, Stiavelli M, et al. 2010. *Ap. J. Lett.* 708:L69
Bradač M, Vanzella E, Hall N, Treu T, Fontana A, et al. 2012. *Ap. J.* 755:L7
Bradford C, Nikola T, Stacey GJ, Bolatto AD, Jackson JM, et al. 2003. *Ap. J.* 586:891–901
Brown RL, Vanden Bout PA. 1991. *Astron. J.* 102:1956–59
Bryant PM, Scoville NZ. 1999. *Ap. J.* 117:2632–55
Carilli CL, Blain AW. 2002. *Ap. J.* 569:605–10
Carilli CL, Cox P, Bertoldi F, Menten KM, Omont A, et al. 2002. *Ap. J.* 575:145–49
Carilli CL, Hodge J, Walter F, Riechers D, Daddi E, et al. 2011. *Ap. J. Lett.* 739:L33
Carilli CL, Menten KM. 2002. *Highlights Astron.* 12:481
Carilli CL, Rawlings S. 2004. *New Astron. Rev.* 48:979

Carilli CL, Riechers D, Walter F, Maiolino R, Wagg J, et al. 2013. *Ap. J.* 763:120
Carilli CL, Yun MS. 1999. *Ap. J. Lett.* 513:L13–16
Carilli CL, Yun MS. 2000. *Ap. J.* 530:618–24
Casey C, Chapman SC, Daddi E, Dannerbauer H, Pope A, et al. 2009. *MNRAS* 400:670–76
Casey C, Chapman SC, Neri R, Bertoldi F, Smail I, et al. 2011. *MNRAS* 415:2723–43
Chapman SC, Blain AW, Ivison RJ, Smail IR. 2003. *Nature* 422:695–98
Chapman SC, Neri R, Bertoldi F, Smail I, Greve TR, et al. 2008. *Ap. J.* 689:889–96
Chung A, Narayanan G, Yun MS, Heyer M, Erickson NR. 2009. *Astron. J.* 138:858
Coe D, Zitrin A, Carrasco M, Shu X, Zheng W, et al. 2013. *Ap. J.* 762:32
Combes F. 2008. *Ap. Space Sci.* 313:321
Combes F, García-Burillo S, Braine J, Schinnerer E, Walter F, Colina L. 2011. *Astron. Astrophys.* 528:124
Combes F, García-Burillo S, Braine J, Schinnerer E, Walter F, Colina L. 2013. *Astron. Astrophys.* 550:41
Combes F, Maoli R, Omont A. 1999. *Astron. Astrophys.* 345:369–79
Combes F, Rex M, Rawle T, Egami E, Boone F, et al. 2012. *Astron. Astrophys.* 538:L4
Condon JJ. 1992. *Annu. Rev. Astron. Astrophys.* 30:575–611
Coppin KEK, Danielson ALR, Geach JE, Hodge JA, Swinbank AM, et al. 2012. *MNRAS* 427:520
Coppin KEK, Smail I, Alexander DM, Weiß A, Walter F, et al. 2009. *MNRAS* 395:1905–14
Coppin KEK, Swinbank AM, Neri R, Cox P, Alexander DM, et al. 2008. *MNRAS* 389:45–62
Coppin KEK, Swinbank AM, Neri R, Cox P, Smail I, et al. 2007. *Ap. J.* 665:936–43
Cormier D, Madden SC, Hony S, Contursi A, Poglitsch A, et al. 2010. *Astron. Astrophys.* 518:L57
Cox P, Krips M, Neri R, Omont A, Güsten R, et al. 2011. *Ap. J.* 740:63
Croton DJ, Springel V, White SDM, De Lucia G, Frenk C, et al. 2006. *MNRAS* 365:11–28
da Cunha E, Groves B, Walter F, Decarli R, Weiß A, et al. 2013. *Ap. J.* 766:13
Daddi E, Bournaud F, Walter F, Dannerbauer H, Carilli CL, et al. 2010a. *Ap. J.* 713:686–707
Daddi E, Cimatti A, Renzini A, Fontana A, Mignoli M, et al. 2004. *Ap. J.* 617:746–64
Daddi E, Dannerbauer H, Elbaz D, Dickinson M, Morrison G, et al. 2008. *Ap. J. Lett.* 673:L21–24
Daddi E, Dannerbauer H, Krips M, Walter F, Dickinson M, et al. 2009a. *Ap. J. Lett.* 695:L176
Daddi E, Dannerbauer H, Stern D, Dickinson M, Morrison G, et al. 2009b. *Ap. J.* 694:1517–38
Daddi E, Elbaz D, Walter F, Bournaud F, Salmi F, et al. 2010b. *Ap. J. Lett.* 714:L118
Dame TM, Hartmann D, Thaddeus P. 2001. *Ap. J.* 547:792–813
Danielson ALR, Swinbank AM, Smail I, Cox P, Edge AC, et al. 2011. *MNRAS* 410:1687–702
Dannerbauer H, Daddi E, Riechers DA, Walter F, Carilli CL, et al. 2009. *Ap. J. Lett.* 698:L178–82
Dannerbauer H, Lehnert MD, Lutz D, Tacconi L, Bertoldi F, et al. 2004. *Ap. J.* 606:664–82
Davé R, Finlator K, Oppenheimer B, Fardal M, Katz N, et al. 2010. *MNRAS* 404:1355–68
De Breuck C, Downes D, Neri R, van Breugel W, Reuland M, et al. 2005. *Astron. Astrophys.* 430:L1–4
De Breuck C, Maiolino R, Caselli P, Coppin K, Hailey-Dunsheath S, Nagao T. 2011. *Astron. Astrophys.* 530: L8
De Breuck C, Neri R, Morganti R, Omont A, Rocca-Volmerange B, et al. 2003. *Astron. Astrophys.* 401:911–25
De Breuck C, Neri R, Omont A. 2003. *New Astron. Rev.* 47:285–89
Decarli R, Walter F, Neri R, Bertoldi F, Carilli C, et al. 2012. *Ap. J.* 752:2
Dekel A, Birnboim Y. 2006. *MNRAS* 368:2–20
Dekel A, Birnboim Y, Engel G, Freundlich J, Goerdt T, et al. 2009. *Ap. J.* 457:451–54
Dekel A, Sari R, Ceverino D. 2009. *Ap. J.* 703:785–801
Dickman RL. 1975. *Ap. J.* 202:50–57
Dickman RL. 1978. *Ap. J. Suppl.* 37:407–27
Dickman RL, Snell RL, Schloerb FP. 1986. *Ap. J.* 309:326–30
Downes D, Solomon PM. 1998. *Ap. J.* 507:615–54
Draine BT, Dale DA, Bendo G, Gordon KD, Smith JDT, et al. 2007. *Ap. J.* 663:866–94
Draine BT, Li A. 2007. *Ap. J.* 657:810–37
Dressler A, Oemler A, Gladders M, Bai L, Rigby J, Poggianti B. 2009. *Ap. J. Lett.* 699:L130–33
Dyson JE, Williams DA. 1980. *Physics of the Interstellar Medium.* New York: Halsted
Elbaz D. 2002. *Ap. J.* 281:449–52

Elbaz D, Dickinson M, Hwang HS, Diaz-Santos T, Magdis G, GOODS-Herschel team. 2011. *Astron. Astrophys.* 533:119
Elmegreen BG, Burkert A. 2010. *Ap. J.* 712:294–302
Emonts BHC, Feain I, Mao M, Norris R, Miley G, et al. 2011. *Ap. J. Lett.* 734:L25
Emonts BHC, Feain I, Röttgering HJA, Miley G, Seymour N, et al. 2013. *MNRAS* 430:3465
Engel H, Tacconi LJ, Davies R, Neri R, Smail I, et al. 2010. *Ap. J.* 724:233–43
Erb DK, Shapley AE, Pettini M, Steidel CC, Reddy NA, Adelberger KL. 2006. *Ap. J.* 644:813
Evans AS. 2006. *New Astron. Rev.* 50:657
Evans AS, Frayer DT, Surace JA, Sanders DB. 2001. *Astron. J.* 121:1893
Fabian AC. 2012. *Annu. Rev. Astron. Astrophys.* 50:455–89
Fan X, Carilli CL, Keating B. 2006. *Annu. Rev. Astron. Astrophys.* 44:415–62
Feldmann R, Gnedin NY, Kravtsov AV. 2011. *Ap. J.* 732:115
Feldmann R, Gnedin NY, Kravtsov AV. 2012a. *Ap. J.* 747:124
Feldmann R, Gnedin NY, Kravtsov AV. 2012b. *Ap. J.* 758:127
Ferkinhoff C, Brisbin D, Nikola T, Parshley SC, Stacey GJ, et al. 2011. *Ap. J. Lett.* 740:L29
Ferkinhoff C, Hailey-Dunsheath S, Nikola T, Parshley S, Stacey GJ, et al. 2010. *Ap. J. Lett.* 714:L147–51
Feruglio C, Aussel H, Le Floc'h E, lbert O, Salvato M, et al. 2010. *Ap. J.* 721:607
Finkelstein SL, Papovich C, Ryan RE, Pawlik AH, Dickinson M, et al. 2012. *Ap. J.* 758:93
Finlator K, Davé R, Papovich C, Hernquist L. 2006. *Ap. J.* 639:672–94
Flower DR, Launay JM. 1985. *MNRAS* 214:271
Flower DR, Pineau des Forêts G. 2003. *MNRAS* 343:390–400
Franx M, Labbé I, Rudnick G, van Dokkum PG, Daddi E, et al. 2003. *Ap. J.* 587:L79–82
Frayer DT, Ivison RJ, Scoville NZ, Evans AS, Yun M, et al. 1999. *Ap. J. Lett.* 514:L13–16
Frayer DT, Ivison RJ, Scoville NZ, Yun M, Evans AS, et al. 1998. *Ap. J. Lett.* 506:L7–10
Fu J, Kauffmann G, Li C, Guo Q. 2012. *MNRAS* 424:2701
Fukugita M, Peebles PJE. 2004. *Ap. J.* 616:643–68
Gallerani S, Neri R, Maiolino R, Martin S, De Breuck C, et al. 2012. *Astron. Astrophys.* 543:A114
Gao Y, Solomon PM. 2004a. *Ap. J. Suppl.* 152:63–80
Gao Y, Solomon PM. 2004b. *Ap. J.* 606:271–90
García-Burillo S, Graciá-Carpio J, Guélin M, Neri R, Cox P, et al. 2006. *Ap. J. Lett.* 645:L17
Geach JE, Papadopoulos PP. 2012. *Ap. J.* 757:156
Geach JE, Smail I, Moran SM, MacArthur LA, Lagos CDP, Edge AC. 2011. *Ap. J.* 730:L19
Genzel R, Burkert A, Bouché N, Cresci G, Förster Schreiber NM, et al. 2008. *Ap. J.* 687:59–77
Genzel R, Cesarsky CJ. 2000. *Annu. Rev. Astron. Astrophys.* 38:761–814
Genzel R, Newman S, Jones T, Förster Schreiber NM, Shapiro K, et al. 2011. *Ap. J.* 733:101
Genzel R, Tacconi LJ, Combes F, Bolatto A, Neri R, et al. 2012. *Ap. J.* 746:69
Genzel R, Tacconi LJ, Eisenhauer F, Förster Schreiber NM, Cimatti A, et al. 2006. *Ap. J.* 442:786–89
Genzel R, Tacconi LJ, Graciá-Carpio J, Sternberg A, Cooper MC, et al. 2010. *MNRAS* 407:2091–108
Gerin M, Phillips T. 2000. *Ap. J.* 537:644–53
Giavalisco M. 2002. *Annu. Rev. Astron. Astrophys.* 40:579–641
Glover SCO, Clark PC. 2012. *MNRAS* 421:9
Glover SCO, Mac Low MM. 2011. *MNRAS* 412:337
Goldsmith PF, Langer WD. 1978. *Ap. J.* 222:881
González-Alfonso E, Fischer J, Isaak K, Rykala A, Savini G, et al. 2010. *Astron. Astrophys.* 518:L43
Grazian A, Salimbeni S, Pentericci L, Fontana A, Nonino M, et al. 2007. *Astron. Astrophys.* 465:393–404
Greve TR, Bertoldi F, Smail I, Neri R, Chapman SC, et al. 2005. *MNRAS* 359:1165–83
Greve TR, Ivison RJ, Papadopoulos PP. 2004. *Astron. Astrophys.* 419:99–107
Greve TR, Papadopoulos PP, Gao Y, Radford S. 2009. *Ap. J.* 692:1432–46
Greve TR, Pope A, Scott D, Ivison RJ, Borys C, et al. 2008. *MNRAS* 389:1489–506
Gromke JJ, Bradford CM, Bock JJ, Dragovan M, Duband L, et al. 2002. *Low Temp. Detect.* 605:543–46
Guilloteau S, Omont A, McMahon RG, Cox P, Petitjean P. 1997. *Astron. Astrophys.* 328:L1
Guo Q, White S. 2008. *Ap. J.* 384:2–10
Habart E, Dartois E, Abergel A, Baluteau J-P, Naylor D, et al. 2010. *Astron. Astrophys.* 518:L116

Hailey-Dunsheath S, Nikola T, Stacey GJ, Oberst T, Parshley S, et al. 2010. *Ap. J. Lett.* 714:L162–66
Hailey-Dunsheath S, Sturm E, Fischer J, Sternberg A, Graciá-Carpio J, et al. 2012. *Ap. J.* 755:57
Harris AI, Baker AJ, Frayer DT, Smail I, Swinbank AM, et al. 2012. *Ap. J.* 752:152
Harris AI, Baker AJ, Zonak S, Sharon C, Genzel R, et al. 2010. *Ap. J.* 723:1139–49
Harris AI, Stutzki J, Graf UU, Russell APG, Genzel R, Hills RE. 1991. *Ap. J. Lett.* 382:L75
Hayward CC, Jonsson P, Kereš D, Magnelli B, Hernquist L, Cox T. 2012. *MNRAS* 424:951
Helou G, Soifer B, Rowan-Robinson M. 1985. *Ap. J.* 298:L7
Henkel C, Downes D, Weiß A, Riechers D, Walter F. 2010. *Astron. Astrophys.* 516:111
Henkel C, Mauersberger R, Wiklind T, Hüttemeister S, Lemme C, Millar TJ. 1993. *Ap. J.* 268:L17–20
Hezaveh YD, Marrone DP, Fassnacht CD, Spilker JS, Vieira JD, et al. 2013. *Ap. J.* 767:132
Hickox R, Wardlow JL, Smail I, Myers A, Alexander DM, et al. 2012. *MNRAS* 421:284
Hodge JA, Carilli CL, Walter F, de Blok WJG, Riechers D, et al. 2012. *Ap. J.* 760:11
Hollenbach D, Kaufman MJ, Bergin EA, Melnick GJ. 2008. *Ap. J.* 690:1497–521
Hollenbach DJ, Tielens AGGM. 1999. *Rev. Mod. Phys.* 71:173–230
Hopkins PF, Bundy K, Croton D, Hernquist L, Kereš D, et al. 2010. *Ap. J.* 715:202–29
Hopkins PF, Hernquist L, Cox TJ, Di Matteo T, Robertson B, Springel V. 2006. *Ap. J. Suppl.* 163:1–49
Hughes DH, Serjeant S, Dunlop J, Rowan-Robinson M, Blain A, et al. 1998. *Nature* 394:241–47
Hunter SD, Bertsch DL, Catelli JR, Dame TM, Digel SW, et al. 1997. *Ap. J.* 481:205–40
Ikeda M, Oka T, Tatematsu K, Sekimoto Y, Yamamoto S. 2002. *Ap. J. Suppl.* 139:467–85
Ilbert O, Salvato M, Le Floc'h E, Aussel H, Capak P, et al. 2010. *Ap. J.* 709:644–63
Iono D, Tamura Y, Nakanishi K, Kawabe R, Kohno K, et al. 2006a. *Publ. Astron. Soc. Pac.* 58:957–63
Iono D, Yun MS, Elvis M, Peck AB, Ho PTP, et al. 2006b. *Ap. J.* 645:L97–100
Israel FP. 2005. *Ap. J.* 295:171–76
Israel FP, Baas F. 2002. *Nature* 383:82–90
Israel FP, Maloney P. 2011. *Astron. Astrophys.* 531:A19
Ivison RJ, Greve TR, Dunlop JS, Peacock J, Egami E, et al. 2007. *MNRAS* 380:199–228
Ivison RJ, Papadopoulos PP, Smail I, Greve TR, Thomson A, et al. 2011. *MNRAS* 412:1913–25
Ivison RJ, Smail I, Amblard A, Arumugam V, De Breuck C, et al. 2012. *MNRAS* 425:1320
Ivison RJ, Smail I, Barger A, Kneib J-P, Blain AW, et al. 2000. *MNRAS* 315:209–22
Ivison RJ, Smail I, Le Borgne J, Blain AW, Kneib J-P, et al. 1998. *MNRAS* 298:583–93
Ivison RJ, Smail I, Papadopoulos PP, Wold I, Richard J, et al. 2010a. *MNRAS* 404:198–205
Ivison RJ, Swinbank AM, Swinyard B, Smail I, Pearson C, et al. 2010b. *Astron. Astrophys.* 518:L35
Jiang L, Fan X, Brandt WN, Carilli CL, Egami E, et al. 2010. *Nature* 464:380–83
Kacprzak GG, Churchill CW, Steidel CC, Spitler LR, Holtzman JA. 2012. *MNRAS* 427:3029
Kennicutt RC Jr. 1998a. *Annu. Rev. Astron. Astrophys.* 36:189–232
Kennicutt RC Jr. 1998b. *Ap. J.* 498:541
Kennicutt RC Jr, Calzetti D, Walter F, Helou G, Hollenbach DJ, et al. 2007. *Ap. J.* 671:333–48
Kennicutt RC Jr, Evans NJ. 2012. *Annu. Rev. Astron. Astrophys.* 50:531–608
Kereš D, Katz N, Fardal M, Davé R, Weinberg DH. 2009. *Ap. J.* 395:160–79
Kereš D, Katz N, Weinberg D, Davé R. 2005. *MNRAS* 363:2–28
Kereš D, Yun MS, Young JS. 2003. *Ap. J.* 582:659–67
Khandai N, Feng Y, DeGraf C, Di Matteo T, Croft RAC. 2012. *Ap. J.* 423:2397–406
Klypin AA, Trujillo-Gomez S, Primack J. 2011. *Ap. J.* 740:102
Komatsu E, Smith KM, Dunkley J, Bennett C, Gold B, et al. 2011. *Ap. J. Suppl.* 192:18
Kovács A, Chapman SC, Dowell CD, Blain AW, Ivison RJ, et al. 2006. *Ap. J.* 650:592–603
Kovács A, Omont A, Beelen A, Lonsdale C, Polletta M, et al. 2010. *Ap. J.* 717:29–39
Kriek M, van Dokkum PG, Franx M, Quadri R, Gawiser E, et al. 2006. *Ap. J.* 649:L71–74
Kristensen LE, Ravkilde TL, Pineau des Forêts G, Cabrit S, Field D, et al. 2008. *Astron. Astrophys.* 477:203–11
Krumholz MR, Dekel A, McKee CF. 2011. *Ap. J.* 745:69
Krumholz MR, Thompson TA. 2012. *Ap. J.* 760:155
Lagos CDP, Baugh CM, Lacey CG, Benson AJ, Kim H-S, Power C. 2011. *MNRAS* 418:1649–67
Lagos CDP, Bayet E, Baugh CM, Lacey CG, Bell T, et al. 2012. *MNRAS* 426:2142

Lapi A, Cavaliere A, Menci N. 2005. *Ap. J.* 619:60–72
Larson RB. 1981. *MNRAS* 194:809–26
Leipski C, Meisenheimer K, Klaas U, Walter F, Nielbock M, et al. 2010. *Astron. Astrophys.* 518:L34
Leipski C, Meisenheimer K, Walter F, Besel M-A, Dannerbauer H, et al. 2013. *Ap. J.* In press (arXiv:1305.3999)
Lequeux J. 2005. *The Interstellar Medium, EDP Sciences.* Astron. Astrophys. Libr. Berlin: Springer
Leroy AK, Bolatto A, Gordon K, Sandstrom K, Gratier P, et al. 2011. *Ap. J.* 737:12
Leroy AK, Walter F, Bigiel F, Usero A, Weiß A, et al. 2009. *Astron. J.* 137:4670
Leroy AK, Walter F, Brinks E, Bigiel F, de Blok WJG, et al. 2008. *Astron. J.* 136:2782–845
Leroy AK, Walter F, Sandstrom K, Schruba A, Munoz-Mateos J-C, et al. 2013. *Astron. J.* 146(2):19
Lestrade J-F, Combes F, Salomé P, Omont A, Bertoldi F, et al. 2010. *Astron. Astrophys.* 522:L4
Leurini S, Wyrowski F, Herpin F, van der Tak F, Guesten R, van Dishoeck EF. 2013. *Astron. Astrophys.* 550:10
Li Y, Hernquist L, Robertson B, Cox TJ, Hopkins PF, et al. 2007. *Ap. J.* 665:187–208
Lilly SJ, Le Fevre O, Hammer F, Crampton D. 1996. *Ap. J. Lett.* 460:L1
Liu G, Koda J, Calzetti D, Fukuhara M, Momose R. 2011. *Ap. J.* 735:63
Luhman ML, Satyapal S, Fischer J, Wolfire MG, Sturm E, et al. 2003. *Ap. J.* 594:758
Madau P, Ferguson HC, Dickinson ME, Giavalisco M, Steidel CC, Fruchter A. 1996. *MNRAS* 283:1388–404
Magdis GE, Daddi E, Béthermin M, Sargent M, Elbaz D, et al. 2012a. *Ap. J.* 760:6
Magdis GE, Daddi E, Elbaz D, Sargent M, Dickinson M, et al. 2011. *Ap. J. Lett.* 740:L15
Magdis GE, Daddi E, Sargent M, Sargent M, Elbaz D, et al. 2012b. *Ap. J. Lett.* 758:L9
Magnelli B, Elbaz D, Chary RR, Dickinson M, Le Borgne D, et al. 2011. *Astron. Astrophys.* 528:A35
Magnelli B, Lutz D, Berta S, Altieri B, Andreani P, et al. 2010. *Astron. Astrophys.* 518:L28
Magnelli B, Saintonge A, Lutz D, Tacconi LJ, Berta S, et al. 2012. *Astron. Astrophys.* 548:A22
Maiolino R, Neri R, Beelen A, Bertoldi F, Carilli CL, et al. 2005. *Astron. Astrophys.* 472(2):L33–37
Maiolino R, Caselli P, Nagao T, Walmsley M, De Breuck C, Meneghetti M. 2009. *Astron. Astrophys.* 500:L1–4
Maiolino R, Gallerani S, Neri R, Cicone C, Ferrara A, et al. 2012. *MNRAS* 425:L66–70
Malhotra S, Helou G, Stacey G, Hollenbach D, Lord S, et al. 1997. *Ap. J.* 491:L27–30
Malhotra S, Kaufman MJ, Hollenbach D, Helou G, Rubin R, et al. 2001. *Ap. J.* 561:766–86
Manoj P, Watson DM, Neufeld DA, Megeath ST, Vavrek R, et al. 2013. *Ap. J.* 763:83
Mao R-Q, Henkel C, Schulz A, Zielinsky M, Mauersberger R, et al. 2000. *Ap. J.* 358:433–50
Marchesini D, van Dokkum PG, Förster Schreiber NM, Franx M, Labbé I, Wuyts S. 2009. *Ap. J.* 701:1765–96
Martig M, Bournaud F, Teyssier R, Dekel A. 2009. *Ap. J.* 707:250–67
Martin CL. 1998. *Ap. J.* 506:222–52
McNamara B, Nulsen P. 2007. *Annu. Rev. Astron. Astrophys.* 45:117
Meijerink R, Kristensen LE, Weiß A, van der Werf PP, Walter F, et al. 2013. *Ap. J. Lett.* 762:L16
Meijerink R, Spaans M. 2005. *Astron. Astrophys.* 436:397
Meijerink R, Spaans M, Israel FP. 2006. *Ap. J.* 650:L103–6
Miley G, De Breuck C. 2008. *Astron. Astrophys. Rev.* 15:67–144
Momjian E, Carilli CL, Riechers DA, Walter F. 2007. *Astron. J.* 134:694–97
Mookerjea B, Kramer C, Buchbender C, Boquien M, Verley S, et al. 2011. *Astron. Astrophys.* 532:A152
Moster BP, Somerville RS, Maulbetsch C, van den Bosch FC, Maccio AV, et al. 2010. *Ap. J.* 710:903–23
Murphy EJ, Chary R-R, Dickinson M, Pope A, Frayer DT, Lin L. 2011. *Ap. J.* 732:126
Naab T, Johansson PH, Ostriker JP. 2009. *Ap. J.* 699:L178–82
Nagao T, Maiolino R, De Breuck C, Caselli P, Hatsukade B, Saigo K. 2012. *Astron. Astrophys.* 542:L34
Narayanan D, Cox TJ, Hayward CC, Hernquist L. 2010a. *Ap. J.* 412:287–94
Narayanan D, Hayward CC, Cox TJ, Hernquist L, Jonsson P, et al. 2010b. *Ap. J.* 401:1613–19
Narayanan D, Hopkins P. 2013. *MNRAS*. Accepted (arXiv:1210.2724)
Narayanan D, Krumholz MR, Ostriker EC, Hernquist L. 2012. *MNRAS* 421:3127
Negrello M, Hopwood R, De Zotti G, Cooray A, Verma A, et al. 2010. *Science* 330:800
Neri R, Genzel R, Ivison RJ, Bertoldi F, Blain AW, et al. 2003. *Ap. J.* 597:L113–16
Neufeld DA, Kaufman MJ. 1993. *Ap. J.* 418:263
Neufeld DA, Lepp S, Melnick GJ. 1995. *Ap. J. Suppl.* 100:132

Nikola T, Stacey GJ, Brisbin D, Ferkinhoff C, Hailey-Dunsheath S, et al. 2011. *Ap. J.* 742:88
Noeske K, Weiner B, Faber S, Papovich C, Koo D, et al. 2007. *Ap. J. Lett.* 660:L43–46
Oberst T, Parshley S, Stacey GJ, Nikola T, Löhr A, et al. 2006. *Ap. J.* 652:L125–28
Obreschkow D, Croton D, De Lucia G, Khochfar S, Rawlings S. 2009a. *Ap. J.* 698:1467
Obreschkow D, Heywood I, Klöckner H-R, Rawlings S. 2009b. *Ap. J.* 702:1321–35
Ojha R, Stark AA, Hsieh HH, Lane AP, Chamberlin RA, et al. 2001. *Ap. J.* 548:253–57
Omont A. 2007. *Rep. Prog. Phys.* 70:1099
Omont A, Cox P, Bertoldi F, McMahon R, Carilli C, Isaak KG. 2001. *Astron. Astrophys.* 374:371–81
Omont A, Neri R, Cox P, Lupu R, Guélin M, et al. 2011. *Astron. Astrophys.* 530:L3
Omont A, Petitjean P, Guilloteau S, McMahon RG, Solomon PM, Pécontal E. 1996. *Nature* 382:428–31
Onodera S, Kuno N, Tosaki T, Kohno K, Nakanishi K, et al. 2010. *Ap. J. Lett.* 722:L127
Ostriker E, Shetty R. 2011. *Ap. J.* 731:41
Pannella M, Carilli CL, Daddi E, McCracken H, Owen F, et al. 2009. *Ap. J. Lett.* 698:L116–20
Panuzzo P, Rangwala N, Rykala A, Isaak KG, Glenn J, et al. 2010. *Astron. Astrophys.* 518:L37
Papadopoulos PP, Pelupessy FI. 2010. *Ap. J.* 717:1037–42
Papadopoulos PP, Röttgering H, van der Werf PP, Guilloteau S, Omont A, et al. 2000. *Ap. J.* 528:626–36
Papadopoulos PP, van der Werf P, Xilouris E, Isaak KG, Gao Y. 2012. *Ap. J.* 751:10
Peacock JA, Cole S, Norberg P, Baugh CM, Bland-Hawthorn J, et al. 2001. *Nature* 410:169–73
Peng Y-J, Lilly SJ, Kovac K, Bolzonella M, Pozzetti L, et al. 2010. *Ap. J.* 721:193–221
Pentericci L, Fontana A, Vanzella E, Castellano M, Grazian A, et al. 2011. *Ap. J.* 743:132
Perley R, Chandler CJ, Butler B, Wrobel J. 2011. *Ap. J. Lett.* 739:L1
Pety J, Beelen A, Cox P, Downes D, Omont A, et al. 2004. *Astron. Astrophys.* 428:L21–24
Planck Collab., Ade PAR, Aghanim N, Armitage-Caplan C, Arnaud M, Ashdown M, et al. 2013. In press (arXiv:1303.5062)
Pope A, Scott D, Dickinson M, Chary R-R, Morrison G, et al. 2006. *MNRAS* 370:1185–207
Power C, Baugh C, Lacey CG. 2010. *Ap. J.* 406:43–59
Priddey RS, Isaak KG, McMahon RG, Robson EI, Pearson C. 2003. *MNRAS* 344:L74–78
Rahman N, Bolatto AD, Wong T, Leroy AK, Walter F, et al. 2011. *Ap. J.* 730:72
Rahman N, Bolatto AD, Xue R, Wong T, Leroy AK, et al. 2012. *Ap. J.* 745:183
Reddy NA, Steidel CC, Pettini M, Adelberger KL, Shapley AE, et al. 2008. *Ap. J. Suppl.* 175:48–85
Reid BA, Percival WJ, Eisenstein DJ, Verde L, Spergel DN, et al. 2010. *MNRAS* 404:60–85
Renzini A. 2006. *Annu. Rev. Astron. Astrophys.* 44:141–92
Ribaudo J, Lehner N, Howk JC, Werk JK, Tripp TM, et al. 2011. *Ap. J.* 743:207
Riechers DA. 2011. *Ap. J.* 730:108
Riechers DA, Bradford CM, Clements DL, Dowell CD, Pérez-Fournon I, et al. 2013. *Nature* 496:329–33
Riechers DA, Capak P, Carilli CL, Cox P, Neri R, et al. 2010a. *Ap. J. Lett.* 720:L131–36
Riechers DA, Carilli CL, Maddalena RJ, Hodge J, Harris AI, et al. 2011a. *Ap. J. Lett.* 739:L32
Riechers DA, Carilli CL, Walter F, Momjian E. 2010b. *Ap. J. Lett.* 724:L153–57
Riechers DA, Cooray A, Omont A, Neri R, Harris AI, et al. 2011b. *Ap. J. Lett.* 733:L12
Riechers DA, Hodge J, Walter F, Carilli CL, Bertoldi F. 2011c. *Ap. J. Lett.* 739:L31
Riechers DA, Walter F, Bertoldi F, Carilli CL, Aravena M, et al. 2009a. *Ap. J.* 703:1338–45
Riechers DA, Walter F, Brewer BJ, Carilli CL, Lewis GF, et al. 2008a. *Ap. J.* 686:851–58
Riechers DA, Walter F, Carilli CL, Bertoldi F. 2007a. *Ap. J. Lett.* 671:L13–16
Riechers DA, Walter F, Carilli CL, Bertoldi F, Momjian E. 2008b. *Ap. J.* 686:L9–12
Riechers DA, Walter F, Carilli CL, Cox P, Weiß A, et al. 2011d. *Ap. J.* 726:50
Riechers DA, Walter F, Carilli CL, Knudsen KK, Lo KY, et al. 2006a. *Ap. J.* 650:604–13
Riechers DA, Walter F, Carilli CL, Lewis GF. 2009b. *Ap. J.* 690:463–85
Riechers DA, Walter F, Carilli CL, Weiß A, Bertoldi F, et al. 2006b. *Ap. J. Lett.* 645:L13–16
Riechers DA, Walter F, Cox P, Carilli CL, Weiß A, et al. 2007b. *Ap. J.* 666:778–83
Riechers DA, Weiß A, Walter F, Wagg J. 2010c. *Ap. J.* 725:1032–39
Robertson B, Bullock JS, Cox TJ, Di Matteo T, Hernquist L, et al. 2006. *Ap. J.* 645:986–1000
Robertson BE, Bullock JS. 2008. *Ap. J.* 685:L27–30
Rodighiero G, Daddi E, Baronchelli I, Cimatti A, Renzini A, et al. 2011. *Ap. J. Lett.* 739:L40

Rodriguez-Fernandez NJ, Braine J, Brouillet N, Combes F. 2006. *Astron. Astrophys.* 453:77–82
Röllig M, Abel NP, Bell T, Bensch F, Black J, et al. 2007. *Astron. Astrophys.* 467:187
Salomé P, Guélin M, Downes D, Cox P, Guilloteau S, et al. 2012. *Astron. Astrophys.* 545:A57
Sanders DB, Mazzarella JM, Kim DC, Surace J, Soifer B. 2003. *Astron. J.* 126:1607–64
Sandstrom K, Leroy A, Walter F, Bolatto A, Croxall K, et al. 2013. *Ap. J.* Submitted (arXiv:1212.1208)
Sargent MT, Béthermin M, Daddi E, Elbaz D. 2012. *Ap. J.* 747:L31
Sargsyan L, Lebouteiller V, Weedman D, Spoon H, Bernard-Salas J, et al. 2012. *Ap. J.* 755:171
Schinnerer E, Carilli CL, Capak P, Martinez-Sansigre A, Scoville NZ, et al. 2008. *Ap. J. Lett.* 689:L5–8
Schmidt M. 1959. *Ap. J.* 129:243
Schöier FL, van der Tak FFS, van Dishoeck EF, Black JH. 2005. *Astron. Astrophys.* 432:369–79
Schruba A, Leroy AK, Walter F, Sandstrom K, Rosolowsky E. 2010. *Ap. J.* 722:1699–706
Scott K, Lupu R, Aguirre J, Auld R, Aussel H, et al. 2011. *Ap. J.* 733:29
Scoville NZ. 2012. *Proc. XXIII Canary Islands Winter Sch. Astrophys.: Secular Evolution of Galaxies*, ed. J Falcon-Barroso, JH Knapen. Cambridge, UK: Cambridge Univ. Press (arXiv:1210.6990)
Scoville NZ, Frayer DT, Schinnerer E, Christopher M. 2003. *Ap. J. Lett.* 585:L105
Scoville NZ, Yun MS, Windhorst RA, Keel WC, Armus L. 1997. *Ap. J. Lett.* 485:L21
Shapiro KL, Genzel R, Förster Schreiber NM, Tacconi LJ, Bouché N, et al. 2008. *Ap. J.* 682:231–51
Shapley AE. 2011. *Annu. Rev. Astron. Astrophys.* 49:525–80
Shetty R, Glover SC, Dullemond CP, Klessen RS. 2011. *MNRAS* 412:1686
Shields G, Menezes K, Massart C, Vanden Bout P. 2006. *Ap. J.* 641:683–88
Silk J, Mamon GA. 2012. *Res. Astron. Astrophys.* 12:917
Silva L, Granato GL, Bressan A, Danese L. 1998. *Ap. J.* 509:103
Smail I, Ivison RJ, Blain AW. 1997. *Ap. J. Lett.* 490:L5
Solomon P, Vanden Bout P, Carilli CL, Guélin M. 2003. *Nature* 426:636–38
Solomon PM, Downes D, Radford S. 1992. *Ap. J.* 398:L29–32
Solomon PM, Downes D, Radford S, Barrett J. 1997. *Ap. J.* 478:144–61
Solomon PM, Rivolo A, Barrett J, Yahil A. 1987. *Ap. J.* 319:730–41
Solomon PM, Vanden Bout PA. 2005. *Annu. Rev. Astron. Astrophys.* 43:677–725
Spergel D, Bean R, Doré O, Nolta M, Bennett C, et al. 2007. *Ap. J. Suppl.* 170:377–408
Spinoglio L, Malkan MA. 1992. *Ap. J.* 399:504
Spinoglio L, Pereira-Santaella M, Busquet G, Schirm MRP, Wilson CD, et al. 2012. *Ap. J.* 758:108
Spitzer L. 1978. *Physical Processes in the Interstellar Medium*. New York: Wiley-Intersci.
Springel V, White S, Jenkins A, Frenk C, Yoshida N, et al. 2005. *Nature* 435:629–36
Stacey GJ. 2011. *IEEE Trans. Terahertz Sci. Technol.* 1:241
Stacey GJ, Geis N, Genzel R, Lugten JB, Poglitsch A, et al. 1991. *Ap. J.* 373:423
Stacey GJ, Hailey-Dunsheath S, Ferkinhoff C, Nikola T, Parshley S, et al. 2010. *Ap. J.* 724:957–74
Steidel CC, Shapley AE, Pettini M, Adelberger KL, Erb DK, et al. 2004. *Ap. J.* 604:534–50
Strickland DK, Heckman TM. 2009. *Ap. J.* 697:2030–56
Strong AW, Mattox JR. 1996. *Astron. Astrophys.* 308:L21–24
Sturm E, Verma A, Graciá-Carpio J, Hailey-Dunsheath S, Contursi A, et al. 2010. *Astron. Astrophys.* 518:L36
Stutzki J, Graf UU, Haas S, Honingh CE, Hottgenroth D, et al. 1997. *Ap. J.* 477:L33–36
Swinbank AM, Chapman SC, Smail I, Lindner C, Borys C, et al. 2006. *MNRAS* 371:465–76
Swinbank AM, Karim A, Smail I, Hodge J, Walter F, et al. 2012a. *MNRAS* 427:1066
Swinbank AM, Papadopoulos PP, Cox P, Krips M, Ivison RJ, et al. 2011. *Ap. J.* 742:11
Swinbank AM, Smail I, Longmore S, Harris AI, Baker A, et al. 2010. *Nature* 464:733
Swinbank AM, Smail I, Sobral D, Theuns T, Best PN, Geach JE. 2012b. *Ap. J.* 760:130
Tacconi LJ, Genzel R, Neri R, Cox P, Cooper MC, et al. 2010. *Nature* 463:781–84
Tacconi LJ, Genzel R, Smail I, Neri R, Chapman SC, et al. 2008. *Ap. J.* 680:246–62
Tacconi LJ, Neri R, Chapman SC, Genzel R, Smail I, et al. 2006. *Ap. J.* 640:228–40
Tacconi LJ, Neri R, Genzel R, Combes F, Bolatto A, et al. 2013. *Ap. J.* 768:74
Thacker RJ, Scannapieco E, Couchman HMP. 2006. *Ap. J.* 653:86–100
Thompson TA. 2009. *Ap. J.* 408:128
Thompson TA, Quataert E, Murray N. 2005. *Ap. J.* 630:167–85

Thomson A, Ivison RJ, Smail I, Swinbank AM, Weiß A, et al. 2012. *MNRAS* 425:2203–11
Tielens AGGM. 2005. *The Physics and Chemistry of the Interstellar Medium*. Cambridge, UK: Cambridge Univ. Press
Tielens AGGM, Tokunaga AT, Geballe TR, Baas F. 1991. *Ap. J.* 381:181
Townes CH, Schawlow AL. 1975. *Microwave Spectroscopy*. New York: Dover
Valtchanov I, Virdee J, Ivison RJ, Swinyard B, van der Werf P, et al. 2011. *MNRAS* 415:3473–84
van der Tak FFS, Black JH, Schöier FL, Jansen DJ, van Dishoeck EF. 2007. *Astron. Astrophys.* 468:627
van der Wel A, Rix HW, Holden B, Bell EF, Robaina A. 2009. *Ap. J. Lett.* 706:L120–23
van der Werf PP, Berciano Alba A, Spaans M, Loenen AF, Meijerink R, et al. 2011. *Ap. J. Lett.* 741:L38
van der Werf PP, Isaak KG, Meijerink R, Spaans M, Rykala A, et al. 2010. *Astron. Astrophys.* 518:L42
van Kempen TA, Kristensen LE, Herczeg GJ, Visser R, van Dishoeck EF, et al. 2010. *Astron. Astrophys.* 518:L121
Veilleux S, Cecil G, Bland-Hawthorn J. 2005. *Annu. Rev. Astron. Astrophys.* 43:769–86
Venemans BP, McMahon R, Walter F, Decarli R, Cox P, et al. 2012. *Ap. J. Lett.* 751:L25
Vieira JF, Marrone DP, Chapman SC, De Breuck C, Hezaveh YD, et al. 2013. *Nature* 495:344–47
Wagg J, Carilli CL, Wilner DJ, Cox P, De Breuck C, et al. 2010 *Astron. Astrophys.* 519:L1
Wagg J, Kanekar N. 2012. *Ap. J. Lett.* 751:L24
Wagg J, Kanekar N, Carilli CL. 2009. *Ap. J. Lett.* 697:L33–37
Wagg J, Wiklind T, Carilli CL, Espada D, Peck A, et al. 2012. *Ap. J. Lett.* 752:L30
Wagg J, Wilner DJ, Neri R, Downes D, Wiklind T. 2006. *Ap. J.* 651:46–50
Walter F, Bertoldi F, Carilli C, Cox P, Lo KY, et al. 2003. *Nature* 424:406
Walter F, Brinks E, de Blok WJG, Bigiel F, Kennicutt RC, et al. 2008. *Astron. J.* 136:2563
Walter F, Carilli C, Bertoldi F, Menten K, Cox P, et al. 2004. *Ap. J.* 615:L17–20
Walter F, Decarli R, Carilli C, Bertoldi F, Cox P, et al. 2012a. *Nature* 486:233–36
Walter F, Decarli R, Carilli C, Riechers D, Bertoldi F, et al. 2012b. *Ap. J.* 752:93
Walter F, Riechers D, Cox P, Neri R, Carilli C, et al. 2009a. *Nature* 457:699–701
Walter F, Weiß A, Downes D, Decarli R, Henkel C. 2011. *Ap. J.* 730:18
Walter F, Weiß A, Riechers DA, Carilli CL, Bertoldi F, et al. 2009b. *Ap. J. Lett.* 691:L1–4
Walter F, Weiß A, Scoville N. 2002. *Ap. J. Lett.* 580:L21
Wang R, Carilli CL, Neri R, Riechers DA, Wagg J, et al. 2010. *Ap. J.* 714:699–712
Wang R, Carilli CL, Wagg J, Bertoldi F, Walter F, et al. 2008a. *Ap. J.* 687:848–58
Wang R, Wagg J, Carilli CL, Benford DJ, Dowell CD, et al. 2008b. *Astron. J.* 135:1201–6
Wang R, Wagg J, Carilli CL, Walter F, Lentati L, et al. 2013. *Ap. J.* In press (arXiv:1302.4154)
Ward JS, Zmuidzinas J, Harris AI, Isaak KG. 2003. *Ap. J.* 587:171–85
Weiß A, De Breuck C, Marrone DP, Vieira JD, Aguirre JE, et al. 2013. *Ap. J.* 767:88
Weiß A, Downes D, Henkel C, Walter F. 2005a. *Astron. Astrophys.* 429:L25–28
Weiß A, Downes D, Neri R, Walter F, Henkel C, et al. 2007a. *Astron. Astrophys.* 467:955–69
Weiß A, Downes D, Walter F, Henkel C. 2007b. In *ASP Conf. Ser. 375*, *From Z-Machines to ALMA: (Sub)Millimeter Spectroscopy of Galaxies*, p. 25
Weiß A, Henkel C, Downes D, Walter F. 2003. *Astron. Astrophys.* 409:L41–45
Weiß A, Ivison RJ, Downes D, Walter F, Cirasuolo M, Menten KM. 2009. *Ap. J. Lett.* 705:L45–47
Weiß A, Requena-Torres MA, Güsten R, García-Burillo S, Harris AI, et al. 2010. *Astron. Astrophys.* 521:L1
Weiß A, Walter F, Downes D, Carilli CL, Henkel C, et al. 2012. *Ap. J.* 753:102
Weiß A, Walter F, Scoville NZ. 2005b. *Astron. Astrophys.* 438:533
White G, Ellison B, Claude S, Dent WRF, Matheson DN. 1994. *Ap. J.* 284:L23–26
White S, Rees MJ. 1978. *MNRAS* 183:341–58
Willott C, Omont A, Bergeron J. 2013. *Ap. J.* 770:13
Wilner DJ, Zhao JH, Ho PTP. 1995. *Ap. J. Lett.* 453:L91
Wolfe AM, Gawiser E, Prochaska JX. 2005. *Annu. Rev. Astron. Astrophys.* 43:861–918
Wootten A, Thompson AR. 2009. *IEEE Proc.* 97:1463
Wu J, Evans NJ II, Gao Y, Solomon PM, Shirley YL, Vanden Bout PA. 2005. *Ap. J. Lett.* 635:L173–76
Xia XY, Gao Y, Hao C-N, Tan QH, Mao S, et al. 2012. *Ap. J.* 750:92
Yan L, Tacconi LJ, Fiolet N, Sajina A, Omont A, et al. 2010. *Ap. J.* 714:100–14

Yang B, Stancil PC, Balakrishnan N, Forrey RC. 2010. *Ap. J.* 718:1062
Yang Y, Decarli R, Dannerbauer H, Walter F, Weiß A, et al. 2012. *Ap. J.* 744:178
Young JS, Scoville NZ. 1991. *Annu. Rev. Astron. Astrophys.* 29:581–625
Yun MS, Carilli CL. 2002. 568:88–98
Yun MS, Scott KS, Guo Y, Aretxaga I, Giavalisco M, et al. 2012. *MNRAS* 420:957